

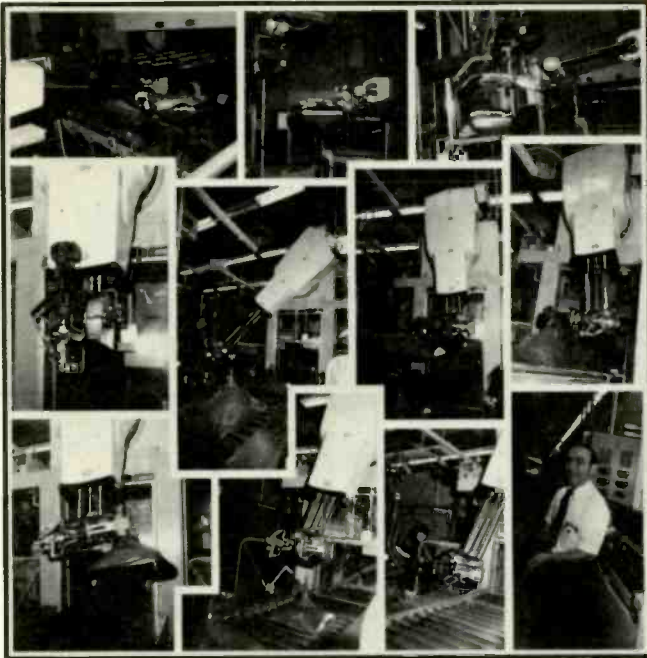
RCA Engineer

Vol. 26 No. 4 Jan./Feb. 1981



Mechanical engineering issue

Cover photos by Louise M. Carr



The cover photos show robot installations at Picture Tube Division manufacturing sites. And the article on p. 6 presents information on the burgeoning applications of robotics, one of several important "hybrid" disciplines encompassing computer science, and manufacturing, electrical and mechanical engineering (see keynote article, p. 4, by W.W. Metzger).

On the front cover, the top row shows Unimates unloading a frit-seal oven and loading a conveyor hanger in the MEGA 1 system at Scranton. The two bottom rows show "Roger," the first Unimate robot in Scranton, transferring different-sized funnels from the coating machines to a conveyor. Joe Holecko (lower right) holds the control used to teach "Roger" its motion. The robot is even programmed to recognize and discard broken funnels (lower row, second photo from right).

— — R.M. Carrell

RCA Engineer

A technical journal published by
RCA Research and Engineering
Bldg. 204-2
Cherry Hill, NJ 08358
TACNET: 222-4254 (609-338-4254)

RCA Engineer Staff

Tom King	Editor
Mike Sweeny	Associate Editor
Louise Carr	Art Editor
Frank Strobl	Contributing Editor
Betty Gutchigian	Composition
Dorothy Berry	Editorial Secretary

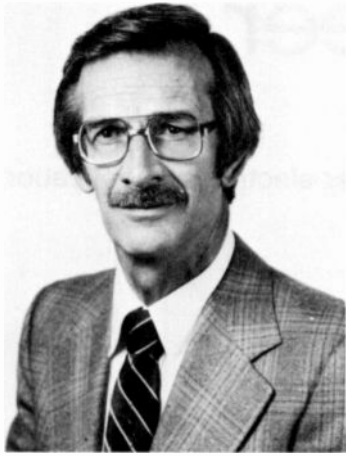
Editorial Advisory Board

Pete Bingham	Division Vice-President, Engineering, Consumer Electronics Division
Jay Brandinger	Division Vice-President, "SelectaVision" VideoDisc Operations
John Christopher	Vice-President, Technical Operations, RCA Americom
Bill Hartzell	Division Vice-President, Engineering, Picture Tube Division
Jim Hepburn	Vice-President, Advanced Programs, RCA Globcom
Hans Jenny	Manager, Engineering Information
Arch Luther	Division Vice-President, Engineering, Commercial Communications Systems Division
Howie Rosenthal	Staff Vice-President, Engineering
Ed Troy	Director, Operations Planning and Support, Solid State Division
Bill Underwood	Director, Engineering Professional Programs
Joe Volpe	Director, Product Operations, Missile and Surface Radar
Bill Webster	Vice-President, Laboratories

Consulting Editors

Ed Burke	Administrator, Marketing Information and Communications, Government Systems Division
Walt Dennen	Director, Public Affairs, Solid State Division
Charlie Foster	Manager, Systems and Procedures, RCA Laboratories
John Phillips	Manager, Proposals and Publicity, Automated Systems

•To disseminate to RCA engineers technical information of professional value •To publish in an appropriate manner important technical developments at RCA, and the role of the engineer •To serve as a medium of interchange of technical information between various groups at RCA •To create a community of engineering interest within the company by stressing the interrelated nature of all technical contributions •To help publicize engineering achievements in a manner that will promote the interests and reputation of RCA in the engineering field •To provide a convenient means by which the RCA engineer may review his professional work before associates and engineering management •To announce outstanding and unusual achievements of RCA engineers in a manner most likely to enhance their prestige and professional status.



Paul E. Wright

Mechanical engineers: building the future

Mechanical engineers have made important contributions to RCA's success throughout its history. An example from RCA's early period is the refinement of radio-loudspeaker quality through applications that combined basic acoustical theory with the theory of vibrations in conical shells. An example from the 1950s is the development of video tape recorders which made possible major improvements in TV production procedures. Recently, mechanical engineers have played a significant role in the creation of new communication systems that use networks of satellites and earth stations. Today, mechanical engineers are providing major innovations to the "SelectaVision" product line. In particular, the VideoDisc players and discs are examples of the rare combination of high performance with low cost.

The future promises even broader opportunities for mechanical engineers to shape the affairs of both RCA and society at large. For instance:

- Declining productivity is everyone's concern. Computer-aided design (CAD), computer-aided manufacturing (CAM), and robotics are areas where mechanical engineers can help to reverse this decline.
- Energy issues must be addressed by RCA and our society if we are to live within the boundaries of the future. New control systems, application of thermodynamics and materials sciences to the development of solar energy, conversion of coal and other materials into synthetic fuels, and the safe use of nuclear energy are appropriate areas for concentration.
- We must protect our environment through innovative approaches to the detection and control of pollutants in the air and water.
- In the 1980s, we will see expanded use of new materials such as composites and plastics.
- Space satellites for communications, navigation and earth observation will explode on the scene in the decade ahead. Space may even provide the "special effects" for radically new manufacturing processes.

These projects demand the management and technical skills of a growing mechanical engineering population. Mechanical engineers — always important professionals in our society — will find the opportunities of the 1980s replete with challenge and reward.

Paul E. Wright
Division Vice-President and General Manager
Government Systems Division

RCA Engineer

Vol. 26|No. 4 Jan.|Feb. 81

interdisciplinary engineering

- 4** Mechanical engineering — for broader electronics applications
W.W. Metzger
- 6** Robots for industry
R.M. Carrell
- 12** Advanced composite structures for satellite systems
R.N. Gounder

finite-element modeling

- 23** Predicting the acoustic response of the 5D-2 satellite
C.R. Voorhees
- 28** A modal vibration test of the 5D-2 satellite
D.F. Chu
- 34** Structural evaluation of plastic parts for television receivers
S.A. Keneman|R.T. Mooney
- 41** Computer analysis for shock testing of AEGIS water coolers
R.J. Pschunder

specific applications

- 46** Precision in large mechanisms —
the near-field-antenna test scanner
W.A. Harmening
- 52** The role of mockups in improved equipment design
C.H. Tipple
- 56** Air-lubricated thermal processor for dry silver film
B.W. Siryj
- 63** Electronic packaging for an artillery-delivered sensor
M.J. Kurina

departments

- 67** Pen and Podium
- 69** News and Highlights

in this issue...

Mechanical Engineering

■ **Metzger** "This separation (of the mechanical from the electrical) has now disappeared in many products as computers and associated electrical gear find their way into mechanical systems..."

■ **Carrell** "The current robot revolution is based on machines that have sophisticated digitally-controlled servo systems and that can 'learn' a series of positions, or 'attitudes', and then repeat them."

■ **Gounder** "Mechanical engineers in the various divisions of RCA are taking advantage of this renaissance technology."

■ **Voorhees** "The special test program required careful planning since the test article was a flight spacecraft, near completion, worth many millions of dollars."

■ **Chu** "These results provide a dynamic model directly from measurements, whereas previously such a model was derived analytically by finite-element analysis."

■ **Keneman|Mooney** "It was not clear in advance that the well-known anisotropic and process-dependent properties of plastics could be suitably modeled with FEM in a cost-effective fashion."

■ **Pschunder** "In an attempt to eliminate barge testing of the AEGIS water coolers, and thus to realize considerable cost savings, the Navy allowed RCA to prove compliance with the specifications by computer analysis."

■ **Harmening** "This approach cuts down the distance required between antenna and test sensor from several hundred feet to a few inches."

■ **Tipple** "They were used as design integration aids, allowing a number of disciplines to participate in the design process..."

■ **Siryj** "If pressurized air is available, the convective processor approach should be considered because it presents a conceptually simple, reliable way to process dry silver film."

■ **Kurina** "Electronic parts and circuits can be gun-hardened for the most severe shock possible, and can survive and function successfully."

in future issues...

increasing your effectiveness, computer-aided design and manufacturing, anniversary issue, microprocessors applications.

Mechanical engineering — for broader electronics applications

Electrical and mechanical engineering categories will meld together into systems approaches that combine technologies, with the help of computers. But mechanical engineers' feats will still attract attention.

Abstract: *An overview of papers in this mechanical engineering issue accompanies predictions on future mechanical engineering tools, products and directions.*

Each year RCA produces electronics products that extend into new areas of technological development. We take pride in these products, from color-television receivers to weather satellites, from national defense systems to commercial-TV cameras. Many of our products lead the field in which they compete. And we all eagerly anticipate the introduction of RCA "SelectaVision" VideoDisc. Mechanical engineering is basic to each of these products. Each depends upon structures — large or small — to give it form, and upon provisions for energy conversion to make it work. Mechanical engineers have the skills to design these structures and make these provisions.

Mechanical engineers and their work

An engineering student at a large state university recently told me, "Mechanical engineers have more fun." She observed that they do a lot of exciting things with conspicuous enthusiasm. Everyone can watch the various contests that they hold out in the open: dropping eggs (or calculators) from the top of the dorm, racing rafts down the river, racing concrete

canoes on the lake, and performing competitive feats with various types of motor-powered rolling and climbing and crawling vehicles. Their clever or ridiculous performances are available for equal scrutiny by both sophisticated and confused observers, whose criticisms may range from cheers to sneers. Dynamometer tests of engines in school laboratories create an attention-getting noisy environment. As kids, these mechanical engineers got their kicks from building and racing model cars, boats and planes, and from squashing pennies on the railroad tracks.

Mechanical engineers as students or as professionals don't really have more fun than other engineers, it just shows more. The things we work on are apt to attract more attention. And when they break apart or won't go, everybody knows about it. During the past year, the whole nation followed the troubles of the DC-10, and Walter Cronkite devoted 90 seconds on national television to one small lost communications satellite. Mechanical engineering is no place for paranoid personalities — it all hangs out, and there is always a crowd watching.

1980: mechanical engineering at the watershed

It has been forecast that two of every three children born this year will work at jobs that don't now exist. Before you doubt that prediction, take out your slide rule, move up closer to your Tektronix keyboard, and contemplate your present job. Did it exist 20 years ago? Of course not, and it won't 20

years hence when you're working with the two out of three. Or will you be?

RCA will be making new products from new hardware. The engineers working on these products will be engaged in new activities, and they'll be using new tools. So if you're going to make the scene in the year 2000, you'll have to develop new skills based on new knowledge. That development will depend upon contacts with colleagues.

The tools, the activities, and the products will be different. I'll leave predictions of new products to others. But I'd like to contemplate the tools and the activities that will comprise engineers' work.

The tools

Have you noticed, in the past year or so, how many computer terminals are appearing in the engineering work areas? Every week, additions of various types spread their connections and carry the engineer's sphere of influence beyond traditional confines. During the 1980s we will see computer terminals become as common a personal tool as the slide rule was in the 1960s and as the pocket calculator became during the 1970s. Terminals will be put to uses which we haven't thought of yet. But most importantly, they'll be as available to us as a TV or a telephone is today.

These new tools will require a whole spectrum of new skills. For example, touch typing will be a valuable asset and will likely be required of all college graduates. Computer terminals will not be restricted to science and engineering, but will be used

in literature, history, music, in many ways not yet invented.

Engineers will have their own terminals, which they will use at work or at home. Probably, just as with calculators, they'll have at least two. These terminals will provide input and output to powerful computer systems both large and small. They'll involve telephone, TV cable, satellites, and small personal computers. It boggles the mind to think of the systems that are already available as a result of combining these elements, and of the uses to which these systems will be applied as they become common tools.

The activities

Computerized instruction and information gathering will promote televised meetings. This will foster a renewed emphasis on team building and on problem solving via groups or task forces. The computer terminal will structure our use of time by imposing its discipline. At the same time, it will open avenues for more effective group work across organizational boundaries. Thus, an individual's daily work will involve a higher order of interpersonal relations.

The products

Recollections of where we've been and predictions of where we'll be provoke some insights as to what's happening now at the cutting edge of progress.

Manufactured products today are engineered with the combination of engineering skills from many fields: mechanical, electrical, materials, and so on. Ten or twenty years ago, most products were either mechanical or electrical, and materials were often taken for granted. Airplanes, trains, and automobiles were mechanical. Television, computers, and telephones were electrical. This separation has now disappeared in many products as computers and associated electrical gear find their way into mechanical systems, taking over control functions that once were mechanical in cars and planes. Meanwhile, television and telephone are providing the basics for building

sophisticated systems of mechanical and electrical equipments devoted to knowledge functions, including systems that handle information and that communicate among people; and machines that learn, remember, and do work per computer instructions. During the 1970s, computers were flown into space as part of the satellite, thus shifting control from the ground to the satellite.

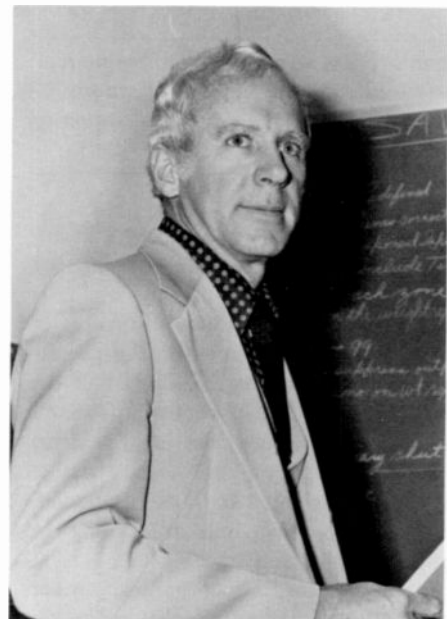
The products from 20 years ago evolved into sophisticated electro-mechanical systems in which a long succession of detailed problems have succumbed to the continued application of engineering from many disciplines. The applications are endless (refrigeration, water heaters, stoves, typewriters, sporting equipment) and crop up in some unlikely places (bathroom fixtures, tires, and toys) that were neglected by engineers for many years.

Thus, the wave of engineering progress carrying us into the 1980s is based on a systems approach to design in which all technical disciplines are combined in products of ever-increasing complexity. There has never been a more exciting time to be a mechanical engineer—but there will be.

The mechanical engineering papers presented in this issue cover diverse applications of mechanical design skills and they attest to the diversity of mechanical engineering activities at RCA. Many authors report finite-element methods of structural analysis. A symposium on that subject nearly three years ago undoubtedly contributed to these efforts reported now. One paper, on robotics, is about direct applications of computers to manufacturing processes. Two of the papers (on the Aegis antenna range and on a satellite's modal vibration test) involve the uses of computers in test facilities. Two papers (on testing Aegis water coolers and on an acoustic test of a satellite) use complicated analytical models to predict mechanical test results. Two papers (on packaging techniques for an artillery-delivered sensor and on thermal processing for dry silver film) describe complicated systems which depend mightily on mechanical engineering skills: structural dynamics and heat transfer,

respectively. Another paper describes the application of new composite materials to build structures with specially tailored characteristics. These works give the authors professional fulfillment and they contribute, each by a small increment, to the success of RCA. They justify the theme: "Mechanical Engineering—Basic Technology for Broader Electronics Applications" for the symposium* of last April and for this issue of the *RCA Engineer*.

*The title of this article is the theme of a symposium which was hosted by RCA Astro-Electronics at the Space Center in Hightstown, New Jersey, last April 29 and 30. It was attended by 80 engineers from 10 different RCA locations. Fourteen papers were presented, many of which are included in the pages of this issue of the *RCA Engineer*.



Bill Metzger has over twenty years' experience in engineering of mechanical systems for aerospace vehicles. Since 1972, he has worked at RCA Astro-Electronics where he is currently Manager, Mechanical Engineering. In this position, he has initiated new methods in finite-element analysis of structures, advanced composite materials applications to spacecraft structures, normal-mode vibration testing of structures, thermal analysis of spacecraft components, and compact electronic packaging.

Contact him at:
RCA Astro-Electronics
Princeton, N.J.
TACNET: 229-2912

Robots for industry

Robots — relatively homeless for twenty years — are heading in dramatically increasing numbers for the factories, where managers believe that their well-programmed assistance will boost sagging productivity.

Abstract: *This paper on robotics surveys the state of the art, notes applications within RCA and predicts the direction of future developments.*

Industrial robots will help U.S. industry make the increases in productivity needed for economic survival during the next decade. The Japanese, astute students of Western technology, now threaten to surpass their teachers by installing half the world's population of robots in Japan's factories. Most of these sophisticated robots incorporate advanced design principles originated by U.S. companies. But now U.S. companies are joining the robotics applications race.

In the last year, U.S. corporations made major commitments to robotics. Westinghouse created a Robotics Division with a charter for extensive internal use of robots. General Electric made large purchase commitments. IBM announced a new division to produce industrial robots for internal use. Texas Instruments used vision-assisted robots for small assembly operations. A new company, Automatix, was founded to produce turnkey robot systems that include CCD (charge-coupled device) cameras to guide the robot in assembly operations.

RCA is keeping up with robotics technology, too. RCA began installing industrial robots in the Picture Tube Division (PTD) plant approximately three years ago. Research is underway at a newly established robotics laboratory at the David Sarnoff Research Center (DSRC), described below.

Industrial robot evolution

We could say that manufacturing consists of making parts and putting them together. The "putting them together" involves a whole technology of material handling on a small scale, and a wide variety of "pick-and-place" mechanisms for handling individual pieces. In this sense, any automatic parts handler is a robot. The Japanese have used simple parts handlers with extreme thoroughness.

Traditional automated parts handlers work with specific parts and specific machines — so-called "hard automation" which a part or process change can make obsolete. Industrial robots started as programmable transfer machines that could endlessly repeat the motions needed to remove parts from a punch press and stack them in a bin. If the part changed, engineers adjusted the motion pattern. If the process changed, the robot was used elsewhere.

In the simplest robots, mechanical stops define the extent of the motions, and a programming drum or, more recently, a solid-state controller, defines the sequence. The current robot revolution is based on machines which have sophisticated digitally controlled servo systems and which can "learn" a series of positions, or "attitudes," and then repeat them. The key to success is repeatability, not absolute accuracy, since the robots are "taught" after their installation in the workplace. In the more sophisticated machines, large memories and computer controls permit hundreds of taught points to be stored. These effectively merge into continuous paths. Such robots can weld and spray-paint with a uniformity that the best humans cannot achieve because of fatigue. The Robot Institute of

America now defines the robot as a "reprogrammable multifunctional manipulator designed to move materials, parts, tools, or specialized devices through variable programmed motions for the performance of a variety of tasks."

At a higher level of sophistication, robots can work on a moving target. For example, they can weld car bodies on a moving conveyor. Once the robot is taught the welding pattern on a stationary car, its computers can then continuously transform the coordinate system as the car moves along the assembly line. These systems are "blind." They require precision placement of the robot and its moving workpiece.

At the leading edge of technology, designers are coupling robots with solid-state cameras and computers that analyze images and direct the robot to grasp randomly oriented parts, and then place them in an assembly.

Robots differ in their precision, load-carrying capacity, ease and flexibility of programming, and basic coordinate systems. Table I summarizes the characteristics of some representative industrial robots illustrated on these pages.

The Unimate® 2000 family, shown in Fig. 1, from Unimation Inc. of Danbury, Connecticut, is a classic design that established the industrial robot as a reliable production machine and made Unimation the industry leader. A telescoping arm, mounted to provide rotation about the vertical and horizontal axes, makes it a basic spherical-coordinate machine. The arm contains two shafts that can be rotated to produce two wrist motions, for a total of five basic motions. Various gripping devices — or "hands" — are attached to the "wrist" to adapt the robot to specific

Table I. A summary of the characteristics of representative industrial robots, showing the various structural, control and performance features available.

Manufacturer	Model	Coordinate system	Repeat accuracy (inches)	Load capacity (pounds)	Power	Control	Program method	Remarks
Unimation Inc.	2000	Spherical	.050	> 100	Hydraulic	Plated wire Shaft encoder	Teach	Industry leader
	500/600	Cartesian, Cylindrical, Arm	.005	5	Electric	LSI-11 Shaft encoders	VAL Language or Teach	Small assembly
Cincinnati Milacron	T ³	Arm	.050	> 100	Hydraulic	Computer Shaft encoder	Teach	Continuous-path tracking
ASEA Inc.		Arm	.050	> 100	Hydraulic	Computer Shaft encoder	Teach	Continuous-path tracking
Prab Conveyors Inc.		Spherical	.005	> 100	Hydraulic	Hard stops	Drum	Old design
	Versatran	Cylindrical	.050	>2000	Hydraulic	Core memory Helical pots	Teach	Modular
Rosenlew Tool Works		Various	.050	100	Various	Limit switches Hydraulic regulation External logic		Modular
Seiko Instruments Inc.		Cylindrical	.001	< 116	Pneumatic	Hard stops	Air logic	Watch assembly

applications.

A digitally controlled hydraulic servo powers all motions. Primary power is given by a 10-hp motor that drives a pump and an associated accumulator, which consists of a confined gas "spring" to provide peak energy for fast acceleration. The pump operates only to maintain pressure in the accumulator. It shuts off during idle periods, thereby saving power. Linear cylinders drive the motions, and linkages or gears produce rotary motions.

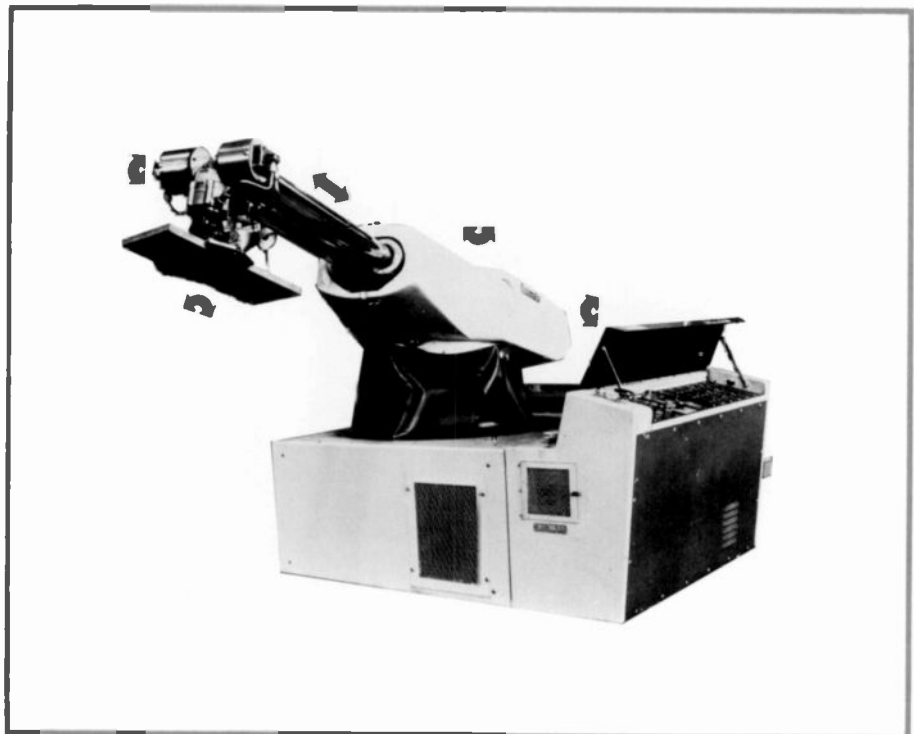
Motions are measured by 14-bit shaft encoders that can resolve 0.050-inch displacements of the arm end at its maximum extension. Shaft positions are recorded in a plated-wire memory. Plated-wire memories have nondestructive readouts, which make them less vulnerable than core memories to error in electrically noisy environments. Until recently, semiconductor memories were too unreliable for robot applications and were vulnerable to power failure. Robots of the 1980s, however, will use semiconductor memories. Electronic reliability is of extreme concern because a single-bit error can cause a wild motion. A faulty robot can severely damage people (and expensive machines).

An operator programs the Unimation robot by using a hand-held control box on the end of a 'teach umbilical' cable that lets him slowly guide the robot to each of a sequence of attitudes comprising the task to be done. For each attitude, the azimuth, elevation and extension of the arm and the position of the shafts which control the wrist are measured by the shaft encoders mentioned above, and recorded as five

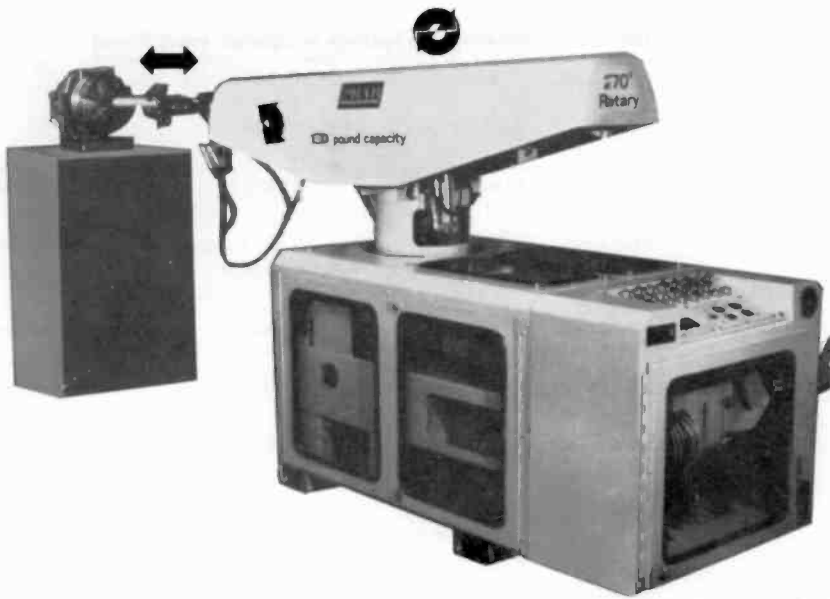
numbers in the memory. A sequence of attitudes becomes a table of numbers in the memory. In the RUN mode, the numbers from the shaft encoders are compared with the numbers recorded in the memory, thereby generating error signals that drive the hydraulic servos. The robot can repeat the taught sequence of attitudes endlessly, without coffee breaks or fatigue.

At each program step, external contacts can be operated or sensed so that the robot can interact with other machines. For example, it can wait for a die casting mold to open or inform a conveyor that a part has been placed upon it. In complex installations, the robot can interface with a programmable controller or computer.

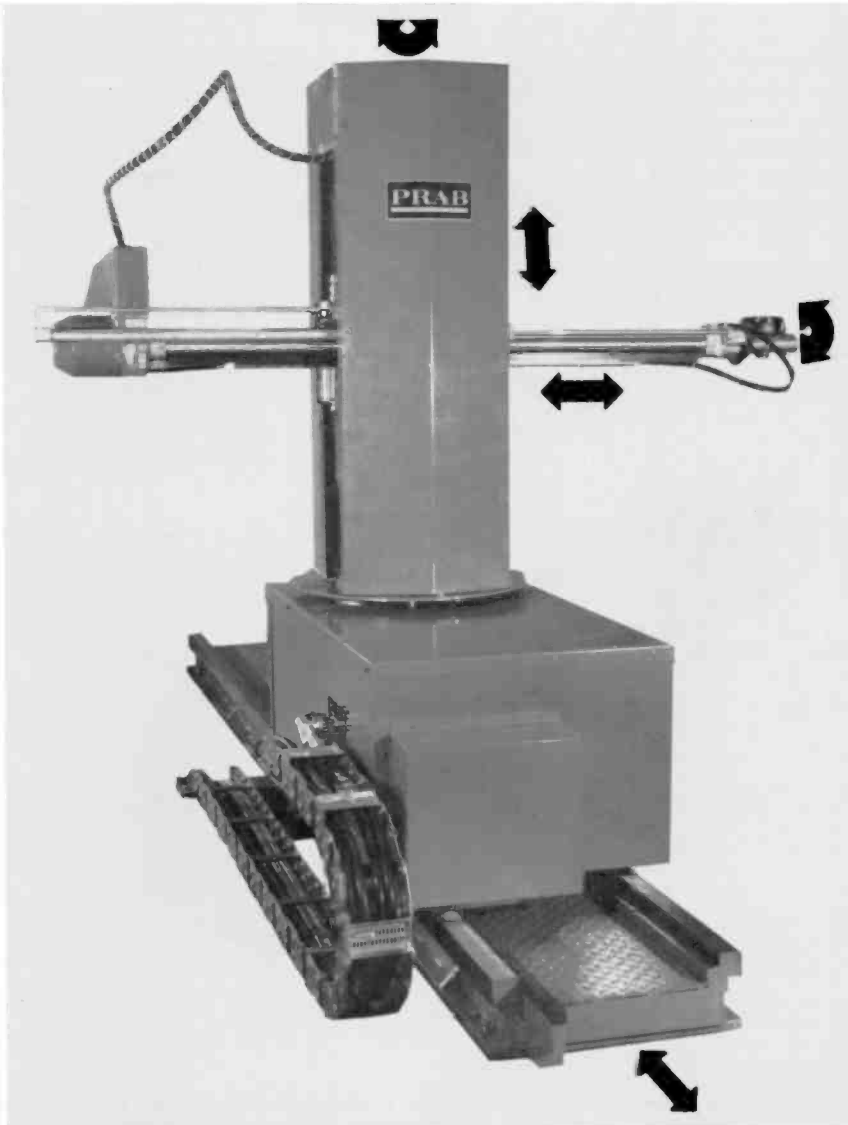
With periodic maintenance, Unimates



The Unimate 2000-series robot has 5 degrees of freedom. The "hand" clamping the workpiece is custom made for each application and may itself be a complex mechanism. The base cabinet contains the controls and hydraulic system. The boom can be separated from the base and mounted in any position.



A Prab Conveyors, Inc. robot uses hard stops and solid-state control. Its repeatability is better than the servo robots, but it is more difficult to program.



A Prab Versatran servo-controlled robot. The entire robot can move on a track. It can be mounted in any position. The Versatran is a modular system.

can be expected to have a service life approaching forty thousand hours of continuous operation, with an uptime of 98 percent or better. This performance exceeds that of many other production machines, and it is an important reason why industry is accepting the Unimates.

RCA has purchased seven large Unimates. Three are installed at the Scranton, Pennsylvania plant, three are to be used at the Marion, Indiana plant and the other is in a developmental laboratory headed by W.R. Kelly at Lancaster, Pennsylvania. These last four machines can track a moving conveyor, so that they can place picture tubes on the conveyor without stopping it.

Another family of robots has structures that imitate the human arm in geometry and function. These robots require computers to coordinate the motions of the joints and can do complex tasks such as continuous path welding of car bodies on a moving conveyor. Examples are the Unimation 600, Cincinnati Milacron's T³ robot, and the two models from ASEA Inc. in Sweden.

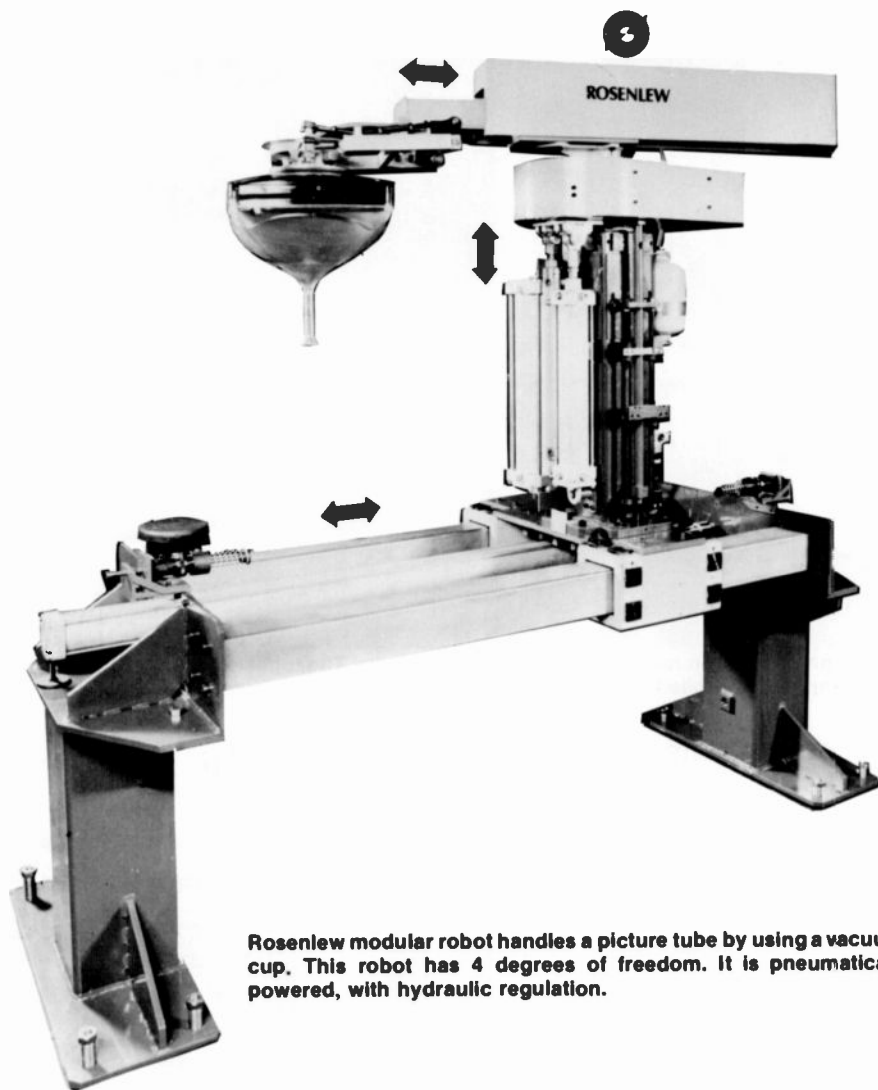
The newest and most interesting of these — the 600 — is intended to be a man-sized companion to human operators in lightweight assembly work. A survey of automobile plant assembly tasks showed that 95 percent of them involved loads of five pounds or less, which is the capacity of the 600.

The 600 is programmed in a special language called VAL that allows the motions to be defined in Cartesian, tool, or joint coordinates. A 'teach umbilical' is also available. Since the computer is a Digital Equipment Corporation LSI-11, the robot communicates with other computers and controllers.

Two 600s are at RCA. One is at Lancaster, Pennsylvania, in W.R. Kelly's Automation and Computer Systems Group, the other at the Robotics Laboratory in DSRC at Princeton, New Jersey. The latter will be coupled to a camera/computer system from SRI International and used for investigation of vision-assisted robotics.

Prab Conveyors Inc., of Kalamazoo, Michigan markets two machines. One is a spherical-coordinate-based machine with mechanical stops to define motion limits. It is an old design, but it can give good repeatability.

AMF Inc. originated the Versatran robot, then sold it to Prab. It is a modular, cylindrical-coordinate machine available in several sizes — the largest can carry



Rosenlew modular robot handles a picture tube by using a vacuum cup. This robot has 4 degrees of freedom. It is pneumatically powered, with hydraulic regulation.

press manufacturer. But this is dedicated, "hard" automation, which can be obsoleted by a minor part change.

The advantage of the teachable machines such as the Unimate is that when a part or operation changes, the machine can "learn" a new program in a matter of minutes, or can accept, via tape cassette, a previously developed program.

The teachable robot is very appealing in management presentations. It is a great concept — bring in the robot on a forklift, teach it a program and push the PLAY button. But it is never that simple. In practice, human adaptability conceals the actual complexity of the task that looks easy. The worker can use his intelligence and ingenuity to respond to new or unusual circumstances. With robots, all possible occurrences must be provided for in a system in which the robot's cost is a minor part of the total project cost. As one industry commentator said: "Robots are easy, it's everything else that's hard."

For example, the robot must be able to recognize and discard broken parts. The robot must sometimes wait for a part. And it should be able to recognize a bigger, heavier object and compensate for varied sizes and weights.

One incentive favoring the increased use of robots is that the cost of robots is coming down and the cost of labor is rapidly going up.

Before designing mechanization systems, the project must be defined to be large enough to give substantial returns without becoming overwhelming in cost and scope. In the PTD plant at Scranton, a single Unimate, called Roger, was installed to perform a simple task in order to gain experience and demonstrate reliability. This installation was illustrated in an article by L. Rarig and W.R. Kelly in the Dec. 78/Jan. 79 issue of the *RCA Engineer* and the two bottom rows of the photo collage on this issue's front cover.

In 1978 a large system, MEGA I, was

also installed at Scranton. In MEGA I, Unimates remove picture tube bulbs from frit-seal fixtures and place them on special hangers in a power-and-free conveyor system (see front cover, top row). A power-and-free conveyor has two rails. One supports the tube hangers, the other supports a drive chain. The hangers can be powered by coupling them to the drive chain, or be free to change from one chain to another, or they can rest idle on a rail.

The power-and-free system allows a hanger to be a fixed target to which the Unimate can transfer the bulb. Next, the hanger can be coupled to the drive chain. This system distributes the bulbs to six lines, each comprised of four process units that perform the air-flush, frit-check and neck-dip operations.

Because several bulb styles are intermixed in the frit seal furnaces, the programmability of the Unimates is an essential feature of the project. The fixtures are coded so that one of several Unimate programs can be selected as each fixture arrives at the pickup position.

Interestingly, studies of these and other tasks showed that the Unimates' programmability was unnecessary in many applications. Engineers found a more cost-effective approach — use a number of simpler robots, rather than one high-performance robot working at its peak capacity. All these projects require well-coordinated teamwork by engineering and manufacturing personnel.

Future trends

Engineers are studying other tasks, some of them requiring new technology. Since robots are handling a variety of different-sized products, we must find a positive-identification technique.

Removing a tube from a fixture and placing it on a moving conveyor is an easy task for today's robots. But when a human places a tube on a conveyor, the tube's attitude is uncontrolled. Getting the robot to pick the tube off the conveyor is a challenging problem in computer-aided vision. This is one of the tasks being studied in the Robotics Laboratory at DSRC.

A number of laboratories are studying vision-assisted robotics. Many of these use a vision module developed by SRI International. It scans a backlit object and computes characteristics from the data, such as perimeter length, center of gravity, and maximum and minimum dimensions. These can be used in recognition and manipulation algorithms. Other ap-



Members of DSRC's robotics laboratory. The Unimate 600 is used to conduct an exercise in handling deflection yoke parts. At the Unimate computer/controller are **M. Herman** (left) and **M. Martinez**. Looking on (left to right) are **S. Noto**, **D. Yang** and **H. Baird**. On the tripod is the CCD camera for the SRI image analyzer used to recognize parts.

proaches use "structured light" to get data on the surface profile of objects. Structured light means that the light illuminating an object has a structure which helps define the object. A camera will see a sphere, illuminated by structured, parallel planes of light, as a series of concentric rings which can be interpreted by a computer. Structured light is useful for high-speed measurement of human body contours. And work is progressing to use structured light with robots that will then recognize parts in a bin.

Westinghouse has a project to assemble fractional horsepower motors using vision-assisted robots. A significant aid in assembly tasks is the remote center-of-compliance hand, developed by the Draper Laboratory at MIT, which enables a robot to quickly insert a pin in a close-fitting

hole. The hand contains linkages which redirect the frictional forces (these might cause a pin to bind as it is put into a close-fitting hole) to align the pin with the hole so it slides in. Since the clearances are only a few thousandths of an inch in many cases, and the robot's margin for error is greater, a "search and jiggle" approach would be needed without the Draper hand.

The use of intelligent robots will spread rapidly during the next decade. They are widely perceived as being one of the key factors in Japan's current high productivity, and in the projected survival of U.S. industry.

Acknowledgments

Many people participated in the projects described above, especially D. Ranlet,

Manager, Industrial Engineering and Standards, and E. Gronka, Manager, Equipment Development of PTD in Scranton, who "took the plunge" and started robot applications in RCA. W.R. Kelly, of Lancaster Equipment Development, has had overall systems responsibility in guiding the PTD projects.

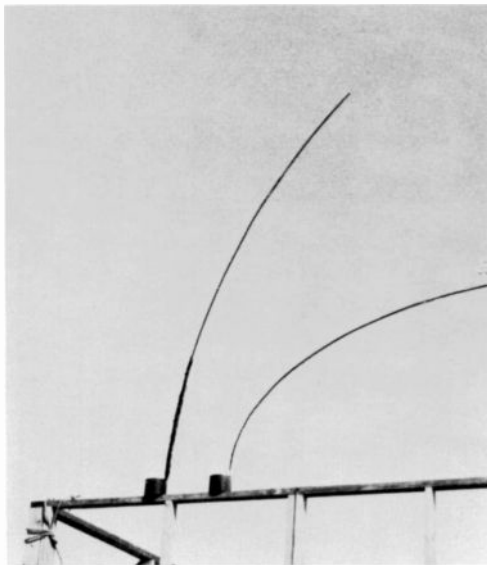


Mike Carrell is a Member of Technical Staff, Manufacturing Systems and Process Control, RCA Laboratories, Princeton, New Jersey. He joined RCA in 1949 and did design and development work on acoustical transducers, magnetic recording devices, and military keyboards and printers. He joined the Graphic Systems Division in 1965, where he was active in product planning and systems engineering. In 1973 he joined the RCA Manufacturing Staff at Cherry Hill, where he worked on computer-based data-collection systems for picture tube and VideoDisc production. For the last three years he has consulted with the Picture Tube Division in its mechanization programs, which use industrial robots.

Contact him at:
RCA Laboratories
Princeton, N.J.
TACNET: 226-2083

Advanced composite structures for satellite systems

Advanced space systems demand complex structures requirements. New and ingenious structures concepts using advanced composites are meeting these demands.



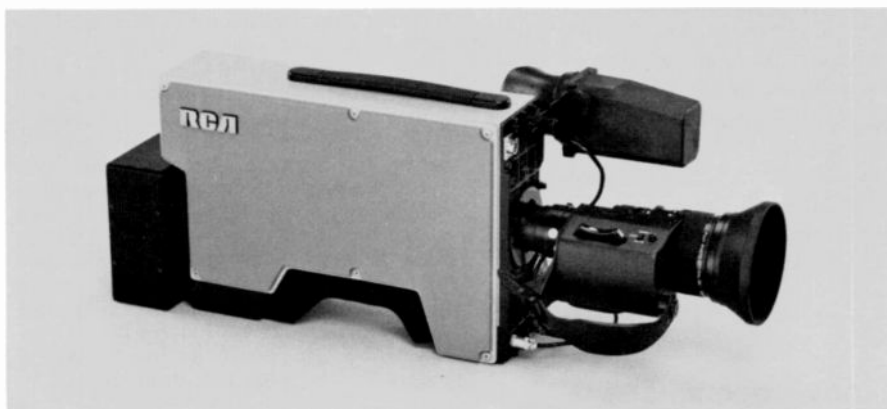
1 (a)

Abstract: *The author explains what advanced composites are, outlines their unique characteristics, and gives the "what and why" of their applications to advanced satellite systems, including types of composites, composite fabrication and structures design.*

Within the last two decades, structural materials technology has changed tremendously with the advent of the man-made advanced composite materials and their structures technologies. Mechanical engineers in the various divisions of RCA are taking advantage of this renaissance technology. They are developing structural products that are lighter, stiffer, stronger, more stable and cost efficient.

At RCA, the unique properties of the advanced composites are put to use in diversified products ranging from TV cameras to spacecraft hardware (Fig. 1). For example, Government Systems Division's Automated Systems is exploring graphite-fiber-reinforced composites to develop 8-foot-high, lightweight, expendable communications-jammer antennas. And injection-molded graphite-fiber-reinforced composite components, now under development, will reduce the weight of portable TV cameras at Government Communications Systems.

We at Government Systems Division's Astro-Electronics are at the very forefront



1 (b)

Fig. 1. At RCA, the unique properties of the advanced composites are put to use in diversified products ranging from TV cameras to spacecraft hardware. (a) GSD Automated Systems' graphite/epoxy composite expendable communications jammer antennas. (b) Portable TV camera of the Government Communications Systems which incorporates several injection-molded graphite/epoxy composite components. (c) RCA Astro-Electronics' Satcom communications satellite which employs advanced composites in a variety of components including antenna reflectors, r.f. waveguides, feedhorns and microwave filters.



1 (c)

of the leading-edge structures and materials technology. We are meeting the structural challenges of tomorrow's space missions with new and ingenious structures concepts using advanced fiber-reinforced composite materials. The following sections explain what advanced composites are, outline their unique characteristics and give the "what and why" of their applications to advanced satellite systems. You may find that composites can help you, too.

Advanced composites

Fibrous reinforcements are embedded in a suitable matrix.

Composite materials—fibrous reinforcements embedded in a suitable matrix—are as old as civilization itself. We can classify several natural materials as composites. Wood and bamboo, for example, are two natural composites that man still uses as structural materials. Man-made composites became popular when primitive societies learned to add straw to mud to make stronger adobe bricks. A more modern example of a man-made composite—reinforced concrete—combines the high tensile properties of steel with the excellent compressive but poor tensile characteristics of concrete.

Thus, a composite may be defined as a combination of two or more materials, differing in composition or form and acting synergistically, to provide properties that may not be obtained from any one of the components when used alone. One of these two components, stronger and often discontinuous, is called the reinforcement (straw, gravel, steel and so on). The second component, usually weaker but always continuous, is termed the matrix (clay, cement, and so on). The reinforcement may take any one of several forms or shapes. Thus, in a laminated composite, the reinforcement is in the form of a sheet. In particulate composites, particulate, platelet-like, or flaky materials are used as the reinforcement. In fibrous composites, the reinforcement material takes the form of continuous or discontinuous fibers. The weaker matrix material, needed to bind the reinforcements together, allows the reinforcements to perform as a unit in resisting loads. The matrix transfers the loads among the reinforcements and acts as a protecting medium for the reinforcements.

The term "advanced composites" is reserved for composite materials consisting of a special class of reinforcement systems.

These reinforcements are made up of advanced fibers whose strength to equivalent weight (specific strength) and stiffness to equivalent weight (specific modulus) are several times that of conventional materials such as steel and aluminum. Such reinforcements include several types of carbon and graphite fibers, boron fibers, filamentary glass and Kevlar® (an organic polyaramid fiber). The matrix material used in advanced composites may be one of three kinds:

- Organic matrix such as epoxy, polyimide, phenolic, polysulfone, polyester, or silicone;
- Inorganic matrix such as carbon and glass; or
- Metallic matrix such as aluminum and magnesium.

To date, epoxy resin has been the primary composite matrix for aerospace applications. Epoxies are lightweight, easily fabricated and produce high reinforcement efficiencies. Epoxies in advanced composites, in addition to their conventional roles, contribute to the shear rigidity and strength between filaments and plies (sheets of fibers and matrix making up a solid form), the transverse strength and modulus, and the determination of the maximum service temperature of the composite.

The most commonly used raw material in the building of an organic-matrix advanced-composite structure is called a "prepreg." The prepreg is a B-staged (semi-rigid and tacky) thin sheet of fiber-resin combination. The prepreg may be:

- Unidirectional tapes (the reinforcement fibers are all parallel, aligned and oriented in one direction);
- Broadgoods of fabric systems (fabric-reinforced prepregs); or
- Chopped mats (randomly or specially oriented, discontinuous, fiber-reinforced prepregs).

These prepreg materials form the building blocks in the construction of three-dimensional, advanced-composite hardware. Plies of prepregs are laid up in different orientations and shapes to meet the final performance and dimensional requirements of the structure. The laid-up forms are then rigidified by curing under suitable pressure and temperature.

Engineers use the metal-matrix and ceramic-matrix composites for special applications, for example, where the design requires high-temperature and high-

environmental stabilities. Metal-matrix composites are built essentially the same way as resin-matrix composites. The reinforcing advanced fibers, collimated and penetrated with a suitable metal alloy under predetermined temperature and pressure, yield three-dimensional solid forms. The metal-matrix can infiltrate the collimated reinforcement fibers via several methods. A common practice employed to distribute the metal matrix throughout an array of reinforcement fibers involves solid-state diffusion. In one technique, the filaments are collimated by drum-winding into a tape or filament array. After adding the matrix to the fiber array by flame spraying or by interleaving the precollimated fiber array with foils of the metal matrix, the fiber-matrix system is then compacted in a heated platen press or in a pressure vessel (hot isostatic pressing). Under very high pressure at 10 to 20 ksi (thousands of pounds per square inch) and at temperatures below the liquidus temperature of the matrix alloy, the metal creeps and forms around and between the filaments, becoming metallurgically bonded to itself and to the filaments.

Types of composites

A wide variety of composites with versatile properties are available to the designer.

Thanks to the successful development of a large number of reinforcement fibers over the last two decades, the structures designer can use a variety of composite systems with versatile properties. Most designers, although blessed with the fiberglass systems since the 1930s, recognized the systems' widespread utility as structural materials only after World War II. A wide variety of glass fibers are now available for use in composite systems. Two types of advanced, glass-reinforced composites—S-glass/epoxy and E-glass/epoxy—are widely used for aerospace structures.

A more recent introduction, an unusual organic material developed by DuPont, is sold under the trade name, Kevlar®. Kevlar is available in yarn, tow, and woven-cloth forms that are subsequently impregnated with a matrix such as epoxy during structural composite fabrication. DuPont makes two types of Kevlar reinforcements: low performance Kevlar-29 and the high performance Kevlar-49 used in aerospace applications. Kevlar-49 has about 450,000 psi tensile strength, a modulus of about 18×10^6 psi, and a density of 0.05 lb per cubic

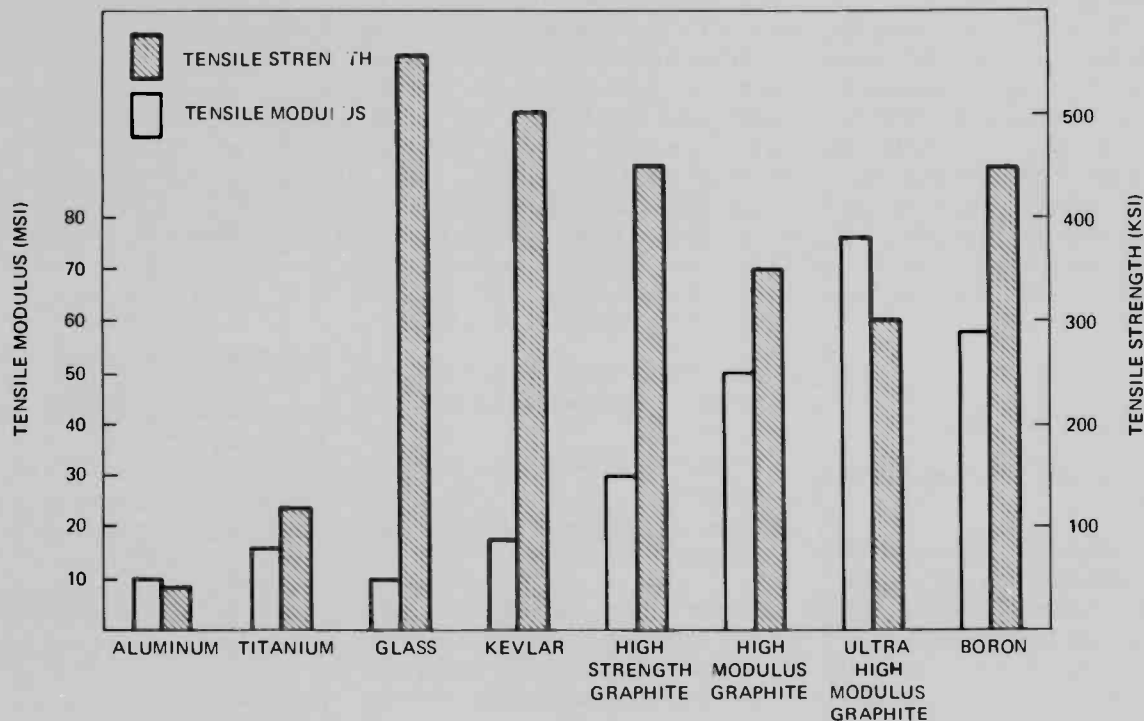


Fig. 2. Tensile modulus and strength characteristics of advanced fiber reinforcements used in composites and conventional materials. The tensile modulus (stiffness) is shown in millions of pounds per square inch (MSI) and strength in thousands of pounds per square inch (KSI).

inch. In addition, Kevlar/epoxy composites are virtually transparent to radio frequency (r.f.) signals, making them ideal for special communication system applications such as polarized antenna reflectors or dichroic (dual-frequency characteristic) subreflectors. Kevlar also has a near-zero coefficient of thermal expansion, making it an excellent candidate for thermally stable structures.

The most versatile advanced reinforcement fiber available for structural applications is the graphite fiber. Manufacturers make graphite fibers using pyrolysis of an organic precursor such as rayon or polyacrylonitrile (PAN) or, more recently, petroleum pitch. Graphite reinforcements offer a range of mechanical properties, ranging from 200,000 to 450,000 psi tensile strength, and 30,000,000 to 100,000,000 psi modulus. Unfortunately, a combination of both ultra-high strength and ultra-high modulus is not yet feasible in any given type of graphite reinforcement. Generally, as the fiber modulus increases, the fiber strength decreases.

Based on their modulus and strength behaviors, graphite fibers may be classified into three different types. The ultra-high-modulus (UHM) graphite fibers offer extremely high stiffnesses ranging from 75,000,000 to 100,000,000 psi combined with

moderate strengths of 200,000 to 300,000 psi. Celanese Company's GY-70[®] graphite fiber and Union Carbide's P75S[®] graphite fiber belong to this class. The high-modulus (HM) graphite fibers are combined with moderate stiffness (approximately 50×10^6 psi) and moderate strength (approximately 340×10^3 psi). Hercules Company's Magnamite HMS[®] graphic fiber and Union Carbide's P50S[®] are examples of this class of reinforcement fibers. The high-strength (HS) graphite fibers offer ultra-high strengths (approximately 450×10^3 psi) combined with a more moderate modulus (approximately 30×10^6 psi). Examples of HS graphite are Hercules Magnamite AS[®], Celanese Celion 3000 and 6000[®], and Union Carbide Thornel 300[®]. These different types of graphite fibers have coefficients of thermal expansion (CTE) that are nearly zero or slightly negative. By varying the type of fiber, the resin fraction, and the layup configuration, laminates or shapes can be produced with CTEs ranging from -2.3×10^{-6} in/in/ $^{\circ}$ F to 12×10^{-6} in/in/ $^{\circ}$ F. Thus, manufacturers can produce components having thermal dimensional stabilities, or components with CTE values matched to materials to which they are attached. The graphite fibers are available as twisted yarns or untwisted "tows" of 300 to 40,000

filaments each.

Another advanced fiber used as a reinforcement for advanced composites is the boron fiber. Boron filaments are produced on a substrate, usually of tungsten or very thin carbon fibers, by a chemical-vapor-deposition process. Boron fibers exhibit a modulus of approximately 55×10^6 psi combined with a strength of up to 450×10^3 psi. Even though resin matrix boron prepregs such as boron/epoxy are on the market, these are not very popular because they are difficult to handle. The extremely stiff and brittle fibers are difficult to manipulate, and the minimum radius around which they can be wrapped is relatively large. A second drawback is ply thickness, which is determined by the filament diameters and the desired fiber-volume fraction. Whereas manufacturers make graphite/epoxy and Kevlar/epoxy prepregs at 0.005-inch thickness (and up to 0.0005-inch thickness at a premium cost), the boron/epoxy prepregs are several times thicker. Optimized spacecraft require extremely thin walls and, therefore, boron/epoxy prepregs are less favorable to these applications. Also, the boron composites do not have the low CTE of graphite- or Kevlar-reinforced structures, thus limiting their suitability in space applications.

Table 1. The structural mechanical properties of fiber/epoxy advanced composites (left) surpass those of conventional materials (right).

	Fiber/Epoxies						Conventional Materials	
	Glass	Kevlar®	Graphite (GR)			Boron	Aluminum	Titanium
	E Glass/Epoxy	Kevlar-49/Epoxy	HS GR/Epoxy	HM GR/Epoxy	UHM GR/Epoxy	Boron/Epoxy		
Tensile Strength (KSI)	260	220	220	170	110	230	82	125
Tensile Modulus (MSI)	8	11	20	28	44	30	10	16
Density (lb/in ³)	0.072	0.05	0.057	0.059	0.061	0.073	0.10	0.16
Coefficient of Thermal Expansion (in/in/°F)	3.5	-2.2	-0.2	-0.3	-0.65	2.5	13	5
Thermal Conductivity (Btu/hr; ft/°F)	2	1	8	31	65	1	70	4
Raw Material Cost (\$/lb)	10	15	50	75	500	500	2	30

HS = High strength HM = High modulus UHM = Ultra-high modulus

Stiffness, strength and thermal properties

Advanced composites combine very high specific stiffness and strength with excellent thermal properties.

Figure 2 compares the stiffness and strength properties of the various types of advanced reinforcement fibers with the conventional materials. The figure readily shows that the stiffness and strength of advanced fibers are much superior to those of conventional materials. Companies are capitalizing on these superior properties of advanced fibers, by reinforcing conventional materials such as organics and metals with these fibers. In a unidirectional prepreg or a lamina, these fibers are parallel to each other in a matrix so that the fiber reinforcement represents approximately one-half the volume. The resulting properties of a unidirectional lamina, therefore, should be approximately 50 percent of the fiber properties, neglecting the properties of the matrix.

Table I and Fig. 3 compare the unidirectional lamina properties of several epoxy-matrix composites with the more conventional structural materials. Table I compares the structural mechanical properties (stiffness and strength) of advanced composites with those of conventional materials for equivalent volumes. The advantages of composites become even more evident when we compare these properties on an equivalent-

weight basis. The specific modulus (modulus/density) and the specific strength (strength/density) characteristics of advanced composites and conventional materials are compared in Fig. 3. The figure illustrates how composites can provide structural characteristics equivalent to metals at much less weight, or can have superior characteristics at equivalent size and weight. Figure 3 readily shows that the unidirectional high-modulus graphite/epoxy, for example, is five times as stiff and three-and-a-half times as strong as 7075-T6 aluminum, on an equivalent weight basis. As shown in Table I, the advanced composites also exhibit excellent thermal characteristics. Both the Kevlar/epoxy and graphite/epoxy unidirectional composites exhibit either negligible or zero coefficients of thermal expansion. This property makes these materials excellent choices for structures requiring exceptional thermal stabilities.

Composites for satellites

RCA Astro-Electronics capitalizes on the unique composite properties for satellite hardware.

The unique properties of advanced fiber-reinforced composites have made it possible to use these materials in a variety of spacecraft subsystems designed and built at RCA's Space Center (RCA Astro-Electronics). Almost every major sub-

system in a satellite can derive special advantages by the application of advanced composites in its design.

The satellites of the 1980s are designed to carry increasing payloads meant for a variety of missions. The goal is to accommodate a maximum payload at a minimum overall weight of the satellite system. This means that lightweight structures using advanced lightweight materials must be developed wherever possible. In the following paragraphs, we will review the past and ongoing applications of composite materials to the design of a variety of subsystem components for the various RCA-built satellite systems.

Advanced composites are being used in lightweight, overlapping, polarized antenna-reflector designs.

The application of advanced composites to a major spacecraft subsystem at RCA began with the Kevlar/epoxy sandwich, polarized, parabolic antenna-reflector design for Satcom I, launched in December, 1975 (Fig. 4) and Satcom II, launched in March, 1976. The Kevlar/epoxy composite has excellent specific strength and specific stiffness characteristics, but this material was selected for the antenna reflector design for two additional reasons.

As mentioned earlier, Kevlar/epoxy laminates can be designed to have a zero coefficient of expansion. This property was

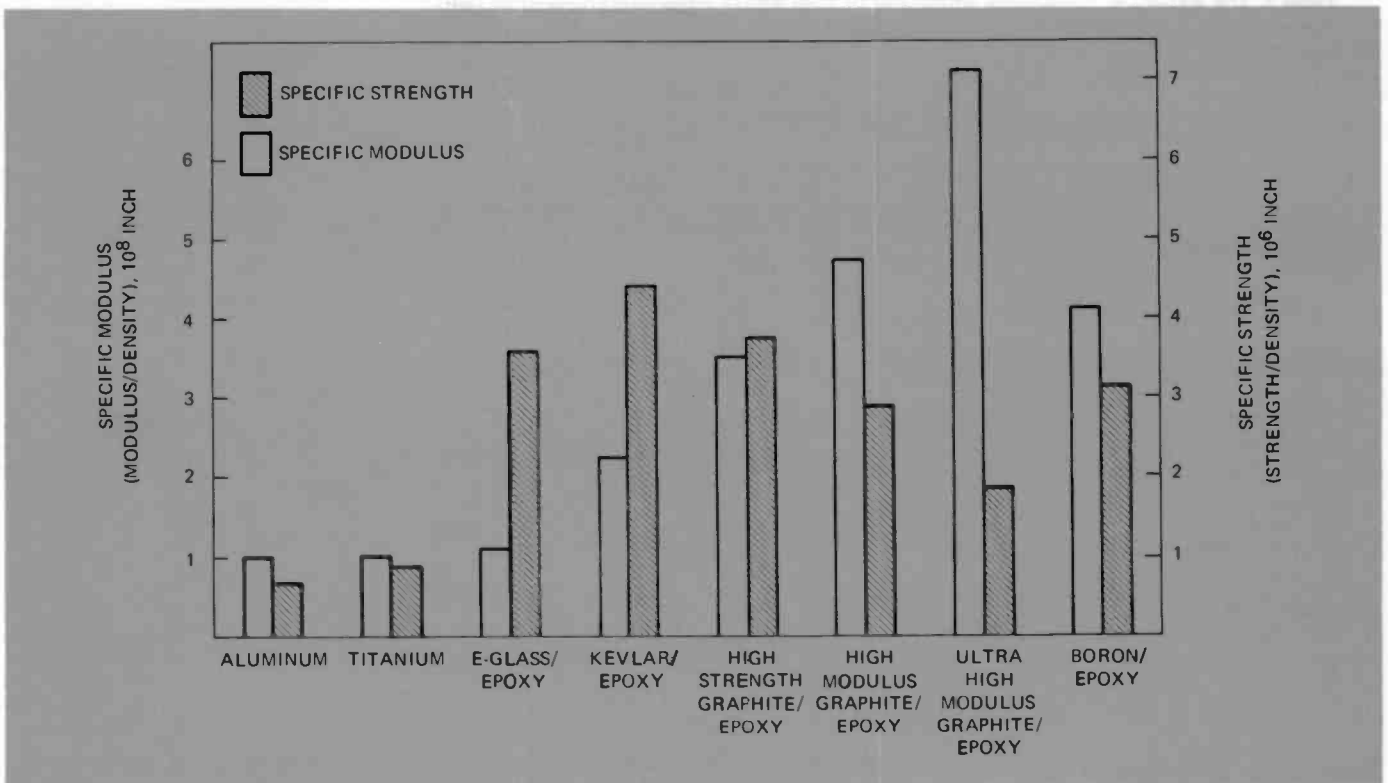


Fig. 3. The specific modulus (modulus/density) and specific strength (strength/density) of advanced composites compared with those of conventional materials. The comparison shows how composites can provide structural characteristics equivalent to metals at much less weight, or superior characteristics at equivalent size and weight.

used to provide distortion-free antenna reflectors as the temperature distribution on the reflector ranges from very cold (approximately -75°C) in shadowed regions to very hot (approximately $+75^{\circ}\text{C}$) in regions directly exposed to solar radiation during the satellite's mission. More importantly, the combined requirements — for polarization isolation, restricted volume constraint of the Delta fairing, and alignment stability — resulted in overlapping reflectors with no deployment. The two reflecting surfaces themselves consisted of grids of parallel copper wires arranged orthogonally to each other. This meant any structure used to support the reflecting grid elements should be transparent to r.f. signals. Kevlar/epoxy was found to be such a material with low-loss dielectric characteristics.

Figure 5 shows one of the two 50-inch-focal-length, 70-by-50-inch aperture, Kevlar/epoxy-composite, C-band antenna reflectors that were designed and fabricated under an IR&D program. The figure also details the Kevlar/epoxy rib structure designed to provide the stiffness and natural frequency required to meet the mission's static and dynamic loads. Each of these reflectors weighs less than 4.5 lb.

These reflectors have been extensively tested for their electrical and mechanical performances for the purpose of developing antenna structures that will meet the

future communications-payloads requirements. The knowledge gained from the design, development and testing of these IR&D reflectors is being applied to



Fig. 4. Kevlar/epoxy antenna reflector assembly of Satcom I. The assembly consisted of an embedded photo-etched polarizing grid structure, making each reflector segment transparent to r.f. energy of one polarization and reflective to energy of the opposite polarization. Similar Kevlar/epoxy composite designs were used for RCA-built ANIK-B satellite reflectors.

the design and fabrication of much larger (94-in x 68-in) antenna reflectors for Satcom F. These reflectors combine the unique properties of Kevlar/epoxy materials with ingenious structures designs to meet the more drastic requirements of ultra-lightweight structures with the ultra-high stiffness, natural frequency, tolerance and stability requirements of the next generation of communications payloads.

Advanced composite feed towers, waveguides, and feedhorns take advantage of the high specific stiffness and strength properties of graphite/epoxy.

In the communications systems area, graphite/epoxy designs that use the high specific stiffness and strength properties have been developed for lightweight feed towers, waveguides and feedhorns. Figure 6 shows examples of straight and ridged waveguides, E-bends, H-bends, and feedhorns that have been designed and fabricated out of graphite/epoxy materials. These structures are coated with special multilayer metallic films which protect the graphite/epoxy from deleterious moisture penetration and provide r.f.-conductive interior surfaces. Similar designs were used for the tower and feed systems of the Satcom I and Satcom II communications satellites, shown in Fig. 7.

Lightweight, thermally stable multiplex microwave filters have been built out of graphite/epoxy.

Invar® (Carpenter Steel Co.) is the common material used to make multiplex microwave filters needed for communications satellites. Although this material meets the frequency stability requirements for the microwave cavities, Invar filters result in a serious weight penalty, even with thin-walled designs. Graphite/epoxy technology has satisfied the requirements for lightweight, thermally stable multiplex microwave filters for communications satellites. RCA has developed a special forming and plating process for graphite/epoxy filters which provides well-adhering and smooth metallic layers, ensuring low r.f. losses. Figure 8 shows the graphite/epoxy multiplex microwave filters used on the Satcom I and Satcom II.

Graphite/epoxy designs meet the difficult weight, alignment, stiffness and strength requirements of precision mounting platforms (PMP).

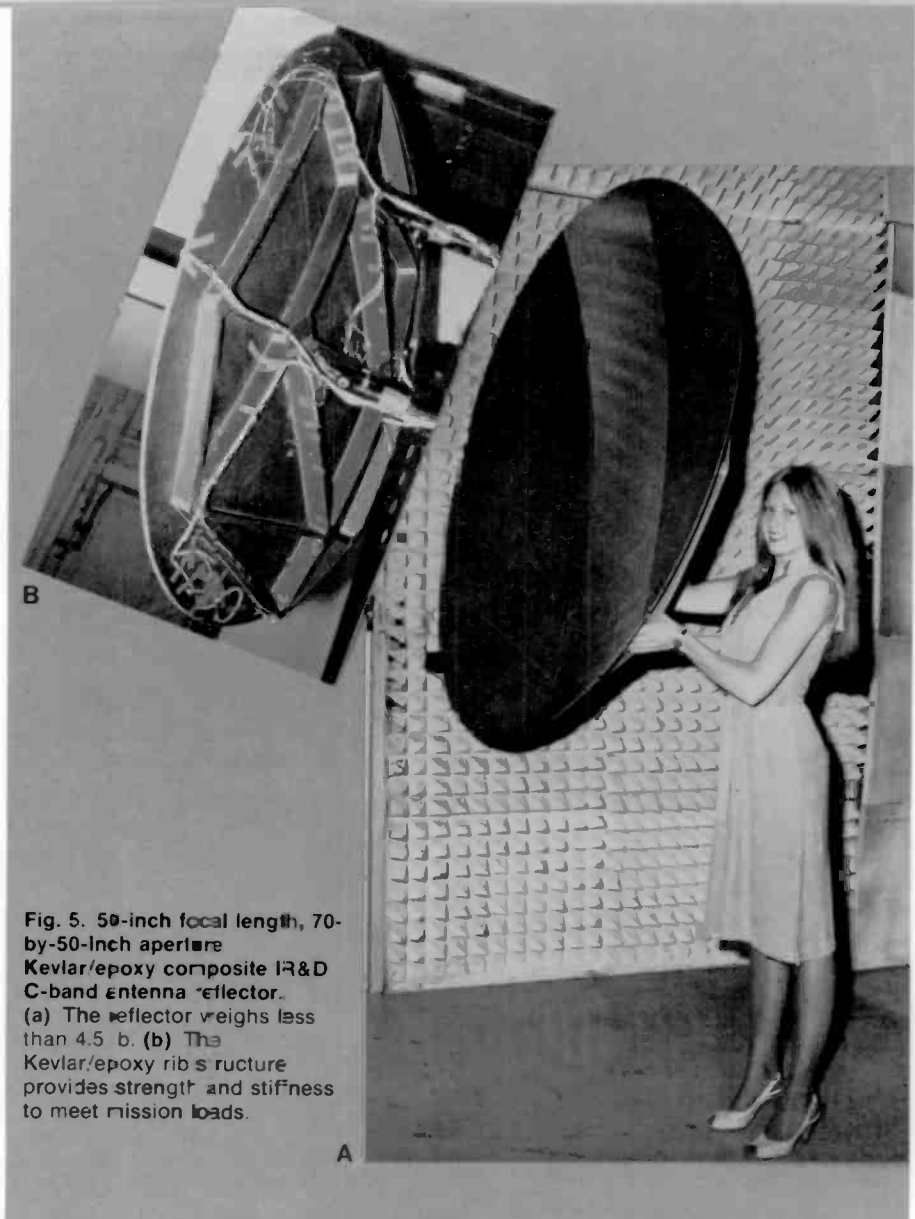


Fig. 5. 50-inch focal length, 70-by-50-inch aperture Kevlar/epoxy composite I&D C-band antenna reflector. (a) The reflector weighs less than 4.5 lb. (b) The Kevlar/epoxy rib structure provides strength and stiffness to meet mission loads.

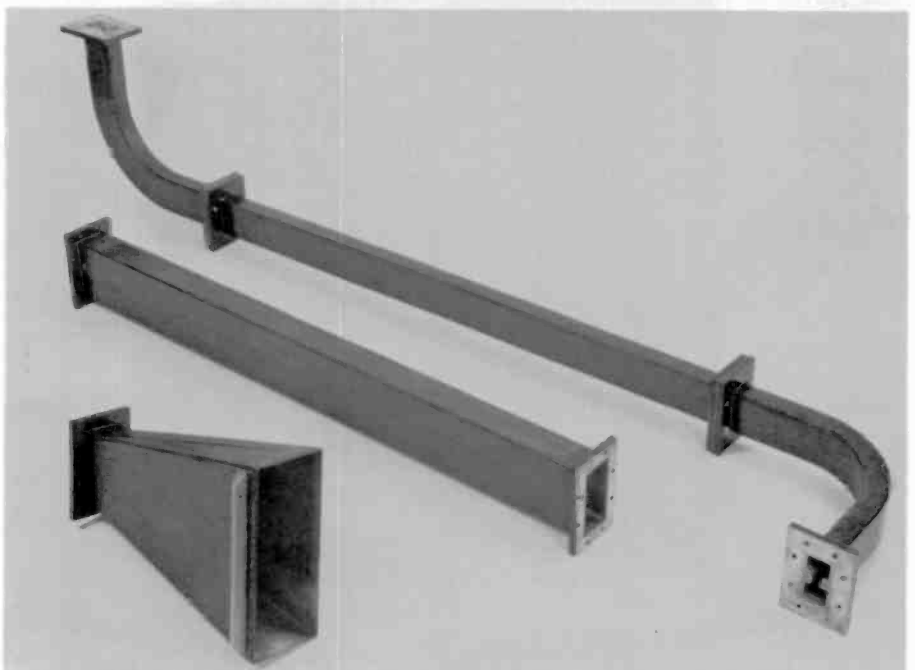


Fig. 6. Graphite/epoxy r.f. waveguides, which include straight and ridged waveguides, E-bends, H-bends and feedhorns.

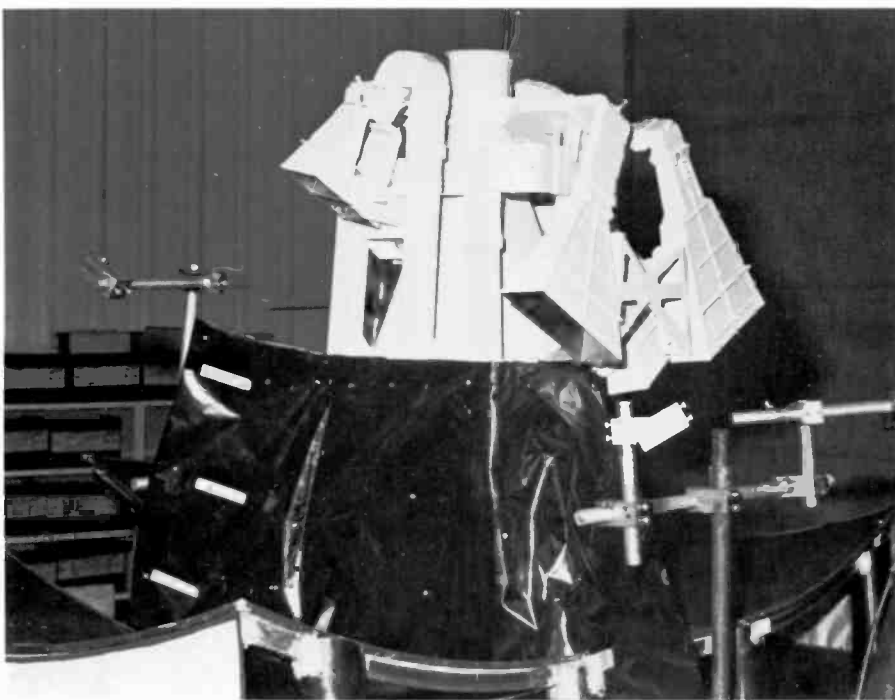


Fig. 7. Graphite/epoxy tower and feed system of Satcom communications satellite.

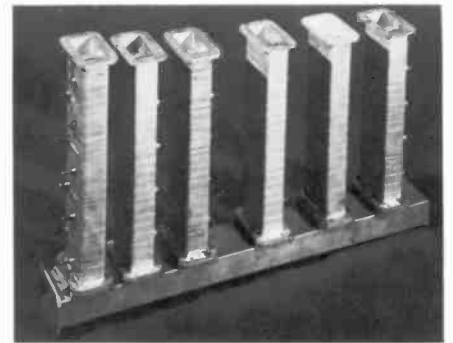


Fig. 8. Graphite/epoxy multiplex microwave filters used on Satcom I.

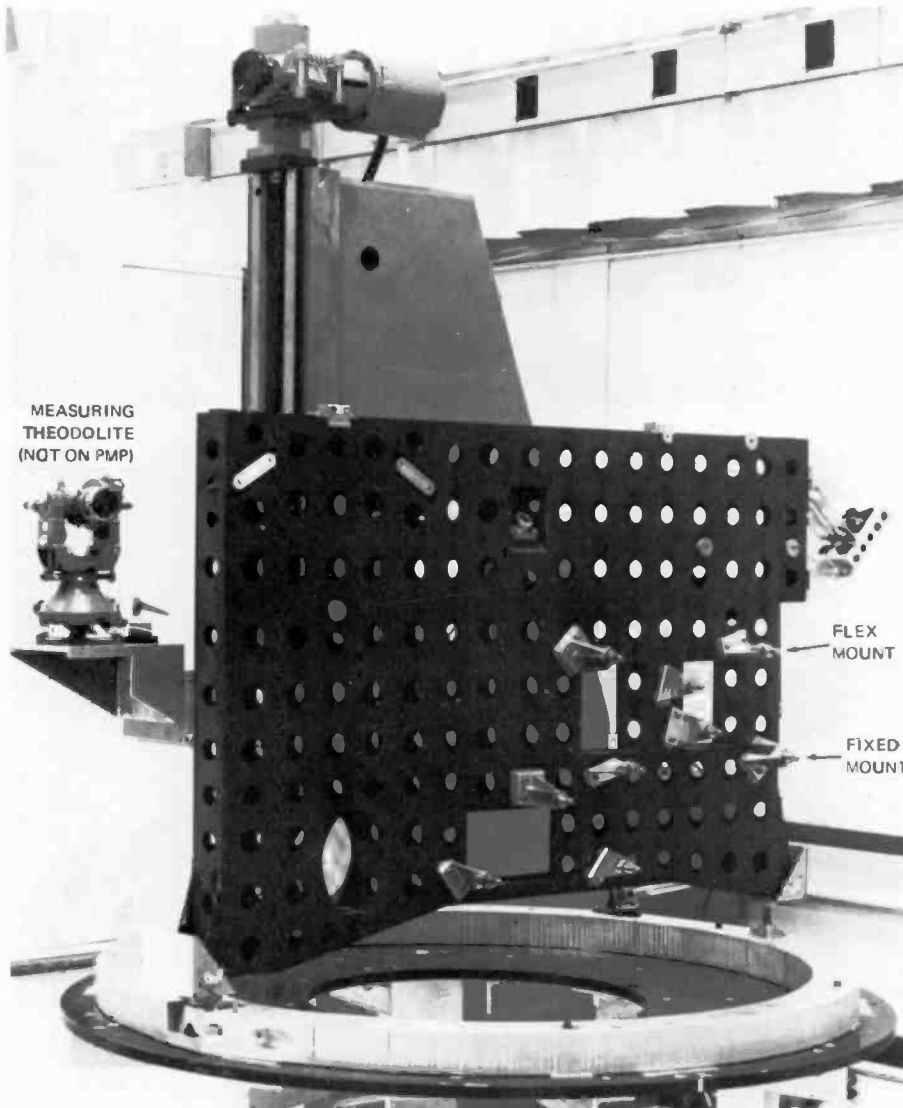


Fig. 9. Advanced graphite/epoxy composite design of the Precision Mounting Platform (PMP) developed for the Air Force DMSP weather satellite.

Figure 9 shows an advanced composite design of a precision mounting platform for the Air Force Defense Meteorological Satellite Program (DMSP) Weather Satellite. The PMP supports several instruments that must be precisely aligned at assembly and remain aligned in space. The conventional design employs a dip-brazed-aluminum structure. The aluminum structure needs to be maintained at a constant temperature to avoid any thermal distortion and, hence, misalignment during the spacecraft's mission. Moreover, the aluminum design is heavy and is limited in its stiffness, strength and natural frequency capabilities. The graphite/epoxy PMP design, shown in Fig. 9, and its improved versions under development promise to alleviate these drawbacks of aluminum and meet the stringent pointing accuracy requirements of future space missions.

RCA Astro-Electronics' composites team is exploring ultra-lightweight, thermally stable composite designs for solar panel substrates on future satellite systems.

With increasing payloads, satellite sizes and mission lives, the power requirements of future satellites are going to be enormous. This will lead to solar panels that are very large, stiff and stable under the mission's mechanical, thermal and other radiation environments. In order to meet these future power systems requirements, RCA Astro-Electronics' composites team has developed several novel designs using the high specific-stiffness-and-strength and low coefficient-of-thermal-expansion properties of graphite/epoxy and Kevlar/epoxy composites. One such design is portrayed in Fig. 10.

More efficient satellite systems will be made from new advanced composites designs.

New advanced composites designs under development will lead to lightweight, ther-



Fig. 10. An advanced composite design of the solar panel substrate.

mally stable satellite structural subsystems that will more efficiently meet the mission requirements of supporting and maintaining the relative locations of components under the mission's mechanical, thermal and other radiation load environments.

A spacecraft structural subsystem has several functions. It primarily provides adequate strength and stiffness to support and maintain the relative locations of components. Secondary functions include providing thermal paths for heat conduction, grounding electronic equipment, shielding equipment from space radiation and protecting against potential thermoelastic and dynamic instabilities. The major constraints on the structure are weight and stability. Historically, aluminum has been the primary material for spacecraft construction. But the limitations of aluminum in terms of weight, stiffness, strength and thermal stability have provided us high incentives to design and develop advanced composites — especially graphite/epoxy — structures for structural subsystems. Figure 11 is an example of such an advanced composite structural subsystem development at RCA. The figure illustrates an advanced composite truss structure for the dual launching of two OSCAR satellites stacked

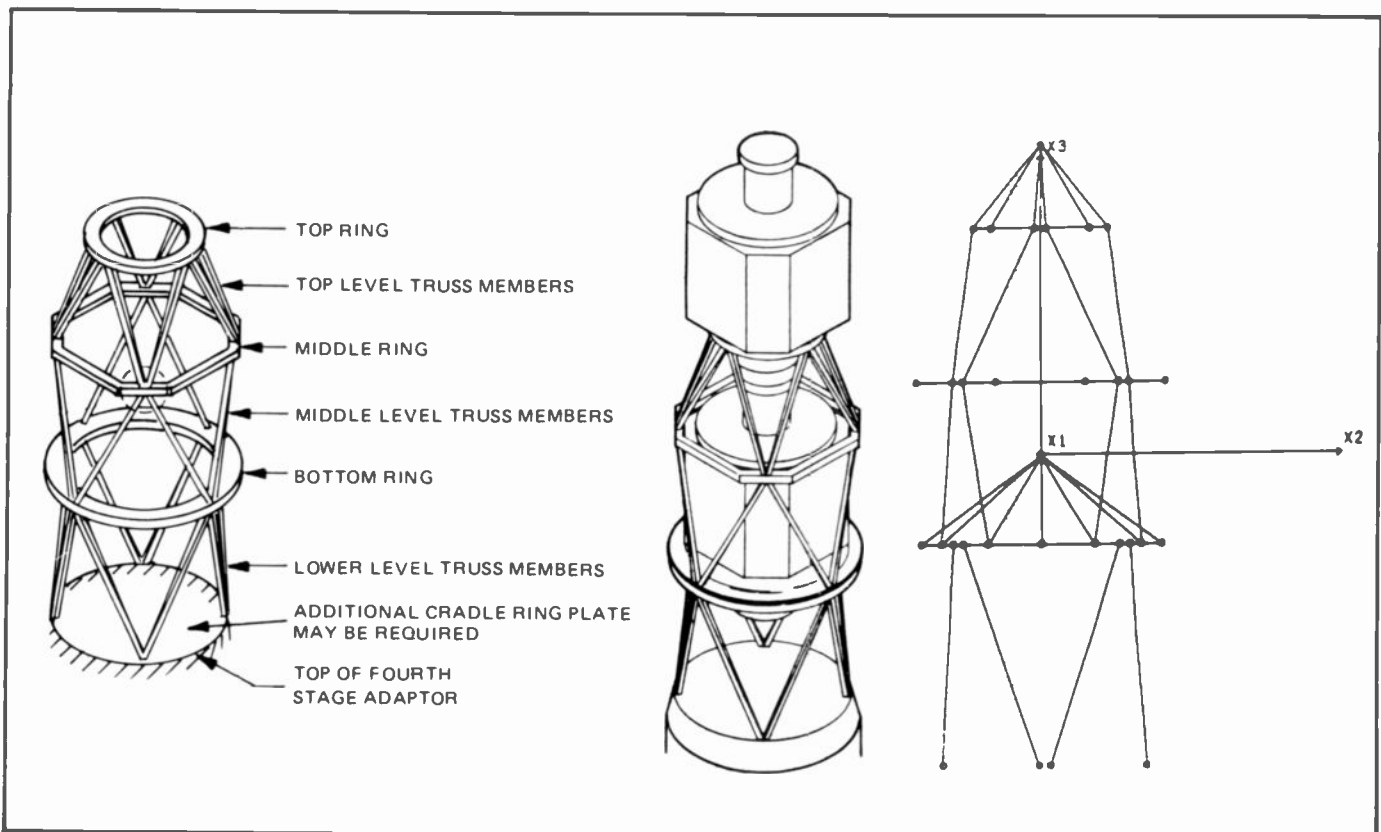


Fig. 11. An advanced composite cradle design for the tandem launching of satellites.

Table II. Arrows show how various constraints (top) characterize laminate performance (bottom).

<i>Elastic Constants</i>	<i>Strength Constants</i>	<i>Physical Constants</i>
Longitudinal Modulus, E_x , (MSI)	Longitudinal Tensile Strength, X , (KSI)	Density, δ , (lb/inch ³)
Transverse Modulus, E_y , (MSI)	Transverse Tensile Strength, Y , (KSI)	Longitudinal CTE, α_x , ($^{\circ}\text{F}^{-1}$)
Shear Modulus, E_s , (MSI)	Longitudinal Compressive Strength, X^1 , (KSI)	Transverse CTE, α_y , ($^{\circ}\text{F}^{-1}$)
Longitudinal Poisson's Ratio, ν_x	Transverse Compressive Strength, Y^1 , (KSI)	Longitudinal Thermal Conductivity, K_x , (Btu/ft/hr- $^{\circ}\text{F}$)
	Shear Strength, S , (KSI)	Transverse Thermal Conductivity, K_y , (Btu/ft/hr- $^{\circ}\text{F}$)
	Strength Ratio Coefficient, F_{xy}	Longitudinal Moisture Coefficient, β_x
		Transverse Moisture Coefficient, β_y

↓	↓	↓
Normal and Flexural Modulus and Compliance Components of Symmetric and General Laminates, Stresses, and Strains in Individual Plies and Laminates.	Strength Parameters of Laminates and Individual Plies, Margins of Safety at Any Applied Load Conditions.	Margins of Safety and Deflections at Any Environmental Condition.

on a single cradle assembly. The truss structure is designed to meet the very stringent requirements of weight, natural frequency and minimum distortion under the mechanical and thermal loads of the mission environment.

Structures design

Composite structures are designed through detailed modeling and stress analyses.

Structural components fabricated from composites are designed as multilayered laminated configurations for more effective use of unidirectional or woven composite materials. Each ply of the laminate has unique orthotropic stress-strain characteristics that contribute to the total stiffness and strength of the multi-ply laminate.

Proper design of a composite laminate structure requires detailed modeling and stress analysis of the individual laminae (plies) to completely define the overall behavior of the structure. The properties of a unidirectional ply may be obtained from the properties of the reinforcing fiber and the reinforced matrix using micromechanics techniques. The most common practice, however, is to measure the stiffness and strength properties of the unidirectional composite by simple tensile, compressive and shear tests performed by loading in directions parallel and transverse to the fiber. One needs a minimum of four different elastic constants, six different strength constants and several physical constants (see Table II) in order to analytically characterize the performance of a multi-ply, multidirectional

laminate. Special computer programs fully characterize multi-ply laminated composite structures. The analyses use linear theories, but are very complex because the number of independent parameters necessary to specify the complete structural behavior is many times greater than that needed for the usual homogeneous isotropic analyses of conventional structures.

The failure in a multi-ply laminate is defined as the onset of failure in the weakest ply in the laminate. Failure envelopes, such as the example shown in Fig. 12 for a cross-ply laminate, are developed to fully characterize the strength behaviors of a laminated composite structure. Computer programs calculate the margins of safety of any laminate orientation under any combined in-plane and out-

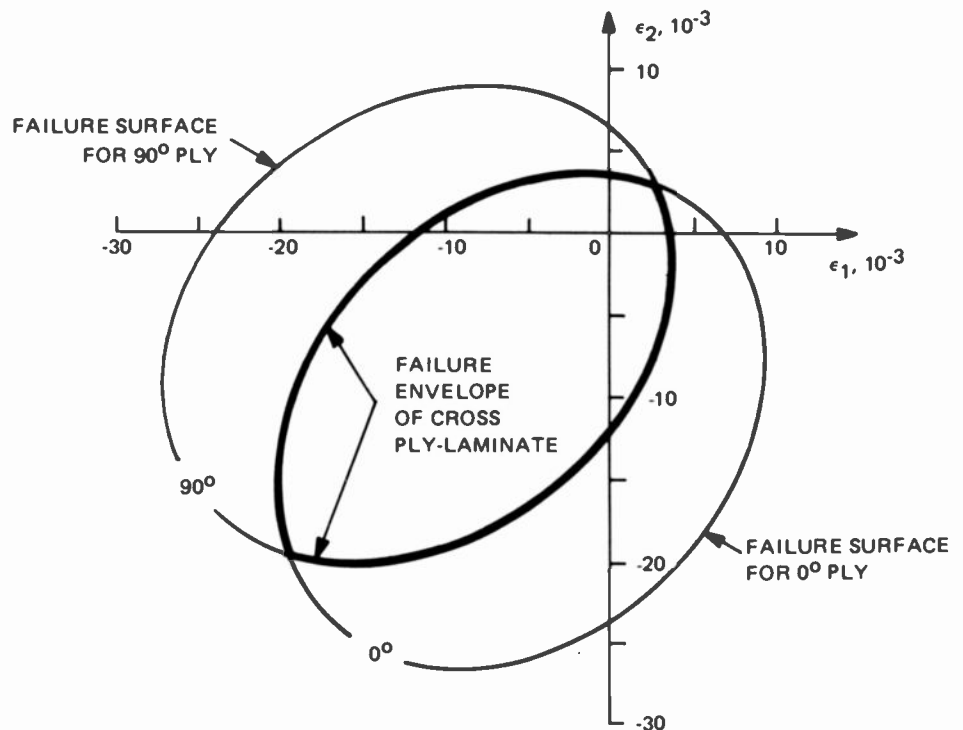


Fig. 12. Failure in a multi-ply laminate is defined as the onset of failure in the weakest ply. The figure illustrates the failure envelope for a cross-ply (0/90) graphite/epoxy laminate in the strain space at an applied shear strain of zero.

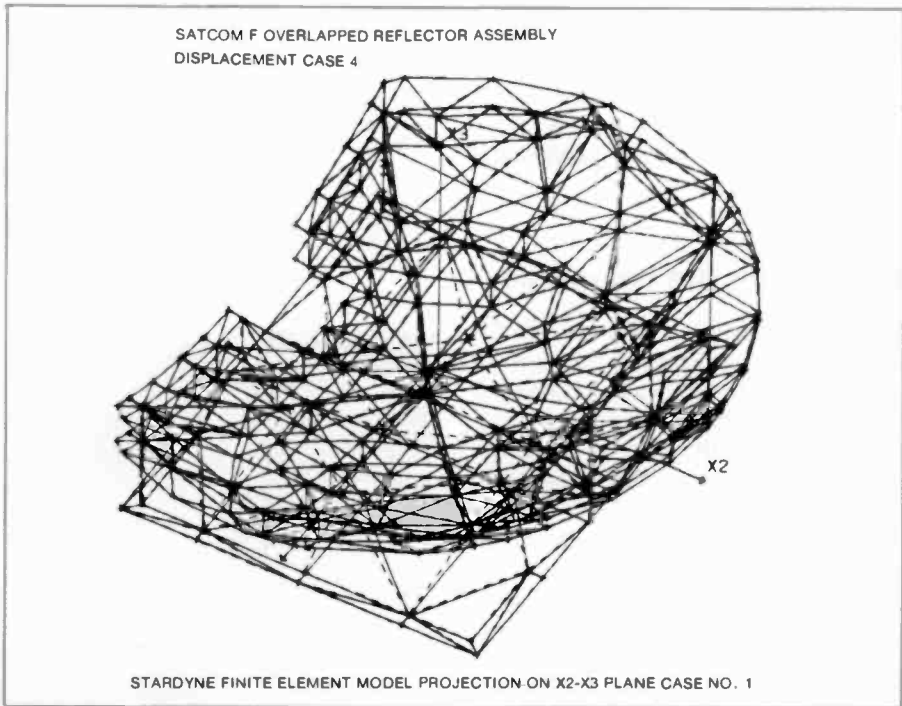


Fig. 13. Finite-element model of a fully overlapping Kevlar/epoxy antenna reflector system showing distortions under mission thermal environments.

of-plane mechanical loads as well as environmental loads such as temperature and humidity. Also, advanced finite-element modeling (Fig. 13) and analyses are extensively employed to characterize the response of complex composite structures under static, dynamic and acoustic loadings.

Specific layup patterns are used for special purposes. For example, maximum strength or stiffness for components such as beams or columns is obtained from unidirectional orientation. Quasi-isotropic properties are obtained with $(0^\circ/+45^\circ/-45^\circ/90^\circ)$, laminates and $(0^\circ/+60^\circ/-60^\circ)$, laminates. Because of the anisotropic thermal expansion behavior of individual laminae, it is necessary, in order to prevent warping due to temperature changes or during fabrication, to use laminate orientations that are symmetric about the mid-plane of symmetry of the laminate, and are balanced (equal number of plus and minus plies). For cylinders or other surfaces of revolution that cannot warp, the layup need not be symmetrical.

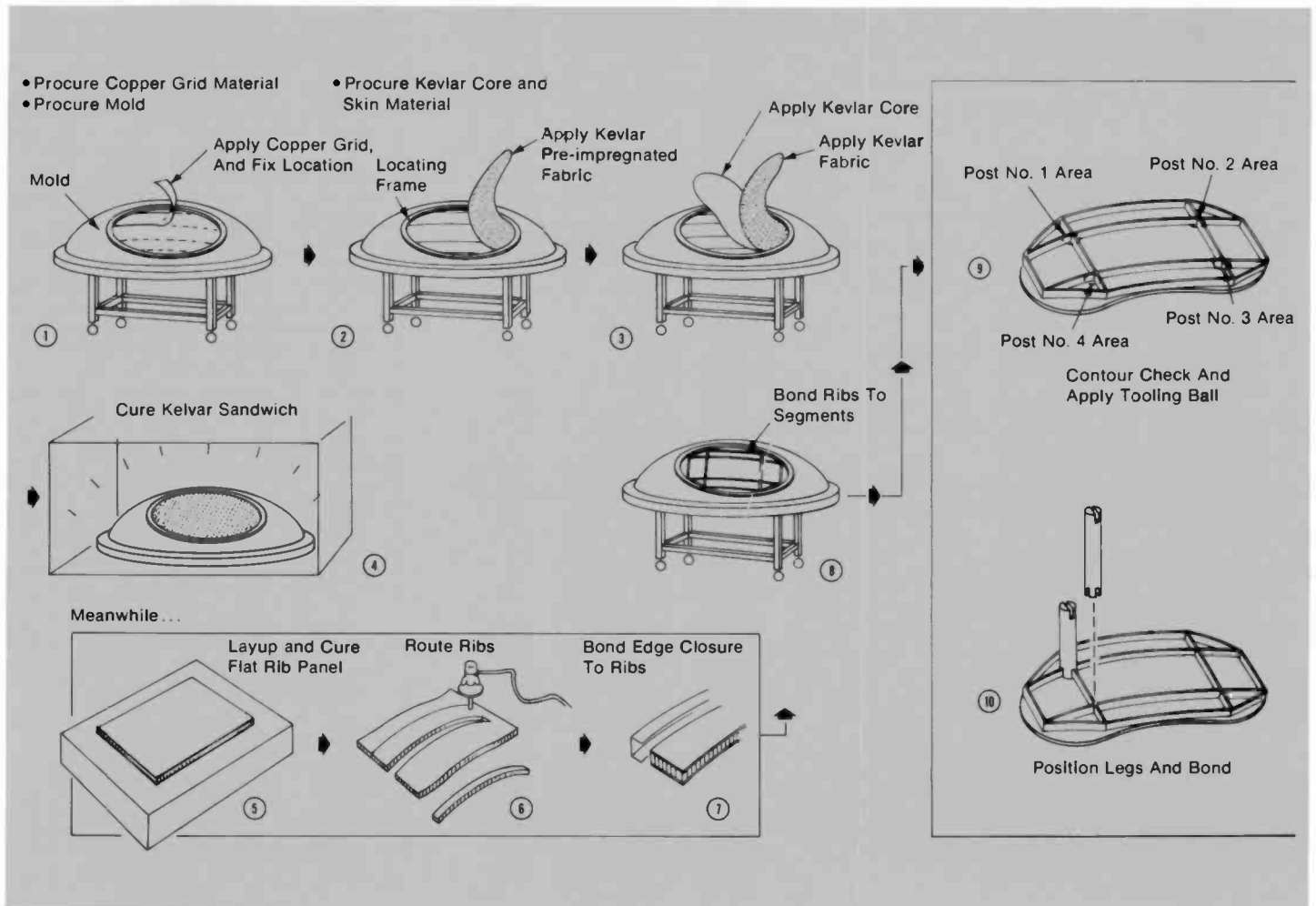


Fig. 14. Processing steps involved in the fabrication of a Kevlar/epoxy antenna reflector.

Composites fabrication

Prepreg layup and filament winding are two common techniques for composites fabrication.

As seen earlier, prepregs may be purchased in forms of unidirectional tapes or woven fabric broadgoods. The most common practice is to fabricate composite structures by laying-up thin (approximately 0.005 inch) plies of prepregs into shapes and filament orientations as dictated by the design. Plies, gores, or patterns are cut from prepreg by use of templates (or by automated cutting machines such as specially designed Gerber machines). The plies are then carefully stacked so that the individual laminae are oriented as required by the design. The next step is to compact the laminate thus assembled by simultaneous application of heat and pressure. Vacuum bagging is a common technique for thin laminates and for composite-skin honeycomb-core sandwich structures which do not require high compacting pressures. For thick laminates which require high pressures for compacting, other means of pressurizing—such as an autoclave or a hydraulic press—are employed. Fig. 14 depicts the sequence of operations involved in the fabrication of a communications antenna reflector.

Composites structures may also be fabricated starting from dry fibers by means of specialty processes. For example, structures which may be described as surfaces of revolution such as tubes, cylinders and pressure vessels can be fabricated by filament winding. In this process, dry fiber rovings are saturated by passing them through a resin bath and are then positioned over a mandrel in a helical pattern. The wound structure is then cured in an oven.

Pultrusion is another specialty technique used for fabricating simple shapes of

composite structures. In this process, bundles of continuous fibers are saturated with a suitable resin and are drawn through a die where compaction and cure are accomplished. Rods and tubes of a variety of cross-sectional shapes may be fabricated through pultrusion.

Composites are here to stay

The satellite systems of the next decade demand stringent pointing accuracies, increased payloads, compatibility with shuttle launch, the attendant weight/size constraints, ability to perform in hostile environments, and cost-efficient hardware and operation. Judicial application of advanced fiber-reinforced composites to selected satellite structures has already satisfied some of these requirements. During the 1980s an expanded total systems approach in the application of advanced composites to RCA Astro-Electronics' satellite systems will meet all of the above future mission requirements. The composites technology is evolving into a more mature and reliable technology. Composites are here to stay.

Acknowledgments

I wish to thank J. Bulinkis (RCA Government Systems Division-FCS), and M. Kurina (RCA Automated Systems) for their contributions to Fig. 1, and W. Metzger (RCA Astro-Electronics) for reviewing the paper.

Selected books on composites

1. Tsai, S.W. and Hahn, H.T., *Introduction to Composite Materials*, Technomic Publishing Co., Westport, Conn. (1980).

2. Agarwal, B.D. and Broutman, L.J., *Analysis and Performance of Fiber Composites*, John Wiley and Sons, N.Y. (1980).
3. Christensen, R.M., *Mechanics of Composite Materials*, John Wiley and Sons, N.Y. (1979).
4. Tewary, V.K., *Mechanics of Fiber Composites*, John Wiley and Sons, N.Y. (1978).
5. Jones, R.M., *Mechanics of Composite Materials*, Scripta Book Company, Washington, D.C. (1975).
6. Garg, S.K., Svalbonas, V. and Gurtman, G.A., *Analysis of Structural Composite Materials*, Marcel Dekker, Inc., N.Y. (1973).



Raj Gounder, Manager, Composite Materials, RCA Astro-Electronics, is responsible for advanced structures design and development, advanced structures analysis and testing, and advanced materials and fabrication technologies required for future satellite missions. At RCA, Dr. Gounder has led the mechanical design of an antenna subsystem for future communications missions and other lightweight structures technology developments including composite solar panel substrates and structural subsystems required for stacked launching of satellites. Before joining RCA in July 1979, he led the application of composite materials to helicopter hardware at Sikorsky Aircraft, Stratford, Connecticut.

Contact him at:
RCA Astro-Electronics
Princeton, N.J.
TACNET: 229-3108

Predicting the acoustic response of the 5D-2 satellite

A special acoustics test program evaluates the impact to the satellite of a larger and noisier launch vehicle.

Abstract: *This paper describes a special acoustics test program designed to safely test a nearly completed spacecraft — via analytical and statistical tools — for acoustic levels higher than those normally encountered on the Thor Delta launch vehicle.*

The regular sequence of environmental testing for spacecraft built at RCA Astro-Electronics includes an acoustics test. The test demonstrates the ability of a spacecraft to withstand the acoustic vibration environment imposed on it during launch and trans-sonic flight. In conducting such a test, engineers place an all-up flight-configuration spacecraft in an acoustic test facility and subject it to an intense sound field that is intended to excite a random vibration environment throughout the structure.

With respect to large panels and equipment mounted on them, this environmental test is the most severe that the spacecraft must withstand. Sound-pressure levels produced during the test may exceed 150 dB, a level far above the human threshold of pain. To survive such levels, some electronic components must be designed to withstand vibration accelerations in excess of 20 times that of gravity.

The first of a series of new Air Force 5D-2 meteorological satellites is shown in Fig. 1. This satellite was designed to be launched on a Thor Delta launch vehicle and under normal qualification procedures would, therefore, be subjected to an acoustic test based on the Thor Delta

acoustic environment. As the buildup of this satellite neared completion, however, the Air Force requested that RCA assess the impact to the satellite of an increased acoustics test level in order to accommodate a larger and noisier launch vehicle and an increased payload. As a result of this request, RCA undertook a special acoustics test program to evaluate the impact of changing the acoustic specification to the proposed higher levels.

Test program

The special test program required careful planning since the test article was a flight spacecraft, near completion, worth many millions of dollars.

Figure 2 is a flowchart of the special acoustics test program. The first step of the program involved making an analytical prediction of the vibration responses of the spacecraft to the Delta acoustic specification. In parallel with this analysis, we performed an actual test in the lab, where we subjected the spacecraft to the Delta acoustic test levels and measured the vibration responses. The predicted and measured responses were then compared in order to ascertain the accuracy of the analytical modeling techniques.

Next, using the same analytical tools developed in the first step, the vibration responses of the spacecraft to the proposed new, higher acoustic test levels were predicted. With these results, it was possible to assess the impact of the proposed new acoustic specification and determine whether or not the resulting vibration responses would be excessive for the spacecraft, its substructures, or components.

Finally, based on this assessment, the okay was given to test the spacecraft to the new proposed acoustic test levels.

The test configuration, as sketched in Fig. 3, consisted of the entire spacecraft and second stage, including solar panels. Only one solar panel is shown for clarity — eight panels were included in the test and are shown in Fig. 1. To give an idea of the size of the satellite, some dimensions are given.

The entire spacecraft was instrumented with forty accelerometers and nine strain gages. The transducers were concentrated primarily on the large surface areas — that is, the equipment-support-module (ESM) panels, the solar panels, the precision-mounting platform (PMP), and on sensitive components.

During the acoustics tests, the vibration responses were recorded on magnetic tape in analog form. The responses were then later used to calculate the power spectral densities (g^2/Hz) and overall responses (grms) for comparison with analytical results.

The acoustic test facility shown in Fig. 1 is typical of those used throughout the

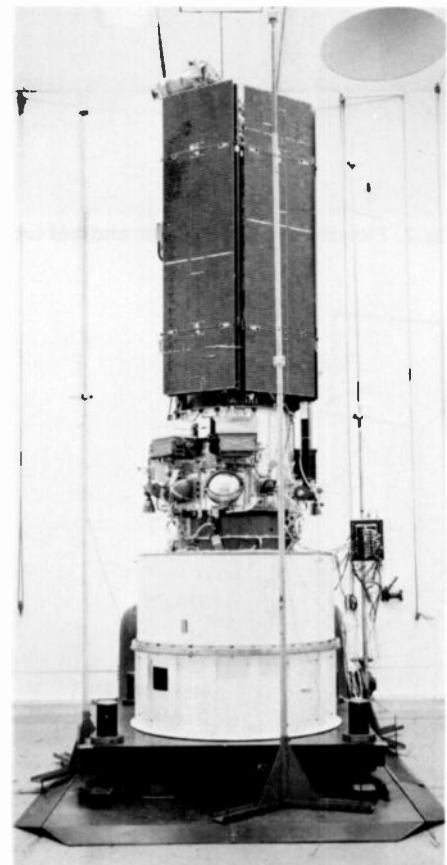


Fig. 1. Air Force 5D-2 meteorological satellite in its acoustic test configuration, mounted in the acoustic test facility at RCA Astro-Electronics.

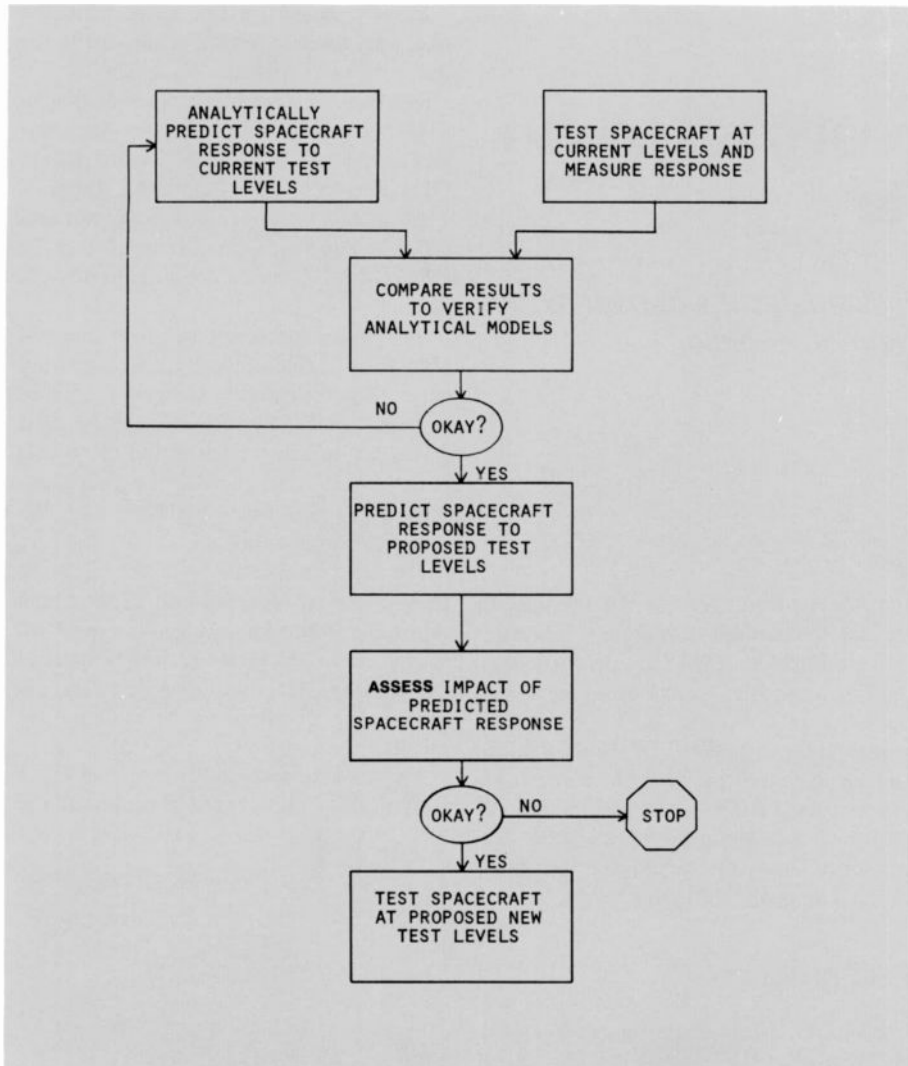


Fig. 2. Flowchart depicting logic and test sequences for the special acoustics test program.

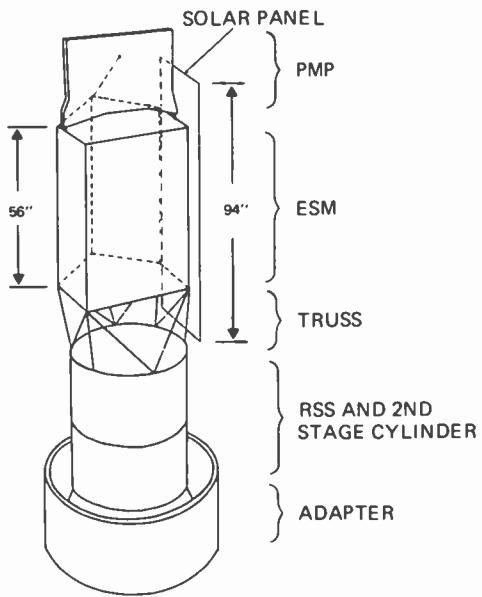


Fig. 3. Sketch of the 5D-2 satellite's acoustic test configuration; one solar panel is shown for clarity—eight were mounted for the test.

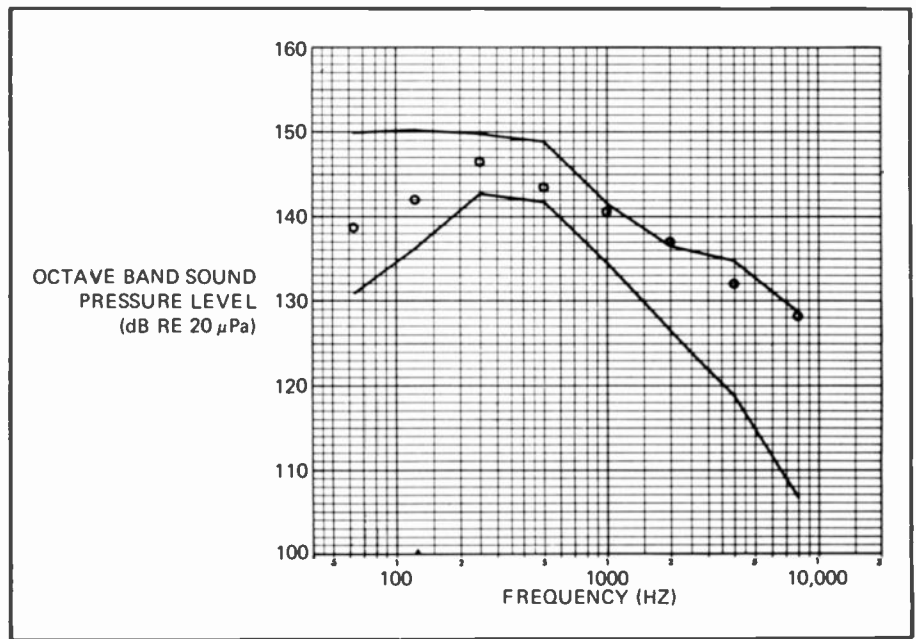


Fig. 4. Measured test levels shown in comparison with the tolerance bounds of the proposed acoustic test specification.

industry for simulating the acoustic environment mentioned above. It consists of a 280 m³ (10,000 ft³) reverberation room located in the environmental test area at the RCA Space Center in Princeton, New Jersey. The room is uniquely constructed from reinforced steel plate and enclosed by an outer steel shell. Excitation is provided by letting cooled nitrogen gas expand through a modulator and chopper which are coupled to the room through a folded, fiberglass exponential horn. An array of six microphones is used to measure the sound-pressure levels in the room.

The acoustic test follows a standardized approach. The complex acoustic excitation environment seen by the satellite is approximated in the form of a shaped, random noise field impinging on the satellite from all angles of incidence. This condition is approximated in the reverberation room where, ideally, the sound field has uniform energy density and equal probability of energy flow in all directions.

Test levels

The acoustic environment is generally specified in the form of a frequency spectrum shape and level, along with allowable tolerance bounds above and below the specified spectrum shape; the frequency spectrum is defined in one-octave bandwidths. The actual test environment

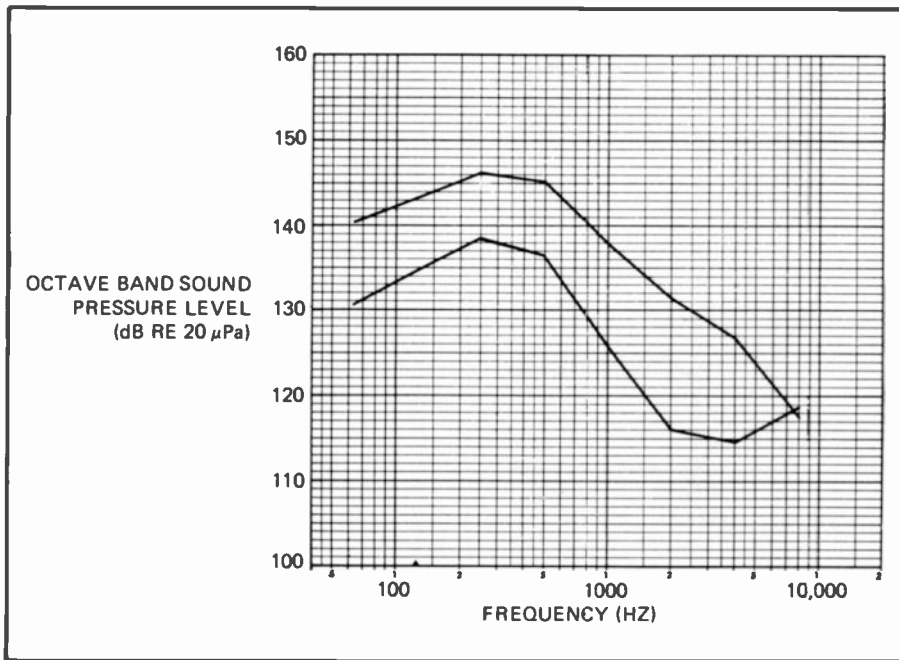


Fig. 5. Proposed (upper curve) and current (lower curve) acoustic test specifications.

may deviate from the specified spectrum shape to the extent permitted within the tolerance bound limits. The tolerance bounds allow for uncertainties and practical limitations of the various acoustic test facilities in use throughout the aerospace testing industry. Figure 4 shows the measured test levels in comparison with the tolerance limits associated with the proposed acoustic test specification.

In most cases, the spacecraft is tested without the shroud, and the insertion loss due to the shroud has been accounted for in the test specification.

The two spectra of octave-band sound-pressure levels shown in Fig. 5 represent the current Delta acoustic specification and the new proposed acoustic specification. The lower curve has an overall sound-pressure level of 141.4 dB re 20 micro-Pascals. The upper proposed curve has a different shape and an overall level of 150.8 dB, 9.4 dB above the current specification.

Finite-element analysis

Finite-element models (FEMs) were constructed for three large flat panels (Fig. 3)—the ESM front panel, an ESM side panel, and a solar panel. The computer-generated display of one of the models shown in Fig. 6 is an example.

The models were formatted for use with the STARDYNE Structural Analysis Program. They were developed specifically for the case of random acoustic loadings. The grid size, therefore, was small enough to adequately support the physical

mechanisms for acoustic excitation of plates, up to 800 Hz. The models used sandwich triangular plate elements to represent the honeycomb panel materials, and beam elements to represent the stiffening members. The components which were mounted on the ESM were modeled by stiff beams connecting each component mounting foot to a mass point concentrated at the component center of gravity. The boundary conditions for the models of ESM panels 1 and 5 were simply supported around the entire perimeter. The solar-

panel model was simply supported at six node points.

Modal analysis was performed on the finite-element models using the STARDYNE Lanczos method. The analysis was restricted to extracting up to 50 natural frequencies and mode shapes in the frequency range up to 800 Hz.

The STARDYNE DYNRE3 program was used to solve for the response of the structural models subjected to stationary random acoustic loading. The execution of the DYNRE3 program requires the results of the modal analysis, as well as specific information describing the acoustic excitation.

The analysis of the dynamic response (DYNRE3) for each model was divided into three separate cases, corresponding to three contiguous frequency ranges of the excitation, which are centered on the panel's critical frequency. The critical frequency is defined as the frequency at which the panel's bending wavelength equals the wavelength of the acoustic excitation, and is a function of the panel's mechanical properties, dimensions, and the speed of sound in air. The three frequency ranges correspond to three distinct mechanisms of random acoustic interaction with a finite panel; it is because of program limitations that each mechanism of acoustic interaction is handled individually, thus producing three computed responses for each panel. At any point on a given panel, the overall response from the three cases is the root of the sum of the squares of the responses from each frequency range.

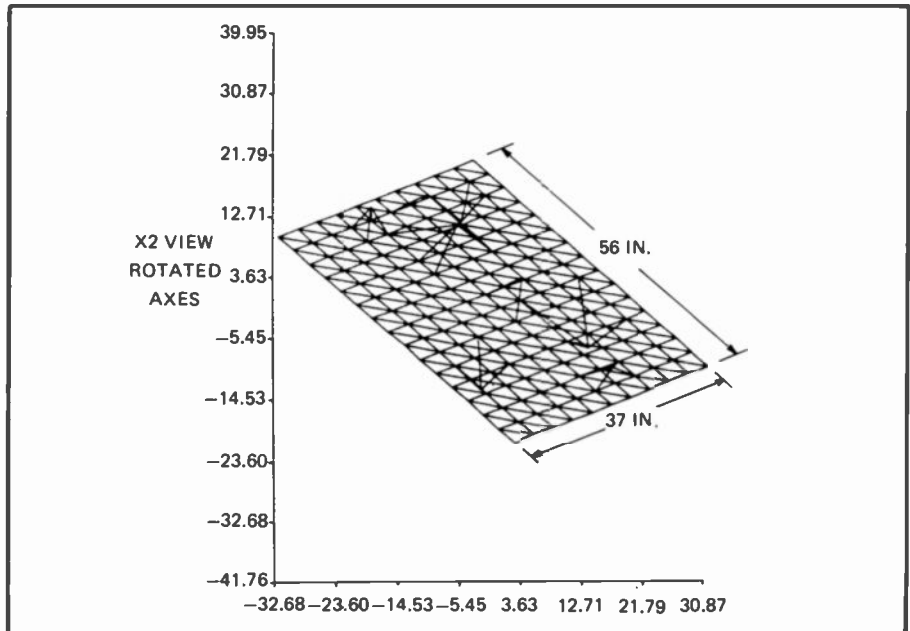


Fig. 6. Computer-generated display of the finite-element grid modeling the ESM front panel and the components mounted on the panel.

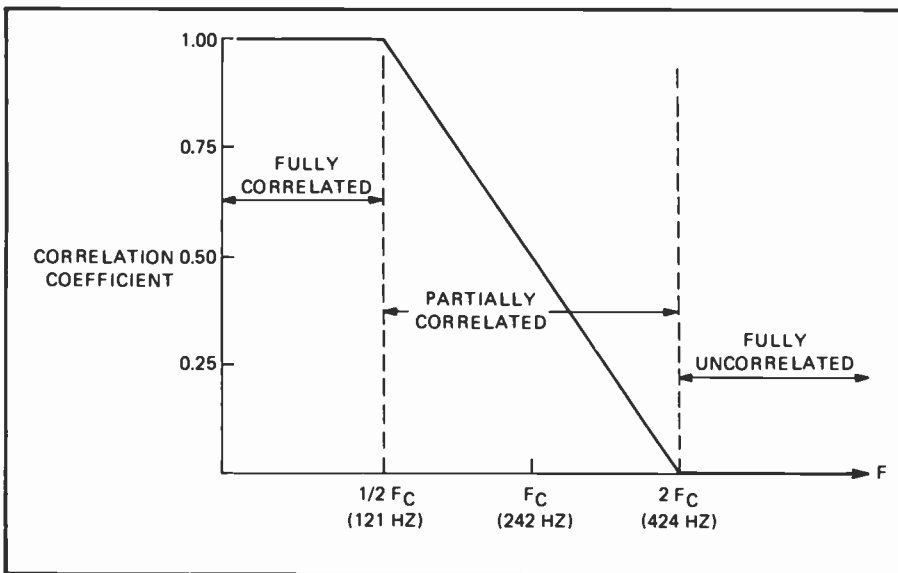


Fig. 7. Curve approximating the correlation of the incident excitation between any two points on the surface of the ESM front panel.

The three mechanisms for acoustic excitation of panels are a function of the statistical properties of the pressure distribution across the panel. In the lower frequency range, the wavelength is large compared to the panel bending wavelength and the phase of the pressure acting on the panel is fully correlated over the entire surface. In the mid-frequency range near the panel's critical frequency, the excitation wavelengths are comparable to the panel bending wavelength, and the degree of correlation between the pressures at any two points on the panel is dependent upon frequency and the distance of separation. In the upper frequency range, the wavelength of the excitation is small compared to the panel bending wavelength and the pressure fluctuations are, therefore, fully uncorrelated over the panel.

Figure 7 shows how the degree of cor-

relation of the incident acoustic excitation between any two nodes on the surface of the panel has been modeled as a function of frequency in the mid-frequency range.

For each model, the DYNRE 3 program was instructed to compute the overall maximum acceleration at every node point, beam end loads, and tri-plate stresses. In addition, the power spectral density (PSD g^2/Hz) of the acceleration response was computed at selected nodes. The PSD responses were computed at the approximate locations of actual accelerometer mountings, thus permitting direct comparison between results of test and analysis.

Figure 8 shows a representative computer-generated PSD curve for a location near the center of the ESM front panel, at the mounting foot of an electronics box. This plot was generated in

three parts corresponding to the three discrete frequency ranges of analysis discussed earlier.

Each part unfortunately has a different horizontal and vertical scale; nevertheless, the primary frequencies of response and their relative amplitude can be read from the curve and can be compared to the corresponding measured frequency response curve. The model identifies the fundamental panel mode at 50 Hz, and two large-amplitude complex modes on either side of 200 Hz. Also, note that less significant modes appear near 320, 400, 500, and 700 Hz.

The computed overall acceleration responses (grms) at locations common to test measurement locations are given in Table I — Column 1 for the current Delta acoustic loads and Column 2 for the new proposed acoustic specification. These overall responses are essentially equal to the areas under the respective computed PSD curves.

Test results

The measured narrowband response at the same location near the center of the ESM front panel is shown in Fig. 9. The computed curve of Fig. 8 has been overlaid onto the measured PSD curve for purposes of direct comparison also. The significant measured modes are seen to occur at 50 Hz, on either side of 200 Hz, just below 500 Hz, and at 750 Hz, and on a narrowband basis the computed response follows the measured response quite well, with all modes represented. The structure's first panel mode appears to be more highly damped than was expected from the analysis, but for the higher modes, the 3-percent damping used in the model seems to be accurate. Computed response amplitudes are seen to be slightly low in the 80- and 100-Hz bands and high in the 400- and 500-Hz bands. Due to the nature of the normal mode analysis in the regions of low modal density, the sharp anti-resonances account for the discrepancy between measured and computed overall responses as seen in the numbers entered in Table I. Measured and calculated responses at representative locations on the ESM side panel and solar panel yield results comparable to those shown for the ESM front panel.

Table I summarizes the overall responses, both calculated and measured, at both levels of acoustic excitation for several ESM front panel response locations. The overall difference between

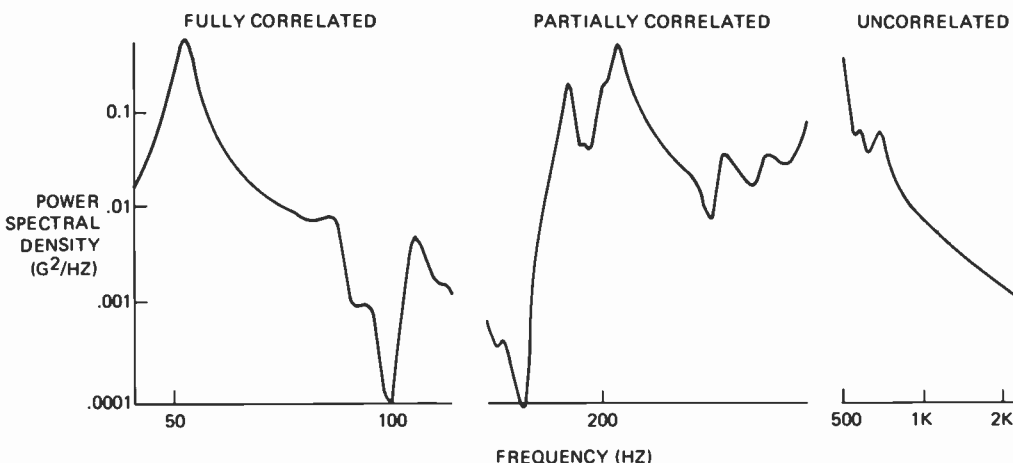


Fig. 8. Computer-generated curve of the analytically derived power spectral density (PSD) acceleration response near the center of the ESM front panel.

Table 1. Summary of selected responses, both calculated and measured, at selected locations on the ESM front panel, for the current and proposed acoustic test levels.

Measurement Location	Calculated FEM Overall Response (rms)		Measured Overall Response (rms)	
	Current Test Level	Proposed Test Level	Current Test Level	Proposed Test Level
A-101X (grms)	0.7	1.8	2.0	6.3
A-102X	1.3	3.4	3.0	5.0
A-103X	0.9	2.5	1.3	3.5
A-104X	1.4	3.6	1.8	7.5
A-105X	1.6	4.1	1.9	5.2
SG-7 ($\mu\epsilon$ rms)	13.6	41.7	10.0	28.0
SG-8	1.7	5.0	7.0	20.0

the two levels of acoustic excitation was 9.4 dB. For identical spectrum shapes and linear systems, 9.4 dB corresponds to a factor of almost three in the rms acceleration responses. From inspection of the numbers in the table, the computed responses at the two levels of excitation are related by a factor of three and for the measured responses this is seen to be generally true also. In a similar manner for the narrowband PSD response, which has the units of power, a 9.4 dB increase in the excitation sound-pressure level results in a factor of almost nine in the PSD responses.

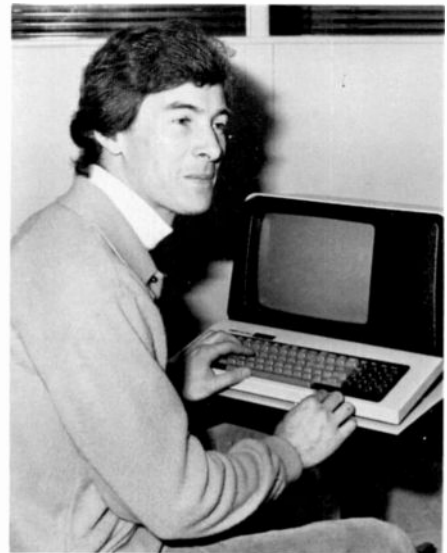
Based on these relationships, it was possible to make engineering estimates of

the responses at various locations on the spacecraft before the high-level test was actually performed. With the estimated spacecraft responses, from the ESM panels and solar panel, and with the corresponding results from response measurements on other areas of the spacecraft, good assurance was given that the spacecraft structure and components could withstand a test at the higher proposed noise levels.

The higher-level test was then performed on the spacecraft; some corresponding responses are included in the last column of Table 1, and these numbers fall within the range of expected results.

Conclusion

In conclusion, this paper covers the reasons for a special acoustics test and the development of an analytical tool which consistently handles a problem, the engineering solution of which is by no means straightforward. In addition, current work in several related areas, for improving the normal-mode analysis method, as well as an investigation into the statistical energy analysis approach, will assure better correlation between the results of analysis and test in the future.



Carl Voorhees is Senior Member of the Technical Staff in the Mechanical Engineering Department at RCA Astro-Electronics, where he is involved in mechanical analysis and structural test. He joined RCA in 1978 with a background in acoustic analysis and measurements from the National Bureau of Standards. Current assignments include work as co-principal investigator of a structural modal testing IR&D program, and on the measurement of spacecraft dynamic properties. He has published or presented nine technical papers, received an RCA Engineering Excellence Award for his contribution to the modal test of the 5D-2 spacecraft, and is a member of the Acoustical Society of America and the American Society of Mechanical Engineers.

Contact him at:
RCA Astro-Electronics
Princeton, N.J.
TACNET: 229-2265

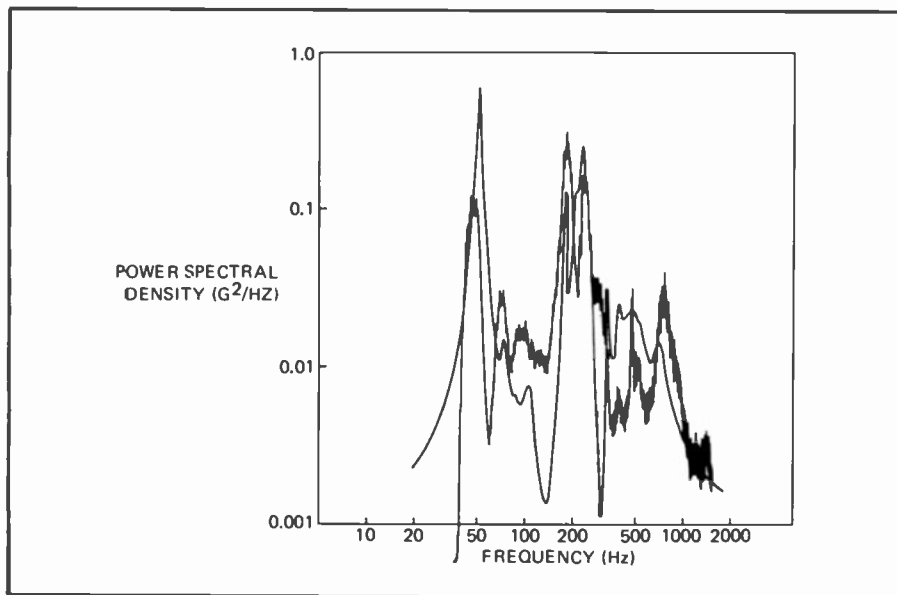


Fig. 9. Analytically derived acceleration response shown in comparison with the measured response at location 105X near the center of the ESM front panel.

A modal vibration test of the 5D-2 satellite

This basic modal test technique is available for application to other satellites, too.

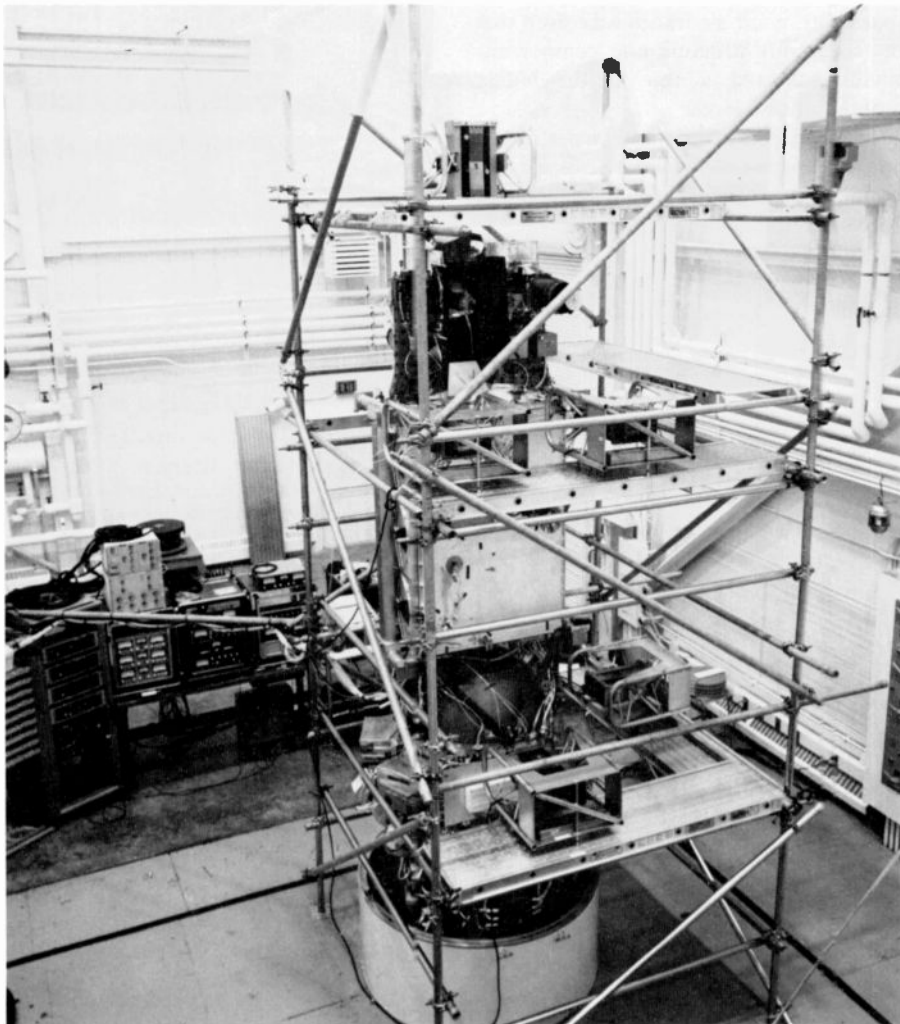


Fig. 1. Defense Meteorological Satellite Program Block 5D-2 spacecraft mounted and instrumented for modal test.

Reprint RE-26-4-5
Final manuscript received Sept. 13, 1980.

Abstract: *The modal test of the 5D-2 satellite efficiently and reliably determines resonant frequencies, mode shapes, and damping properties of satellites developed at RCA Astro-Electronics, using multiple-shaker sine-dwell testing.*

Engineers at RCA Astro-Electronics successfully completed a modal test of Block 5D-2 spacecraft S6 on May 25, 1979. The test created a dynamic model of the spacecraft directly from experimental measurements. The experimental measurements of resonant frequencies, mode shapes, and damping, together with a mass model which is separately derived from weight and dimensional measurements, define the spacecraft dynamic model. The model is necessary for an accurate loads analysis in order to predict spacecraft and launch vehicle loads during lift-off and boost. The procedure used in the test was the multiple-point-excitation, sine-dwell technique required by the task assignment. To give technical assurance of success and to provide accurate, reliable data, RCA used Structural Dynamics Research Corporation (SDRC) as a technical consultant with responsibility for performing the test and for the data recording and data processing.

The successful completion of this test through the coordinated effort of RCA, the Air Force, the Aerospace Corporation, and SDRC not only produced results which satisfied the specific purpose, but also led to the development of new techniques for conducting a multiple-shaker-

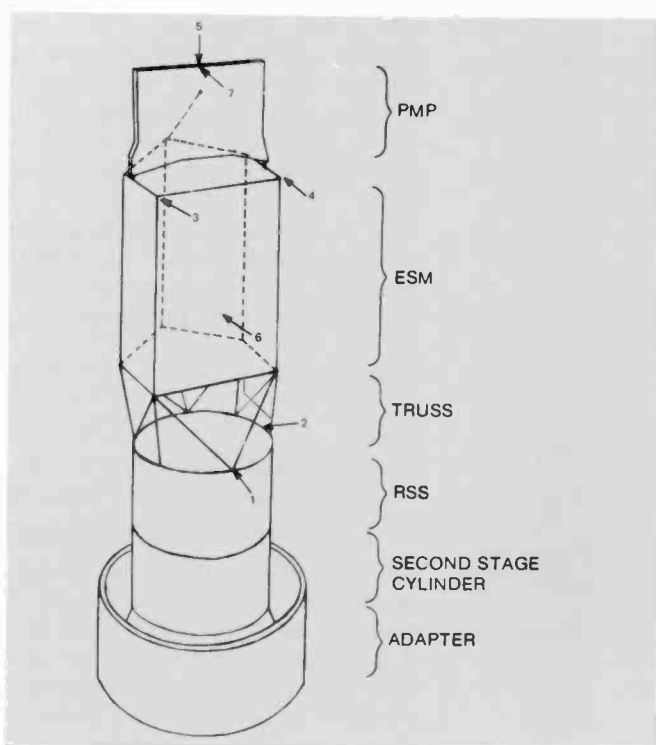


Fig. 2. Exciter locations for the 5D-2 modal test.

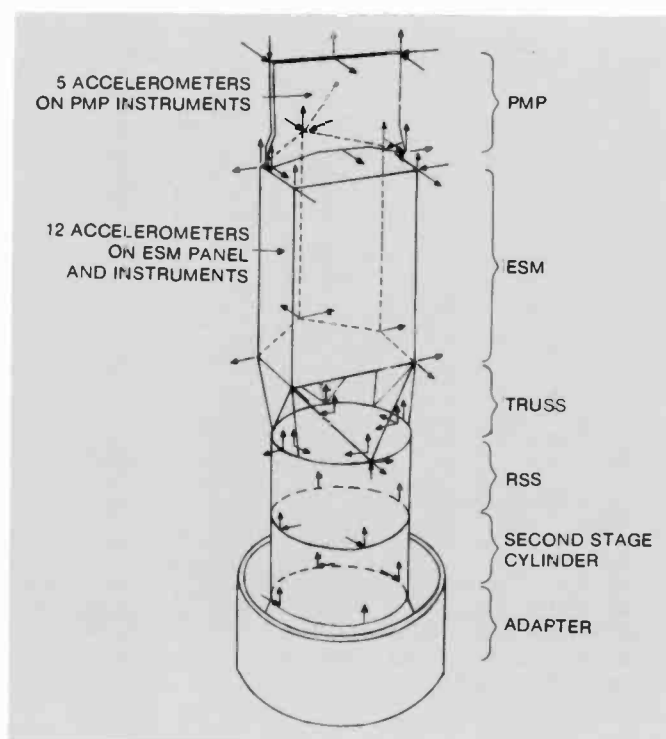


Fig. 3. Accelerometer locations for the 5D-2 modal test.

excitation sine-dwell modal test. Finally, it enabled RCA to develop a technological skill which can now be applied to future programs.

Test setup

The spacecraft used in the test was the first Block 5D-2 configuration built by RCA for the Defense Meteorological Satellite Program (DMSP). The spacecraft was rigidly mounted at its base to a 200-ton seismic block located in the RCA Astro-Electronics' Quad Cluster Room. Figure 1 shows the general setup of the test. Scaffolding, built on the block, completely enclosed the spacecraft. It provided a versatile and flexible means for supporting the shakers, and provided access to all parts of the Integrated Spacecraft System (ISS) during the test. Moving a shaker to a different location on the structure simply involved raising the shaker from the deck via the ceiling crane and either changing the position of the scaffolding deck or placing the shaker onto another deck at the new location.

Seven shaker locations were used during the course of the modal test to excite the spacecraft structure. No more than three shakers were used simultaneously to excite any particular mode of the spacecraft. Figure 2 shows the locations of the shakers. Attachments of the shaker armatures to the spacecraft driving points were ac-

complished with flexures (stingers)-devices specially designed by RCA Astro-Electronics for transmitting purely axial forces to the structure. The flexures reduced the need for precise shaker alignment and eliminated the introduction of bending moments into the force gauges.

Seventy-six accelerometers attached to the spacecraft were used to measure mode shapes. Figure 3 shows the mounting locations of the accelerometers. Data from these transducers was processed by a mini-computer utilizing SDRC software.

The electronic gear setup, visible in Fig. 1, is shown in detail in Fig. 4. A schematic of this equipment is shown in Fig. 5.

Test procedure and results

The test procedure was divided into the following main phases:

- Single exciter sine-sweeps (modal search).
- Multiple exciter mode tuning.
- Multiple exciter sine-dwell (mode survey).
- Data processing.

Force and acceleration data were acquired and stored by the computer during the single exciter sine-sweep phase and during the multiple exciter sine-dwell phase.

The initial exciter locations for the modal search phase of the test were

determined based on the predicted mode shapes from the analytical computer model of the spacecraft. There are a total of five initial exciter locations, that is, positions 1 to 5 in Fig. 2. A single exciter sine sweep was performed between 0 to 55 Hz using one of these five initial exciter locations. The other exciters remained disconnected during this sweep. The frequency response functions (FRF) between the driving point acceleration and force were calculated and the resonant frequencies of the spacecraft were determined from the peaks in the FRF plots. Figure 6 shows the driving point FRF from exciter locations 1 and 2. By inspection of the FRF from all five initial exciter locations, nine modes below 50 Hz were identified to be the structural modes of the spacecraft.

After the resonant frequencies of interest were identified, short, single-exciter sine sweeps were performed for each mode. Responses from the driving point accelerometer and 15 additional well-spaced accelerometers were recorded for each mode. "Coarse" mode shapes were computed and used to calculate the number of shakers, the shaker locations, the force pattern and the relative phasing of the exciters for each mode to be excited.

For a particular mode to be excited, those shakers used for that mode were connected and the force levels and phases adjusted. The sweep oscillator was taken out of the dwell mode and the excitation

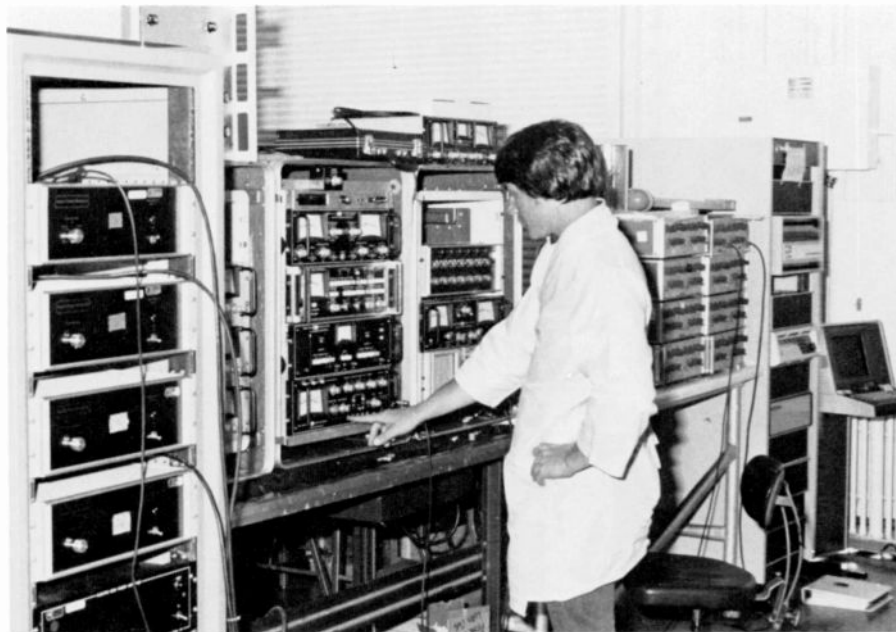


Fig. 4. Electronic equipment for controlling the modal test (center) and for data processing (extreme left and right).

frequency was set to a value of slightly below the frequency of the tuned mode. Using the linear sweep setting, the sweep oscillator swept the exciters through the peak of the mode to a frequency slightly above the resonant frequency. Acceleration and force data from each of the driving points were simultaneously acquired by the data acquisition system. The data were

processed to determine the acceleration/master-force functions. These functions were viewed in the Nyquist plane. The Nyquist plot of a well-tuned mode forms a circle emanating from the origin, symmetric about the imaginary axis. A vector from the origin tracing the low of the point on the circle is maximum at the 90° phase point. This condition is equivalent to peaking quadrature and to having the response 90° out of phase with the master force.

Additional acceleration data (ten channels selected from various locations on the spacecraft) were acquired through the same sweeping operation and the same force signals. The Nyquist circles associated with the acceleration/master-force functions were inspected to further verify a properly tuned mode. Figure 7 shows a typical Nyquist plot from mode No. 1.

If Nyquist plots indicated that the mode was not purely tuned, responses at the resonant frequency from each driving point were recorded and used to calculate the revised force pattern for tuning the mode. The mode tuning phase described above was then repeated.

Once the mode had been tuned, the acceleration data for all of the 76 accelerometers was acquired by dwelling at the resonant peak. The proper force amplitudes were set and controlled through a force feedback loop so that resonance occurred under invariant conditions. The frequency response between the master force and each acceleration

signal was calculated. The mode coefficients were determined from the quadrature values of the measured acceleration response at the resonant frequency. This maximum quadrature point occurs at 90° phase angle for a purely tuned mode.

The measured eigenvectors were transformed to equivalent values at 120 given mass points on the structure using a transformation matrix as follows:

$$[\phi] = [R][U] \quad (1)$$

where

[U] = measured eigenvectors (76 x 1)

[R] = transformation matrix (120 x 76)

[φ] = transformed eigenvectors (120 x 1)

This transformation is necessary for defining the complete mode shape of the spacecraft and for the orthogonality check of the measured modes. Once the complete mode shape coefficients were obtained, an animated mode shape was displayed. Figure 8 shows the mode shape display for the first bending mode of the spacecraft.

The modal damping coefficient is derived from the frequencies of the maximum (ω_a) and minimum (ω_b) coincident (CO) response at each mode. Assuming equivalent viscous damping, the modal damping coefficient ξ_i for mode i is obtained by:

$$\xi_i = \frac{1}{2} \frac{(\omega_a/\omega_b)_i^2 - 1}{(\omega_a/\omega_b)_i^2 + 1} \quad (2)$$

The CO plot from the master shaker on each mode is used for the calculation. Figure 9 shows the calculation of the modal damping coefficient for the first mode of the spacecraft.

Verification of test results

The task assignment required that the orthogonality check be performed to verify the accuracy of the test results. This orthogonality check was carried out between all nine spacecraft modes using the transformed mode shaped from equation (1). Using this complete mode set, the generalized mass for mode i was calculated as:

$$[M]_i = \{\phi\}_i^T [M] \{\phi\}_i \quad (3)$$

Where $\{\phi\}_i^T$ indicates the transpose of $\{\phi\}_i$, [M] is the analytically derived mass matrix

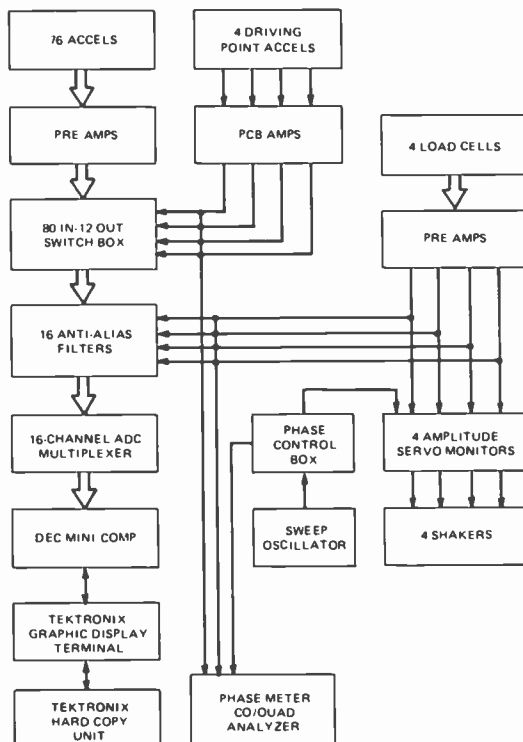


Fig. 5. Schematic of electronic gear for modal test.

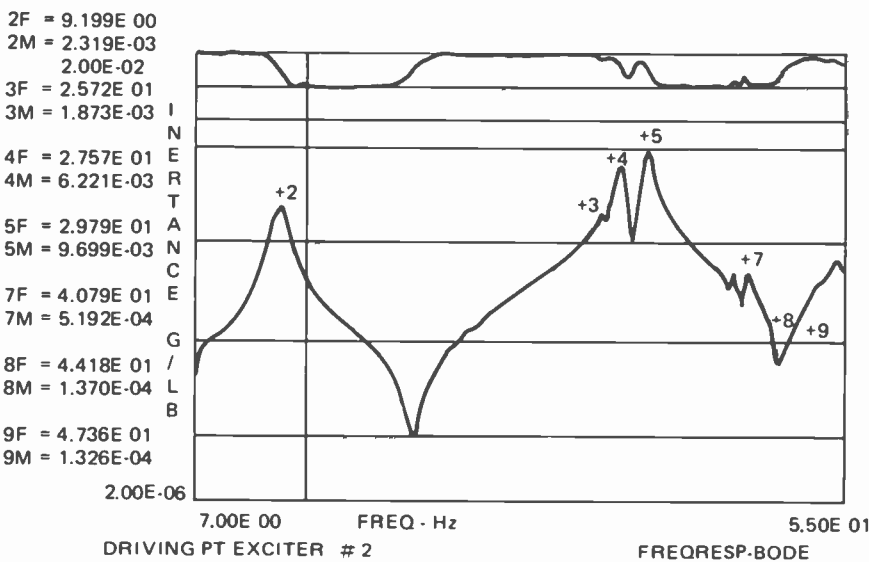
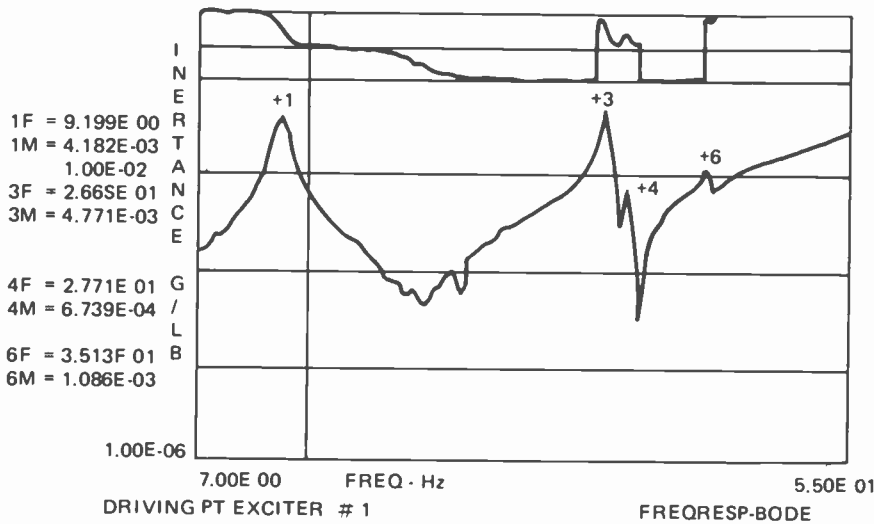


Fig. 6. Frequency response function plot for shaker No. 1 and No. 2.

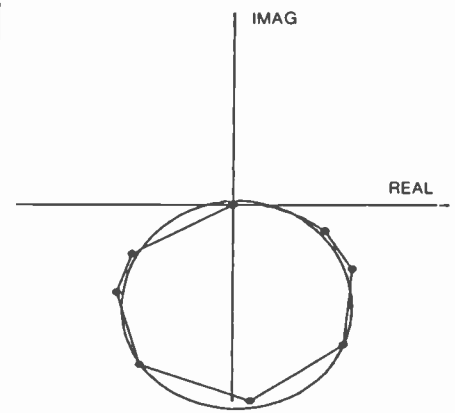


Fig. 7. Driving point Nyquist plot for short sweep of mode No. 1 (f = 9.0 Hz to 9.4 Hz).

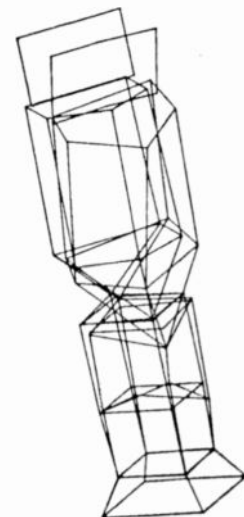


Fig. 8. Animated mode shape plot for mode No. 1.

of the spacecraft, the mode shape, normalized for a unit generalized mass, is:

$$[\bar{\phi}] = \frac{1}{\sqrt{M_i}} \{\phi\}_i \quad (4)$$

The orthogonality error matrix is then calculated by:

$$[E] = \{\bar{\phi}\}^T [M] \{\bar{\phi}\} \quad (5)$$

The test accuracy goal is to achieve off-diagonal terms in the error matrix of magnitude 0.1 or less, where the diagonal terms are normalized to 1. The resulting error matrix, given in Table I, shows very good modal purity. It is noted from this table that only two terms exceed the 0.1 goal. The two high values lie between 0.1 and 0.2, and are for higher order modes, the eighth and ninth. It is therefore believed that the results shown in Table I represent

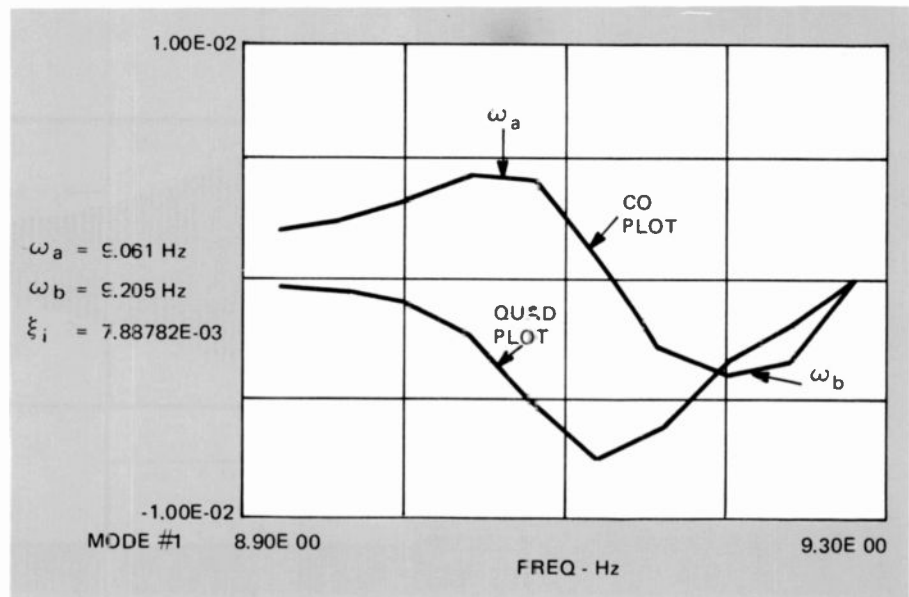


Fig. 9. Modal damping calculation for mode No. 1.

Table I. Error matrix for orthogonality check.

Mode No.	1	2	3	4	5	6	7	8	9
1	1.0	0.014	0.062	0.001	-0.059	0.082	0.005	0.062	-0.002
2		1.0	-0.051	0.062	0.087	0.042	-0.007	-0.015	-0.016
3			1.0	-0.051	-0.016	0.025	-0.021	-0.018	0.091
4				1.0	0.016	0.087	-0.072	0.049	-0.021
5					1.0	-0.049	-0.002	-0.040	-0.012
6						1.0	0.079	0.149	0.103
7							1.0	-0.045	-0.010
8								1.0	-0.115
9									1.0

very good results which in total are better than required.

One traditional way to verify the purity of the tuned mode and to evaluate the modal damping is the decay check. Due to the limitation on testing time and the fact that the modal damping could be calculated more accurately using the driving point CO plot, the decay check was performed only for the first mode using shaker No. 3. The resulting decay curve is given in Fig. 10. The modal damping calculated from this decay curve is equal to 0.0066, as shown in the figure. The tuning purity is indicated by the absence of beating in the decay response.

Comparison of test results with the analytical model

Although the purpose of this test is to create a dynamic model of the spacecraft

directly from the experimental measurements, an analytical finite element model was created for the spacecraft in the test configuration. This was necessary for the construction of the mass matrix which is needed in the orthogonality check of modes. This model was also found to be invaluable in guiding the locations and the tuning of shakers and in sorting out errors and discrepancies discovered when initial measurements did not satisfy the criteria for orthogonality between modes. This computer model, as shown in Fig. 11, consisted of beams and spring elements and 36 mass points with a total of 179 dynamic degrees of freedom. These dynamic degrees of freedom reduce to 120 after Guyan reduction and, hence, the mass matrix [M] for the test has dimension 120 x 120.

The natural frequencies calculated from this computer model are, in general, lower than the frequencies measured from the

test. Modifications were made to this computer model and the updated model gives the natural frequencies of the spacecraft within 3 percent of the test results. Table II gives the comparison of the natural frequencies.

A comparison between the mode shapes from the test measurements and the updated computer model is also given in Table II. The comparison of the mode shapes are made based on the criteria $[\phi]_M^T [M] [\phi]_A$ where $[\phi]_M$ is the measured mode shape, and $[\phi]_A$ is the analytical mode shape from the computer model. If two mode shapes are identical, the value is 1.

Conclusion

Our completion of a modal test of the 5D-2 satellite has paid off with an efficient and reliable method to determine the resonant frequencies, mode shapes, and damping

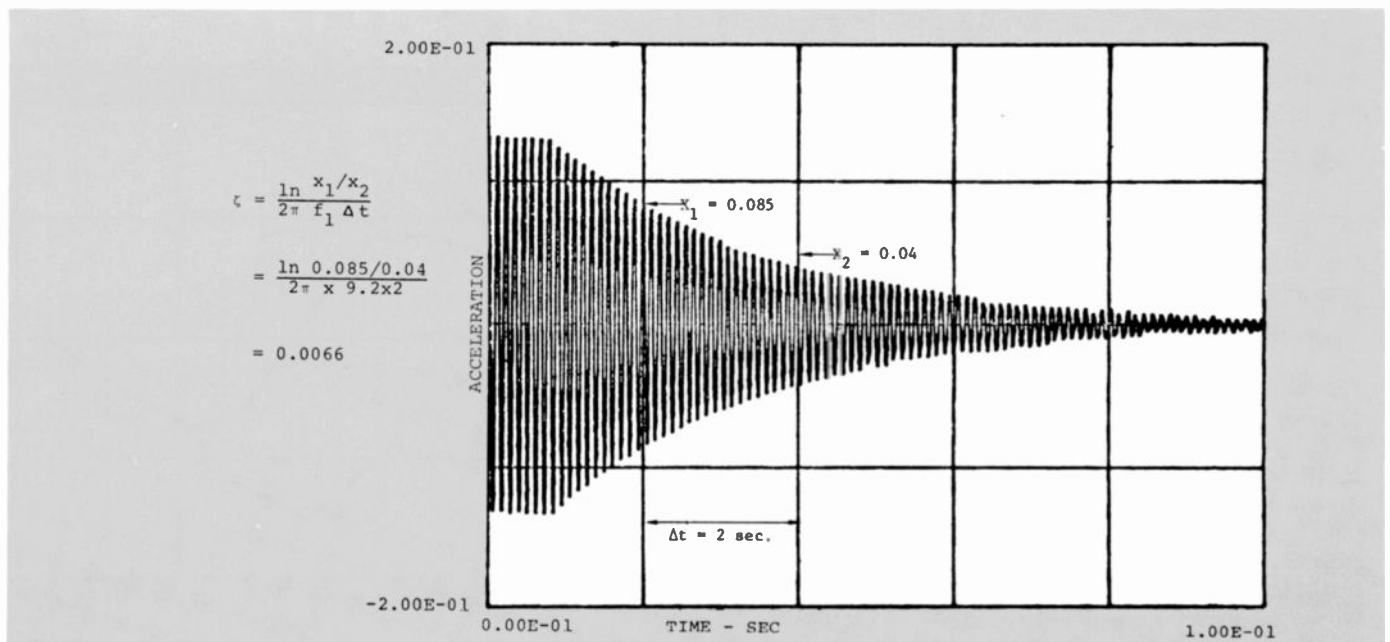


Fig. 10. Decay curve for mode No. 1.

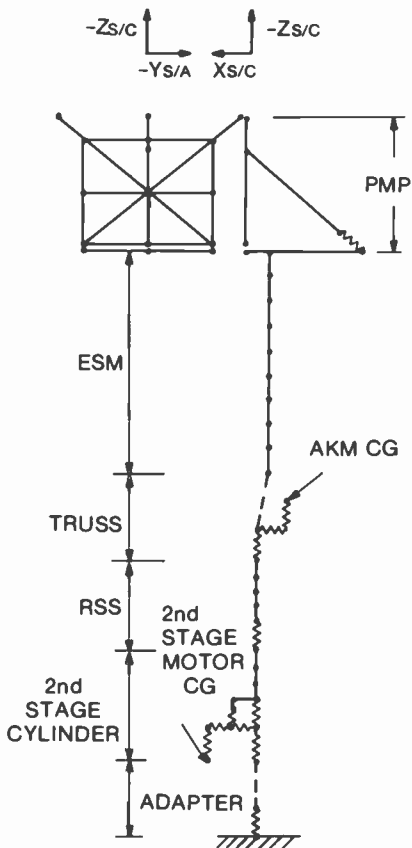


Fig. 11. Dynamic finite-element model of 5D-2 spacecraft.

properties of our satellites. These results provide a dynamic model directly from measurements, whereas previously such a model was derived analytically by finite-element analysis. In either case, this spacecraft model is a necessary part of the total launch vehicle model used by the launch vehicle contractor in his dynamic analysis to determine launch loads.

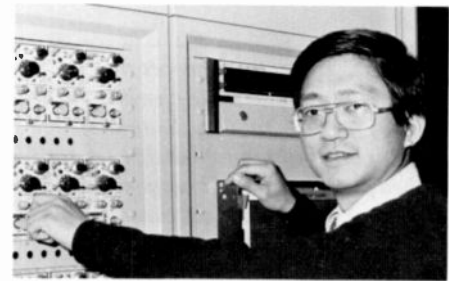
By working closely with our customer

Table II. Comparison of natural frequencies and mode shapes from test and analysis.

Mode No.	Test	Frequency (Hz)		Mode Shape		Description
		Pre-Test Model	Post-Test Model	$[\phi]^T [M] [\phi]_A$		
1	9.13	7.74	9.04	0.98		First Y Bending
2	9.13	7.79	9.09	0.93		First Z Bending
3	25.76	22.92	25.43	0.94		PMP Bending
4	27.56	25.06	27.20	0.91		PMP Torsion
5	29.76	27.24	29.44	0.90		First Torsion
6	35.51	33.27	36.05	0.92		Second Y Bending
7	40.42	37.59	41.17	0.85		Second Torsion
8	44.59	39.87	45.86	0.79		First Thrust
9	47.27	—	—	—		ESM Panel Mode

and with a subcontractor of our selection, we developed a straightforward technique of multiple-shaker sine-dwell modal testing. Procedures were developed for determining the number, locations, and force levels of the shakers for each mode. New techniques were developed for chasing down causes of erroneous results, and the relative significance of error sources was identified. Thus, our modal test method overcame the shortcomings of some previous methods. It was applied to the DMSP 5D-2 spacecraft structure where nine modes below 50 Hz were determined within required accuracy and within cost and schedule constraints.

The basic modal test technique is available for application to other satellites and satellite structures. It has special advantages for large structures, and application to space-shuttle payload interface structures and to future spacecraft structures is anticipated.



David Chu joined RCA Astro-Electronics in 1978 where he is currently a Senior Member of the Technical Staff. While working at RCA, he has been involved in the finite-element modeling, vibration analysis, and modal testing of satellite structures. He is also responsible for an IR&D project for the development of advanced methods for vibration analysis of large structures. He won an RCA Engineering Excellence Award in 1979 for outstanding work on modal vibration testing of the Air Force 5D-2 satellite.

Contact him at:
RCA Astro-Electronics
Princeton, N.J.
TACNET: 229-2352

Structural evaluation of plastic parts for television receivers

Using the finite-element method, RCA Consumer Electronics can "make it right the first time."

Abstract: *The authors report the applicability of the finite-element method (FEM) for structural evaluation of plastic parts prior to tool design. A multi-ribbed plastic mask that supports the 55-lb kinescope within a 25-inch console TV was analyzed. The results of this analysis were compared with drop tests and strain-gauge measurements. Instrument-drop break locations were more accurately predicted than the strain-gauge measurements, since the FEM model did not include the kinescope mounting stresses.*

Motivation to try FEM

Historically, the design of mechanical components (cabinets, chassis, supports, etc.) used in television receivers has been based on experience, extrapolation, and extensive testing of sample parts. On major plastic components, an expensive injection-molding tool is required even before the mechanical testing can begin. After testing, the tool may be found to have deficiencies, leading to parts which have structural weaknesses. The defective tool must be sent back for modifications, and a long delay period is possible. This cycle could repeat itself several times before a sample part finally passes the mechanical approvals.

The above process causes long time delays, scheduling problems, and cost overruns. It was suggested that this cycle of build, test, modify, test, modify, and so on, could be greatly reduced by structural analysis of the component in a finite-

element method (FEM) computer program. FEM routines were developed for the aerospace industry, but several well known programs are now used in many other structural, heat transfer and seismic areas. The ability of an FEM program to accurately calculate the stresses and strains of complex metal structures is what led to our interest in evaluating this method in a plastic part application. As described in detail below, it was not clear in advance that the well known anisotropic and process-dependent properties of plastics could be suitably modeled with FEM in a cost-effective fashion.

Trial problem

To test the FEM approach, we selected for analysis a part having structural weaknesses which caused it to pass marginally the standard engineering instrument drop test.¹ Our trial problem was a 25-inch color-TV mask, called a "60" mask. This component, shown in Fig. 1, showed sufficient complexity to prevent "back of the envelope" solution. The "60" mask, injection molded from Noryl® plastic², serves as a structural support to hold the picture tube, tuner, and controls. It has cosmetic significance as well, therefore we could not introduce arbitrarily sturdy ribs for fear of "sink marks" (unattractive depressions in the surface caused by cooling-induced contractions of the plastic).

For shipping and handling instruments using the "60" mask, adequate strength was assured by adding metal brackets between tube supports and the consoles. However, this is not as cost-effective as making an adequate mask in the first place.

Development of an FEM model

Since this trial problem was our first experience with FEM analysis, we decided to start by modeling a very simple mask configuration and work towards a more complex and realistic model of the "60" mask. We selected the ANSYS Finite-Element-Analysis Program,³ a well-established FEM computer analysis program with capabilities ranging from static-linear modeling to non-linear, dynamic, transient, and others. The ANSYS program has been used in the Picture Tube Division, Lancaster, Pennsylvania,⁴ and at RCA Laboratories, Princeton, New Jersey.⁵ An RCA FEM Symposium was held at RCA Laboratories in March 1978.⁶

Table I. FEM modeling assumptions. More realistic assumptions could have been used at increased model-generation complexity and computer cost. But these assumptions proved sufficient.

- Static
- Linear
- Left-right symmetry
- Mask unstressed after kine-mounting operation
- Kine-mounting lug attached to mask at specific rib-end nodes
- Rib-boss assembly modeled by ribs only
- Isotropic plastic parameters
- Geometry-independent plastic parameters
- All parts weightless — gravitational force on picture tube applied to measured center of gravity

Reprint RE-26-4-6
Final manuscript received Sept. 4, 1980.

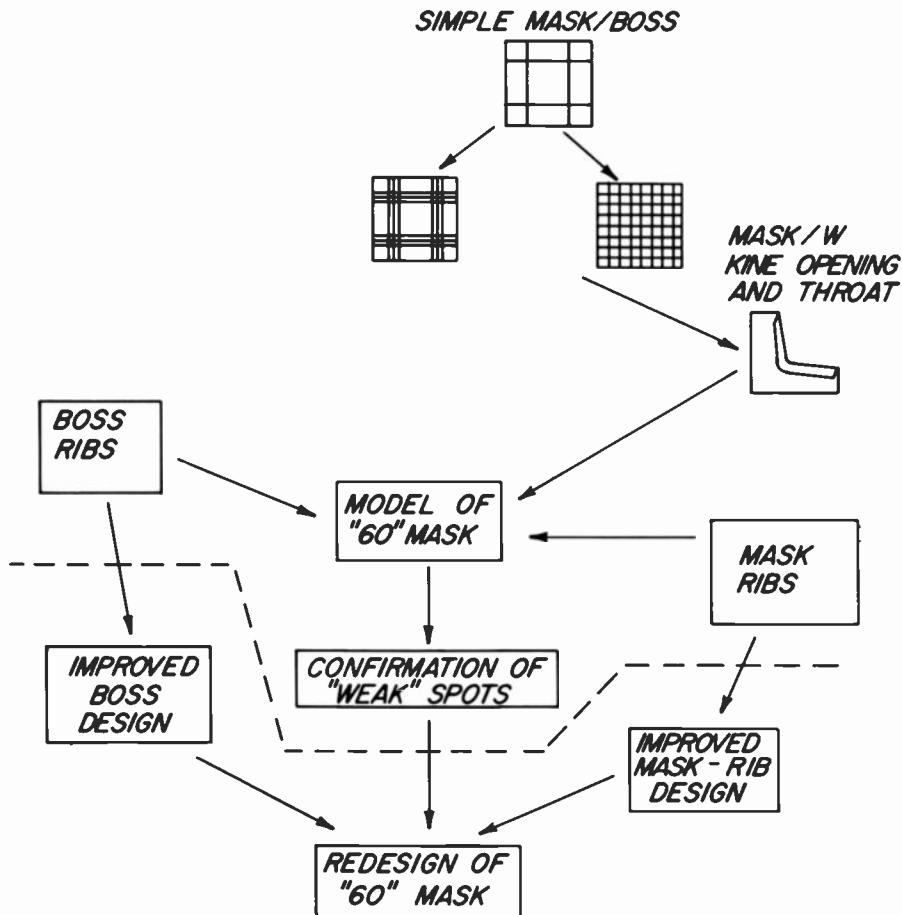


Fig. 2. Flow of modeling the "60" mask. Early attempts were quite simple, while later models bore a high degree of resemblance to the molded part. Tasks below the dashed line were not performed as the utility of FEM modeling was already demonstrated.

Mask 8 was generated in response to the results of Mask 7. The areas of high stress in Mask 7 were resolved into a finer mesh that permitted more detailed contours of the high-stress regions. Mask 8 results showed an improved accuracy in locating areas of maximum stress, but one more refinement (Mask 9) in the mesh density was performed to confirm the areas of high stress. As shown in Fig. 5 and Table III, for each increase in the density of the mesh, the element count increases and so does the computer cost. One must make the model as dense as possible in the area of concern to get accurate results, keeping track of the cost. Mask 9 results showed good agreement with experimental data, as we show in the next section.

Comparison of detailed models with experiment

The utility of FEM models for evaluating plastic part strength cannot be determined by merely looking at the results generated and described earlier in this report. If the FEM method is to be a useful tool, it must yield results which are in agreement with actual experiments. There are a number of

computed parameters that the FEM program gives the modeler for comparison:

1. Normal and shear stresses
2. Principal stresses
3. Von Mises equivalent stress
4. Displacements

Following typical practice in the metal parts field, we relied heavily on the Von Mises equivalent stress as an indicator of local conditions. It should be pointed out that there is a potential shortcoming in so doing. By its very definition, the Von Mises stress is always a positive number; however, plastic parts are known to have very different yield characteristics for compressive and tensile strengths. It is, hence, very important to keep an eye on the principal stresses to see whether the material locally is in a state of tension or compression.

There are a number of experimental techniques which could be used to evaluate the models described earlier in this report:

1. Brittle lacquer
2. Photo-elastic coating
3. Static (or dynamic) strain gauge
4. Drop test

Although the former two tests have received a fair amount of attention in the literature,⁸ we had difficulty achieving calibration in some of the early tests

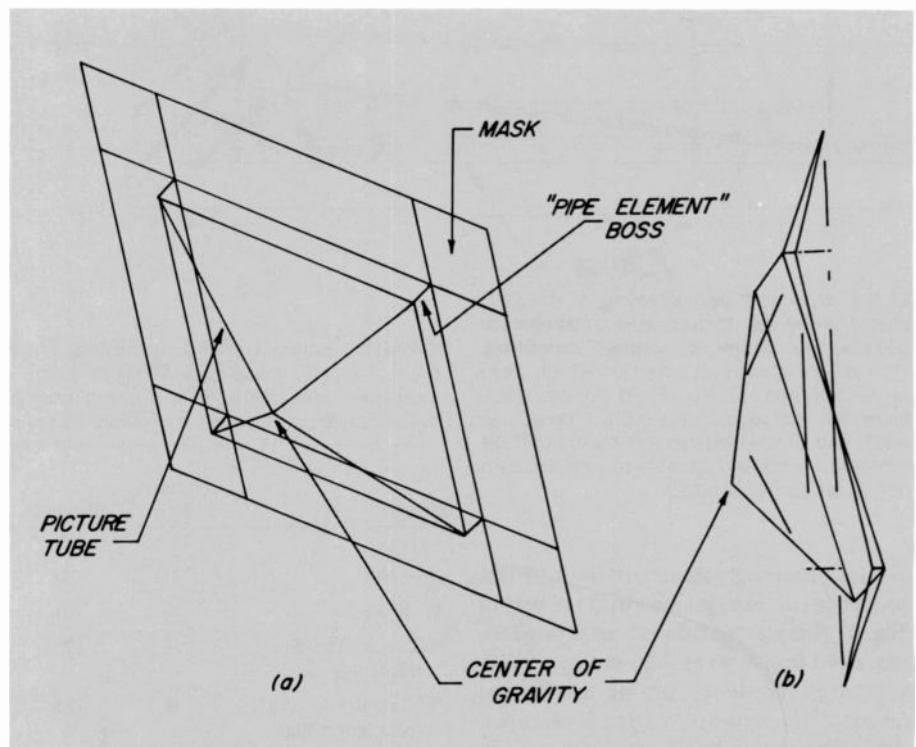


Fig. 3. Simple model of mask with "pipe-element" bosses and attached picture tube. (a) Model geometry. (b) Side view of displaced and initial (dashed) model. The displacement plot shows (exaggerated) shift of the center of gravity of the picture tube, bending down of the bosses, and bending of the mask sheet.

Table III. Comparison of detailed models. The model becomes more detailed, computer cost increases, but so does the accuracy of the model.

Model	Elements	Computer cost (\$)	Prediction of break locations
"60" boss ribs Mask 6	296	72.15	Poor
Mask 7 A	697	142.00 ^a	—
Mask 8 improved "60" Mask	965	270.00 ^a	Good
Mask 9 improved	1233	450.00 ^a	Excellent

a. Evening Computer Rates in June 1979.

performed by our associates. On the other hand, we were able to get meaningful comparisons with the latter two tests. The best correlation occurred with our so-called "uncalibrated drop test." (These results are discussed below.) Our static strain-gauge measurements (described below) did not correlate well with the model, but we believe we now understand these results. The reason for this lack of agreement will be described.

Uncalibrated drop test

In this experiment, the "60" mask under study was mounted into a conventional console receiver. The picture tube was, in turn, mounted on the mask. The console

was supported by several wood shim pieces to assure that the test could be performed consistently with different masks and tubes. The instrument was raised 9 inches and dropped onto standard flooring in a highly repeatable fashion. Due to the presence of the shim pieces, it was not necessary to place the receiver in a shipping carton. (It should be noted that this shimmed cabinet test represents an environment much more drastic than typical handling of receivers in cardboard cartons.) Cushions conventionally used at the mask-interfaces were not used. The weight of the tube, plus the convergence assembly, was roughly 55 lb., as used in our modeling earlier.

In a typical bottom drop of this test arrangement, seven breaks occurred on

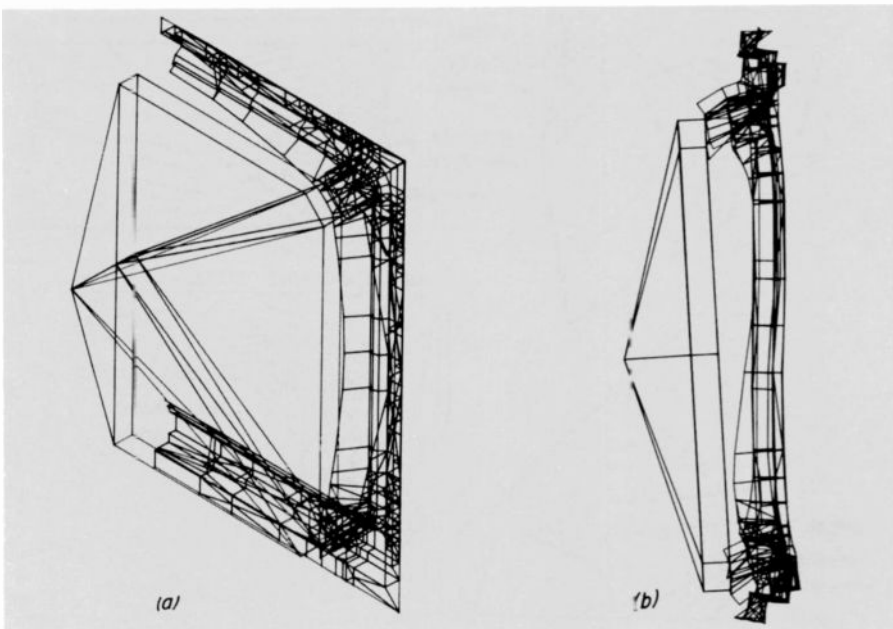


Fig. 4. The Mask-7 model of the "60" mask. (a) Model geometry. (b) Displacement plot. Comparison with Fig. 3a reveals a more complete picture-tube model, permitting incorporation of right-angle mounting lugs. The mask includes more of the detailed contouring of Fig. 1, including throat, flange, and ribs. Comparison with Fig. 3b shows similar changes (except for magnitude) in picture-tube position, boss "sagging", and mask bending.

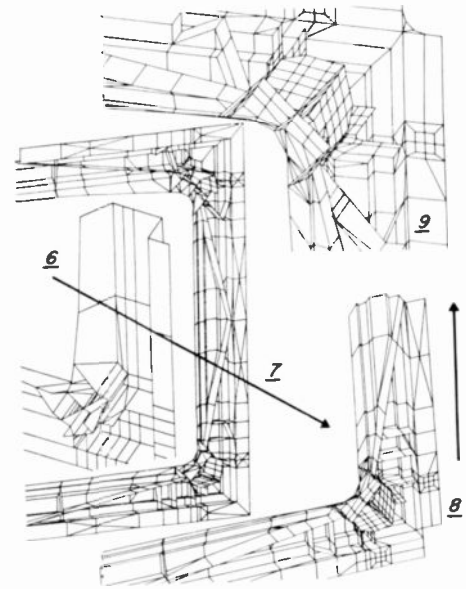


Fig. 5. A series of ANSYS® hidden-line plots shows the increasing element detail used in the boss-support ribbing as the modeling progressed from Mask 6 up through the final model, Mask 9. Increased detail in mask contour and flange attachment can also be seen.

one side of the mask (Fig. 6). Figure 7 shows stress-contour plots for the Von Mises equivalent stress for the rib elements containing those seven breaks. These contour plots are from the Mask 8 model. One can see that in most cases the predicted maximum stress point is extremely close to the break. The principal difference between actual and predicted break locations occurred for breaks 3 and 4. In Mask 9, with improved detail in this and other regions, this discrepancy was drastically reduced. Table IV summarizes the results of this test, giving the element-printout stresses, the indicated maximum stresses from the contour plots, and the distance between the observed break and computed maximum stress point.

Static strain-gauge measurement

In this experiment, the stress results from the Mask 8 model were compared with strain-gauge measurements for gauges placed along critical stress areas of several of the ribs. These locations are shown relative to the model in Fig. 8. Stress measurements were taken at critical times during the assembly process:

1. with the instrument positioned on its face, with the picture tube resting on the mask;

Table IV. Comparison of uncalibrated drop-test results with Mask 8 and Mask 9 results. SGET and SGEB are the Von Mises equivalent stress on the top and bottom of the element platelet, respectively. Break locations are coded to Fig. 7.

Break location	Comparison with element printout (max. SGET or SGEB) (PSI)		Comparison with stress contour plots for SGET or SGEB			
	Mask 8	Mask 9	Indicated maximum stress on plot of rib (PSI)		Distance from break to stress contour maximum (X) (inches)	
	Mask 8	Mask 9	Mask 8	Mask 9	Mask 8	Mask 9
1	408	569	424	556	0.114	0.114
2	501	1075	518	945	0.2	0.04
3	231	324	298	223	0.78	0.24
4	372	646	469	550	0.78	0.249
5	155	307	245	285	0	0
6	602	976	774	880	0	0.141
7	274	395	356	387	0.047	0.188

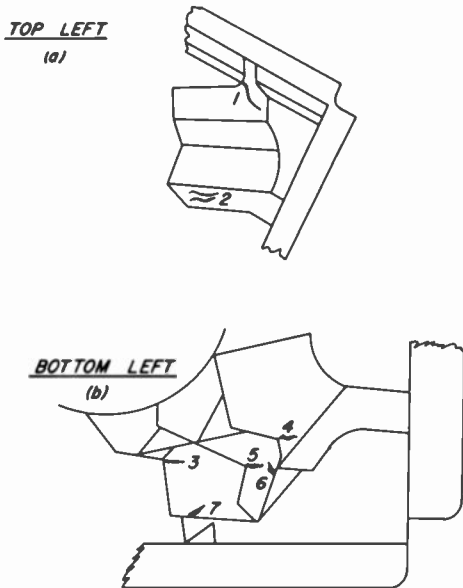


Fig. 6. Schematic sketches show the location of breaks which occurred in the "60" mask bottom-drop experiment. (a) Top-left-corner picture-tube-attachment area. (b) Bottom-left-corner picture-tube-attachment area. (Break #2 was a pair of hairline fractures near the attachment-screw location.)

- with the picture tube assembled to the mask, facedown, with screws; and
- with the instrument set upright, resting on its bottom-side shim pieces.

Instruments were assembled in two fashions:

- in the standard fashion, and
- using no cushions and with special insert pieces between the mask boss and the picture-tube mounting lugs.

The results of this experiment are highlighted in Table V. One can see that the stresses computed for elements in the area

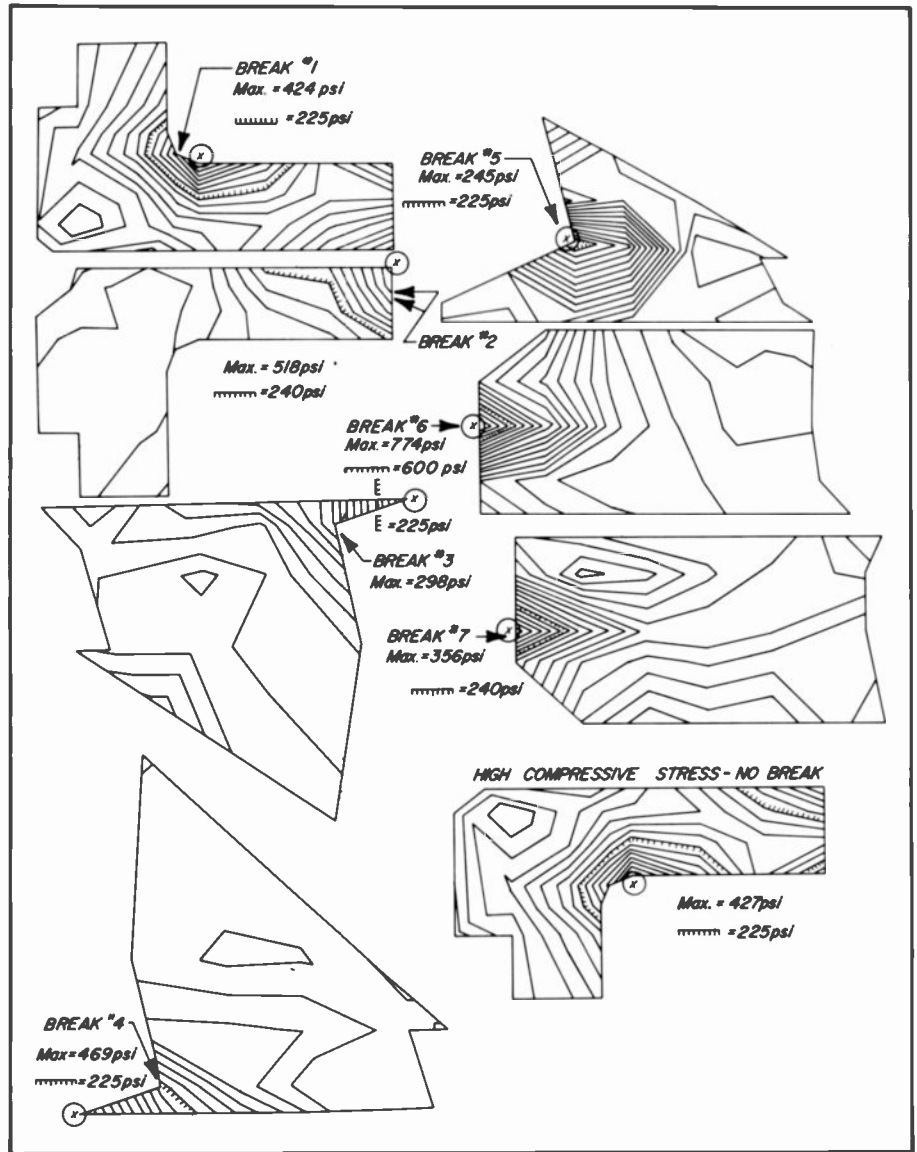


Fig. 7. Stress-contour plots computed with the ANSYS® FEM program for rib sections in the Mask 8 model of the "60" mask, with breaks. The Xs in the center of the circles are computed maximum stress points for the particular ribs. Arrows point to the break locations shown in Fig. 6. The stress contour plots are for the Von Mises equivalent stress.

Table V. Comparison of strain-gauge measurements with computed results. Agreement only in sign, but not magnitude, can be observed for reasons explained in the text.

Strain-gauge location	Plate region	Element number	Mask 8 computed principal stresses (PSI)		Load ^a stress from experiment (PSI)	
			SMX	SMN	I ^b	II ^c
5	TOP	335	163.4		93	246
6	BOT	288		-348	-17	-343
		294		-215		
		297		-446		
8	BOT	805		-168	-121	-288
		758	347			
	TOP	764	213			
		767	443			

a. Load stress = (upright) -(assembly on face with screws) + (positioned on face)

b. Assembly per D/L

c. Assembly as follows: no cushions; lug/boss insert pieces

of the strain gauge are compared with the measured stress. The correlation is not particularly good, although there is, at least, agreement in the sign of the stress. We believe that the correlation problem here relates to the extremely high stresses associated with mounting the picture tube to the mask. These stresses are so large that

they should not be neglected when computing the stress when the instrument is sitting static in its upright condition. However, in our FEM model, such a "pre-stressing" was not taken into account. The reason that the uncalibrated drop-test results are so much more accurate by comparison is because this mounting stress

is purely static. The picture-tube support stress multiplied by an effective g-load at the instant of impact during a drop test far exceeds the mounting stress. Unfortunately, in the static strain-gauge case, these mounting stresses are, in fact, quite significant.

Conclusions

Several significant conclusions can be drawn from the project described here.

1. A static linear FEM analysis can reveal weak points in the mechanical design of a plastic part. This is particularly significant in view of the well-known complex properties associated with injection molded parts.
2. Although quantitative agreement can be improved further, it is clear that alternate structures and materials can be compared for a particular mechanical support application.
3. Since the complete transient, dynamic, and non-linear capabilities of a sophisticated finite-element program are not required to achieve the useful results shown here, it is possible to utilize less expensive linear/static FEM programs that can run easily on CAD/mini-computer systems.

Performing the analysis in this way makes cost-effective analysis of plastic parts design possible.

Important follow-up work to this initial feasibility study would include the creation of interactive programs that would make it easier for more mechanical engineers to utilize the powerful verification tool of an FEM computer program. Such work is now well underway in the design engineering area of the Consumer Electronics Division.⁹

Acknowledgments

The authors would like to acknowledge the assistance provided by a number of other people both in the Consumer Electronics Division and at RCA Laboratories in Princeton, New Jersey. Most especially, we are thankful to W.F. Groene and C.S. Young of the New Products Laboratory for performing the key experiments which were utilized for the model comparison.

Further, a number of individuals contributed substantially to our model development and our understanding of plastic mechanical parts: R.A. Sunshine, M.W. Garlotte, R.J. Ramsbacher, J.A.

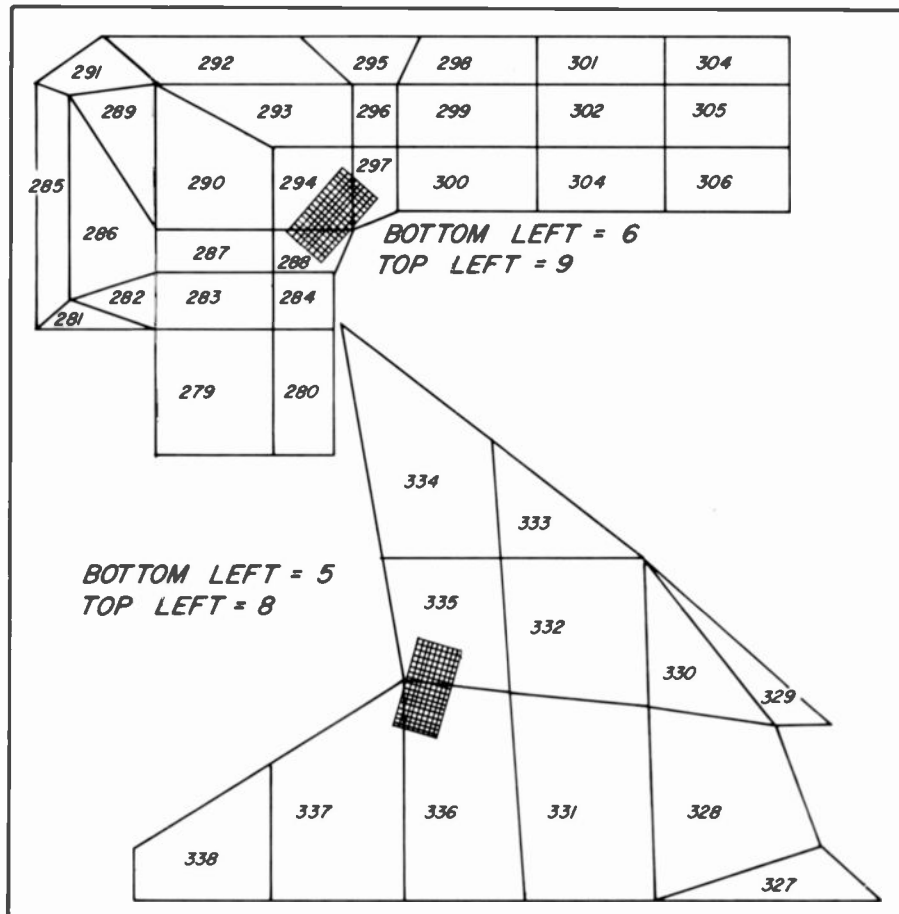


Fig. 8. Geometry plots of two types of ribs on the "60" mask showing where strain gauges were mounted for experiments described in the text. Gauges were placed in corresponding positions in both top and bottom quadrants of the mask.

Milnes, R.E. Enstrom, G.P. Lord, and A.E. Wilson. The computations described here were performed on the ANSYS finite element program through the Westinghouse Computer Service in Pittsburgh. We are indebted to our customer representative, J. Harter, and to the Staff of Swanson Analysis, Inc., for assisting us with the computations.

References

1. "Simulated shipping tests for CE products and electronic components." Engineering Dept., Electronic Industries Assn. Publication, EIA RS-414-A (June 1975).
2. Noryl® is a registered trademark of the General Electric Company, Plastics Division, Noryl Avenue, Selkirk, New York, 12158.
3. ANSYS is a finite element program developed and maintained by Swanson Analysis Systems, Inc., P.O. Box 65, Houston, PA 15342.
4. Bauder, R.C., "Finite Element Analysis of a Twenty-Five Megawatt Power Tube and a High-Energy Water Cooled Heat Sink for Fusion Research." *RCA Review*, Vol. 39, p. 699-717 (Dec. 1978).
5. Enstrom, R.E., Stepleman, R.S., and Appert, J.R., "Application of Finite Element Methods to the Analysis of Stresses in Television Picture Tubes." *RCA Review*, Vol. 39, p. 665-698 (Dec. 1978).
6. Sheffler, A.W., Metzger, M.W., and Varadarajan, G., "The Finite Element Method — A Powerful Tool for Structural Design," *RCA Engineer*, Vol. 24, No. 3, p. 26-33 (Oct./Nov. 1978).
7. "Kent's Mechanical Engineers' Handbook," 12th Edition, C. Carmichael, Editor, John Wiley & Sons, Inc., N.Y., p. 8-45 (1953).
8. See, for instance, Crites, N.A., "Which Type of Stress-Analysis Method?" *Product Engineering*, p. 90 (Oct. 16, 1966). (Available also in Bulletin S1-22, Magnaflux Corp., Chicago, IL 60656.)
9. Sunshine, R.A., and Young, C.W., "The Potential Impact of Computer Technology on Mechanical Engineering Productivity," RCA Mechanical Engineering Symposium, Princeton, New Jersey (April 30, 1980).



Rich Mooney (left) and Scott Keneman (right) with a "60" mask and a drawing of a computer model of the mask (right).

Scott Keneman joined RCA Laboratories in 1964 as a Member of the MIT-RCA Co-Op Program. Dr. Keneman joined the New Products Laboratory of the Consumer Electronics Division in 1978 to assess new technologies for RCA's existing and future product lines. In June 1980, he was made Manager, TV Digital Systems, in the New Products Laboratory, responsible for the development of RCA's TV tuning systems and remote control systems for the mid-80s.

Contact him at:
New Products Laboratory
RCA Consumer Electronics Division
Indianapolis, Ind.
TACNET: 422:6865

Richard Mooney joined RCA in 1967, working in a number of areas including Consumer Electronics Division's TV Engineering Group and "SelectaVision" Video Cassette Recorder Group. He is presently working in the Technology Applications Group of the New Products Laboratory. In this function, he is responsible for applications of computer testing and circuit analysis of ICs under development in Consumer Electronics.

Contact him at:
New Products Laboratory
RCA Consumer Electronics Division
Indianapolis, Ind.
TACNET: 422-6864

Computer analysis for shock testing of AEGIS water coolers

RCA's DYNA3 finite-analysis program proved to be a highly cost-effective alternative to standard Navy shock testing of water cooler systems.

Abstract: *Standard techniques for shock testing Navy shipboard equipment involve potentially destructive measures such as "barge" tests (underwater explosions). For complex, expensive equipment, these tests are time-consuming and costly. Thus, for five large water-cooling systems used on the AEGIS program, the Navy authorized RCA to undertake an analytic approach as an alternative to physical testing. RCA's DYNA3 computer program proved up to the task, satisfying rigorous Government shock and vibration specifications with significant cost savings.*

In ancient mythology, AEGIS was the shield of Zeus. For the U.S. Navy, AEGIS is the shield over its fleet, a combat system designed to protect ships from incoming threats. RCA's Government Systems Division, Missile and Surface Radar (MSR), is the prime contractor responsible to the Navy for coordinating this large project. MSR is also providing detail design of a number of critical system elements.

One of these is the AN/SPY-1A phased-array radar, the heart of the AEGIS system—designed, built, and tested at MSR in Moorestown, New Jersey. This radar dissipates large amounts of heat and requires cooling by purified chilled water; several other major electronic systems require similar cooling. Accordingly, RCA undertook the design of a standardized cooling system for these equipments, in part because cooling systems have historically been a major cause of problems in maintaining large-scale electronic systems.

In the past, such systems have been

"plugged in" to existing ship-cooling equipment, frequently overloading the available cooling capacity. Compounding this problem was a long-standing practice of forcing cooling systems to compete for space in ships. As a result, the systems often ended up disjointed, with components tucked into available corners.

Design of water coolers

Recognizing these problems, and taking advantage of their own naval shipboard expertise, MSR engineers took a systems approach to the design and development of the AEGIS cooling system. They designed

each unit as an integral, palletized assembly. The great advantage of this approach is that a tested, operational unit can be brought into the ship, ready for hookup. Key features of the cooling system include:

- Use of redundant components and parallel cooling loops for reliability;
- Design for ease of maintenance;
- Use of compatible materials to resist electrolytic corrosion;
- Elimination of undesirable turbulence;
- Rapid fault indication and isolation;
- Large heat-dissipation design margin (18 percent) for system growth; and

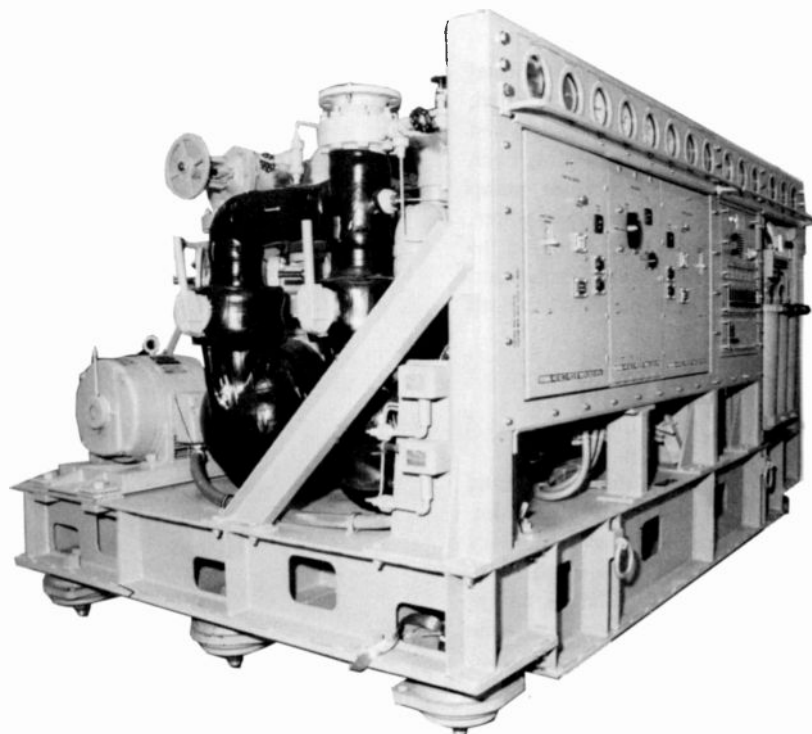


Fig. 1. AN/SPY-1A radar water cooler showing control panel and palletized construction.

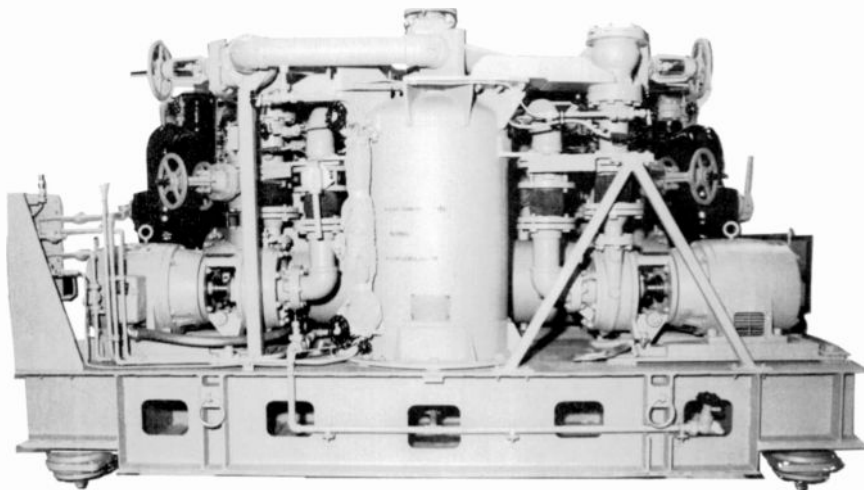


Fig. 2. AN/SPY-1A radar water cooler, rear view.

- Use of combined air and water cooling, achieving a balance between efficiency and weight.

Figures 1 and 2 show the water cooler for the AN/SPY-1A radar. The unit weighs about 9000 pounds and is carried by a heavy frame resting on six heavy-duty Navy shock mounts. In this form, it is ready for direct installation in the AEGIS cruiser. Besides the cooler for the SPY-1A array, MSR provides AEGIS with cooling systems for four other major electronic systems: the AN/SQS-53A sonar static dissipator; the AN/SQS-53A sonar electronics; the AN/SPS-49 radar system; and the command and decision (C&D), display, and external communications (XCOM) equipment. Each of these coolers weighs about 7000 pounds.

All five cooling systems feature dual cooling circuits that work in parallel, enabling half of the unit to be serviced while the other half is still operating. Each cooling circuit consists of a motor/pump unit and heat exchanger fed by sea water. The piping contains valves needed to separate the circuits. A central expansion tank and an instrument panel serve both circuits.

Physical testing

Like all Navy equipment, the coolers must survive rigorous shock and vibration environments imposed by military specifications. MIL-S-901 is a test specification that subjects heavy equipment (more than 6000 pounds) to the shocks of a barge test, where calibrated underwater charges are set off close to the barge (shown in Fig. 3). MIL-STD-167 is a mechanical vibration test specification that

subjects equipment to environmental vibrations, simulating shipboard conditions for at least two hours. Since vibration testing is straightforward and relatively simple, the following discussion is devoted largely to the complexities of shock testing.

Barge tests are very expensive because the equipment must be moved to one of three locations in the United States where these tests are conducted and because the Navy does not permit the units to be used after the test (equipment might be physically strained, leading to early failures). In an attempt to eliminate barge testing of the AEGIS water coolers, and thus to realize considerable cost savings, the Navy

allowed RCA to prove compliance with the specifications by computer analysis.

The standard method of shock analysis is the Navy's Dynamic Design Analysis Method (DDAM), which uses a classified shock-spectrum input. This method is widely used for simple models with few masses, but it is extremely difficult to use on large complex structures such as water coolers. In another approach, the AEGIS water coolers are analytically subjected to equivalent shock pulses such as those shown in Fig. 4, as required by the procurement specifications.

Analytical testing

A closer look at the water coolers indicates that they represent a plumber's nightmare in complexity—any analysis would have to be very detailed to trace large stresses accurately in all elements. MSR decided that the best approach to this problem was to use the finite-element method in sufficient detail to account for every pipe, valve, and supporting bracket in the system.

The finite-element method evolved in the aerospace industry in the early 1960s as a new type of stress analysis. This now commonplace technique is used in the design process for nearly every mass-produced automobile. Finite-element computer programs are used to derive mathematical models of all types of struc-

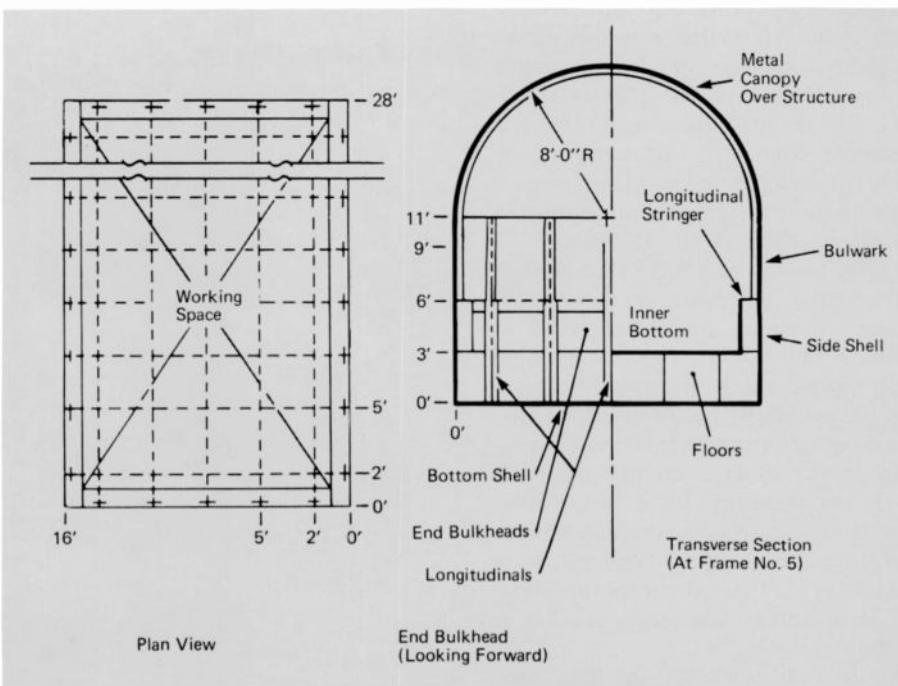


Fig. 3. Standard floating shock platform used in barge testing of Navy equipment weighing more than 6000 pounds.

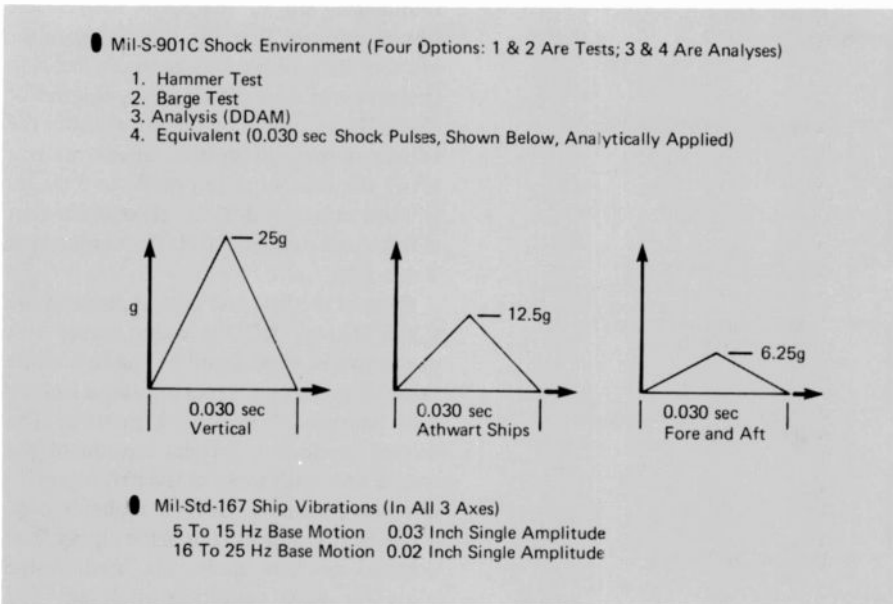


Fig. 4. Specification for shock environment and ship vibrations.

Table I. Parameters of four AEGIS water coolers (WC).

Parameter	SPY-1A WC	AN/SPS-49 Radar WC	Sonar Electronics WC	C&D Display/ XCOM WC
Coordinate Points	239	326	299	260
Elements	381	486	458	391
Elastic Degrees of Freedom	850	1,098	1,284	916
Mass Degrees of Freedom	381	372	375	297
Matrix Bandwidth	246	342	342	318
Resilient Mounts	6	4	4	4
Model Weight (lbs)	8,754	6,739	6,458	6,723
Center of Gravity				
X (inches)	49.53	48.74	48.46	50.72
Y	33.12	29.62	27.67	28.96
Z	16.72	17.70	26.92	15.53

tures by subdividing them into basic elements, each providing a stiffness matrix which is combined into one large global matrix that contains all the elastic properties of the structure. Natural frequencies are derived by solving for the

eigenvalues. The model may then be subjected to static or dynamic loads of various types shown in the flow diagram of Fig. 5.

The analysis produces the responses or deflections to these loads and the associated stresses. Additional routines

Table II. Modal analysis results obtained from DYNA3 vibration tests on SPY-1A water cooler (WC) with and without resilient mounts.

Mode	Natural Frequency (Hz)	
	WC Rigid to Ship's Deck	WC on Soft Resilient Mounts
1	50.37	3.80
2	54.85	5.81
3	63.39	6.89
4	64.47	18.25
5	67.49	19.93
6	75.91	20.84

Table III. Modal analysis results obtained from DYNA3 shock tests on four AEGIS water coolers (WC).

Mode	Natural Frequency (Hz)			
	SPY-1A WC	AN/SPS-49 Radar WC	Sonar Electronics WC	C&D Display/ XCOM WC
1	19.66	25.24	21.34	19.22
2	30.42	27.56	29.01	27.55
3	32.11	34.15	29.98	29.06
4	65.08	42.89	55.45	62.50
5	72.72	44.85	58.05	68.40
6	76.44	49.98	59.20	72.62

provide plotting of structures, deflections, and mode shapes. The finite-element computer program used — RCA-DYNA3 — has served AEGIS for eleven years. It was originally acquired to analyze the AEGIS array structure and has gone through several modifications to become a powerful tool for both static and dynamic analyses.

Of the five water-cooler systems, two were so much alike that only four finite-element analyses had to be made. The four coolers were modeled by assigning grid-coordinate points and connecting them with beams, straight and curved tubings, triangular and four-sided plates. The shock mounts were inputted in the form of flexibility matrices, based on test data for the regular (under vibration) and the bottomed-out (under shock) conditions. Following recommendations by the Navy, all shock analyses were based on bottomed-out shock mounts, whereas the ship's vibration data were based on the regular conditions.

All models were complex and required thorough checking by plotting. A sample of the model of the HD-1014/SPY-1A Array Cooler is shown in Fig. 6. Beam and tubing numbers are shown halfway between endpoints, and plates have arms pointing to the corners.

The model parameters are given in Table I. Elastic degrees of freedom are a measure of model size and run costs. For extensive dynamics analyses, the masses are lumped into significant mass points, reducing the finite-element matrices to those of the mass degrees of freedom. The stiffness matrix has its elements concentrated around the diagonal. The maximum distance of any element from the diagonal is called the matrix bandwidth. To remain within the capacity of the computer memory's core, the matrix bandwidth is kept to a minimum by subjecting the input to the bandwidth-improver subroutine within DYNA3.

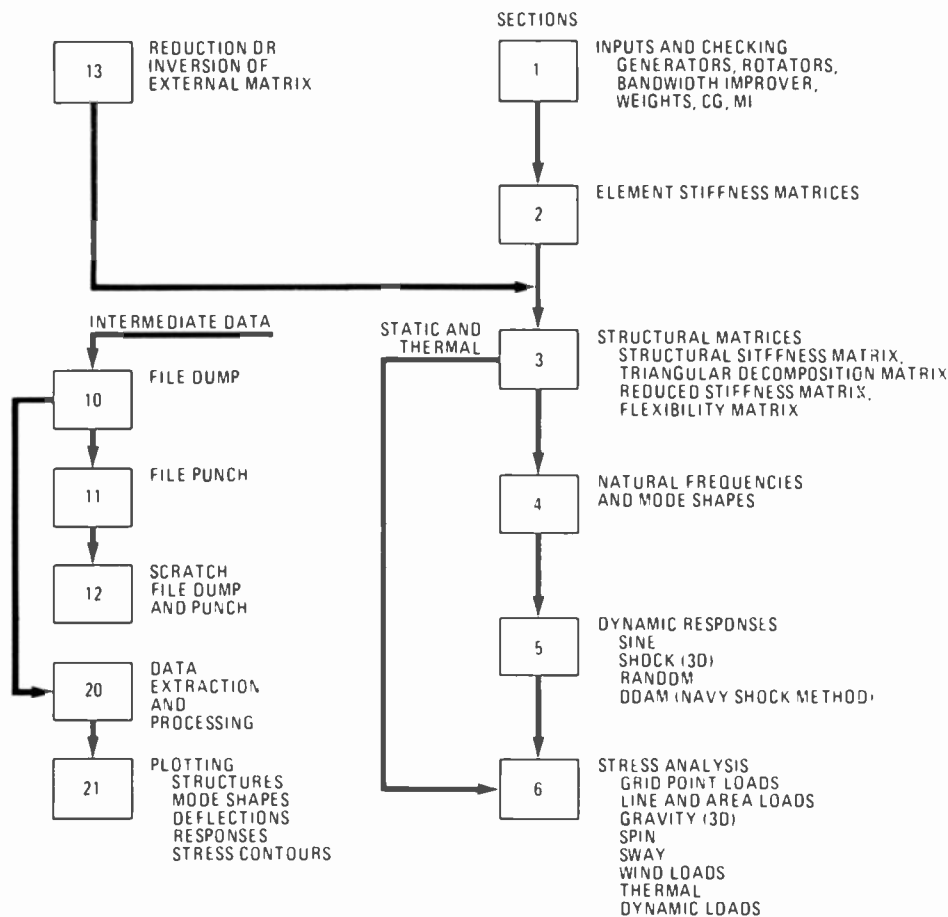


Fig. 5. Flow diagram of RCA DYNA3 computer program for shock analysis.

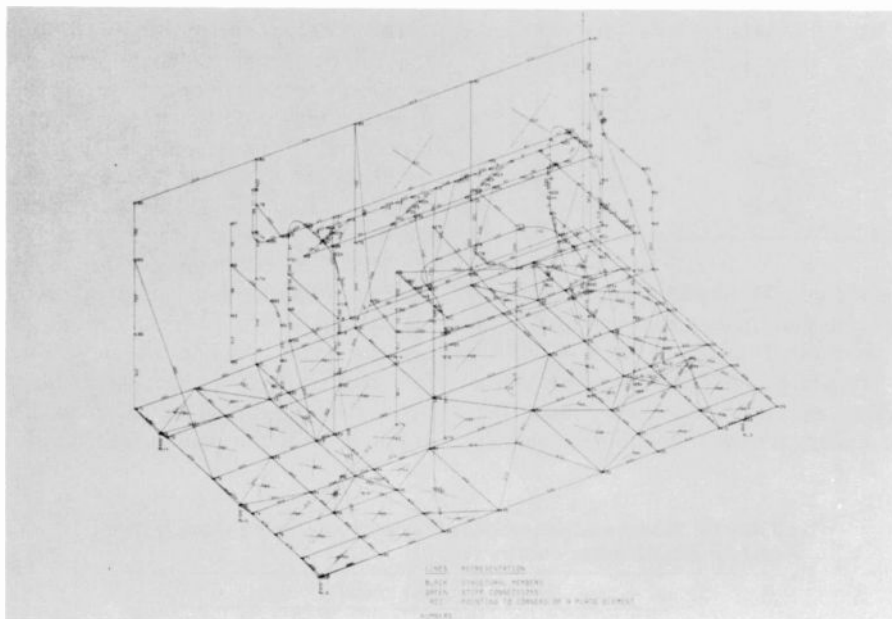


Fig. 6. Structural model of AN/SPY-1A radar water cooler obtained from RCA-DYNA3 computer program.

Analytical results

All analyses of the four models proceeded through a modal analysis in which the lowest natural frequencies and mode shapes were calculated. A mode shape is the preferred shape of deflections that an

elastic body assumes when subjected to an excitation at a natural frequency; it is the pattern of vibration of a structure and is described by the structure's natural frequency and its relative amplitude vector.

Tables II and III present the results of the modal analyses, giving all natural

frequencies up to the sixth mode. The results indicate that the units themselves are very stiff, with a high natural vibration frequency of over 50 Hz (first column of Table II), as shown by the run without the benefit of resilient mounts. Shock mounts lower the first vibration mode to 3.80 Hz (second column of Table II) and the first shock mode to about 20 Hz (first column of Table III).

Plots of the first and second mode of the C&D/Display/XCOM water cooler unit are shown in Figs. 7 and 8. The first mode shows that the unit is rocking about its long axis because of the shock mounts. The second mode is a vertical motion of the cooler unit with most of the deflections in the shock mounts. Only at higher modes are local resonances seen in the piping. The original analysis shows six mode-shape plots for each condition analyzed. The modal plots are used to show the locations of large deflections, thereby indicating the elements requiring stiffening to improve dynamic behavior of the model.

The specified shock inputs of Fig. 4 are used to excite the model. These shocks result in maximum *g* loading of the coolers and in a minimum factor of safety in the elements. The Navy allows a factor of safety (ratio of allowable stress over actual stress) of 1.0 against yield if the proper input level has been used. The factor of safety is based on the properties of the copper-nickel alloys used in the construction of the units. These alloys are very tough and it takes a factor much lower than 1.0 to cause catastrophic damage in the coolers. The lowest factor shown is 1.02 in the search radar (AN/SPS-49) cooler unit (Table IV). The AEGIS water coolers, therefore, meet the requirements for avoiding crippling damage under combat conditions at shock levels exercised in the test by DYNA3.

After the basic analysis report was issued, the HD-1014/SPY-1A cooler incorporated heavier motor/pump assemblies — requiring an updated analysis with practically no change in the results. But a full-fledged DDAM analysis was added using the latest DYNA3 technology; it produced a lower factor of safety of 0.96, compared with the 1.02 factor obtained in the shock-pulse analysis (proving the compatibility of the two methods). As mentioned before, because of the tough material used, no failure of the unit is expected under test or operational conditions.

The analysis of the effects of ship's vibrations was made on only one cooler because the minimum factor of safety

Table IV. Summary mechanical data for AEGIS water coolers (WCs) obtained from RCA-DYNA3 computer program.

<i>Parameter</i>	<i>SPY-1 A WC</i>	<i>AN/SPS-49 Radar WC</i>	<i>Sonar Electronics WC</i>	<i>C&D Display/XCOM WC</i>
Natural Frequency (Hz)				
Soft Mounted	3.80			
Hard	19.66	25.24	21.34	19.22
Rigid	50.37			
Shock				
Maximum Gs	34.04z	35.13z	33.41z	32.57z
Minimum Factor of Safety	1.04	1.02	1.90	1.10
Ship's Vibrations				
Maximum Gs	4.17y			
Maximum Deflection (inches)	.184y			
Minimum Factor of Safety	18.09			

(18.09 in Table IV) was sufficiently high to be representative of the whole family of coolers. The analysis was made by making a sine sweep over all natural frequencies between 3.80 Hz and the AEGIS cutoff frequency, 25 Hz.

Conclusion

A thorough analysis of the AEGIS water-cooler units has demonstrated that all coolers will meet the requirements of the MIL-S-901 and MIL-STD-167 specifications. By using a computer analysis instead of actual shock testing on a barge, the Navy was able to save about \$1 million in testing costs.

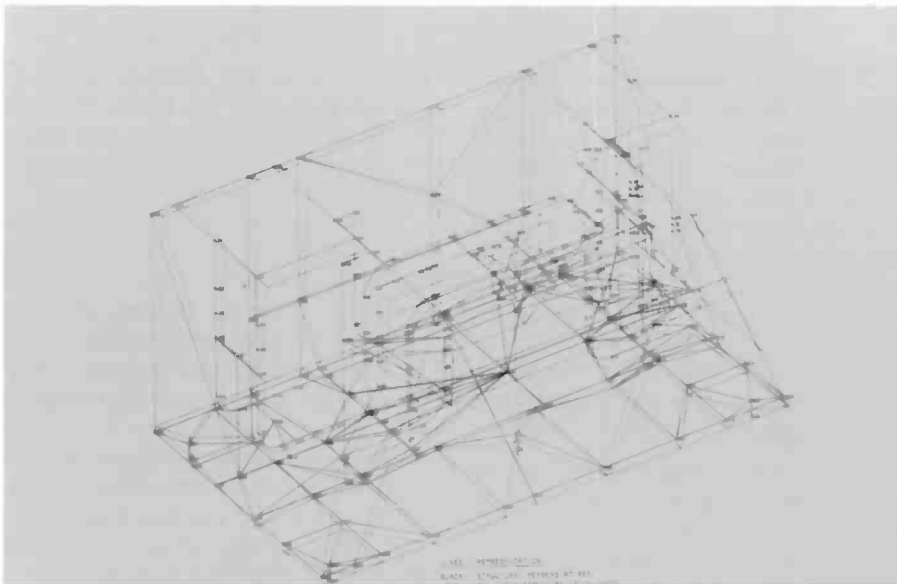


Fig. 7. Structural model of AEGIS C&D/Display/XCOM water cooler in Mode 1 (19.22 Hz) obtained from RCA DYNA3 computer program.

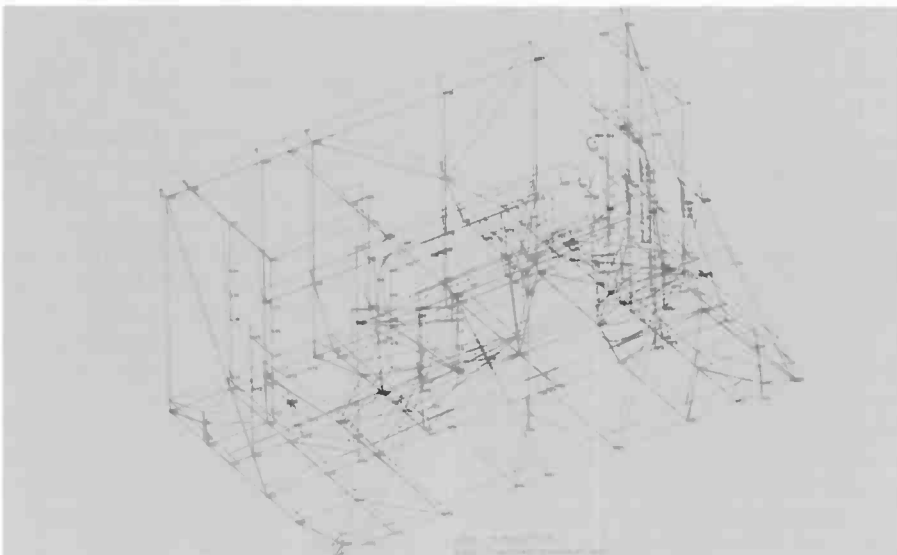


Fig. 8. Structural model of AEGIS C&D/Display/XCOM water cooler in Mode 2 (27.55 Hz) obtained from RCA-DYNA3 computer program.



Ralph Pschunder, Principal Member of the Engineering Staff, Moorestown, joined RCA Missile and Surface Radar (MSR) in 1959, where he contributed to the structural design and analysis of radomes, radar towers and foundations, cable structures, guyed and unguyed TV-towers. In 1969, he became involved in finite-element analysis and created the DYNA system of dynamics analysis, which is used by MSR to analyze ship's structures for the AEGIS project and all other work requiring static or dynamic structural analysis. He has supported other RCA divisions, such as Gibbsboro and Camden, in several projects involving the use of his structural computer programs. Dr. Pschunder was awarded four Chief Engineer's Technical Excellence Awards, one Annual Technical Excellence Award, and one Sarnoff Outstanding Technical Achievement Award.

Contact him at:
Missile and Surface Radar
Moorestown, N.J.
TACNET: 224-2531

Precision in large mechanisms — the near-field-antenna test scanner

Special bearing arrangements, controlled environment, and painstaking alignment by a laser interferometer help assure precision positioning of a large, cantilevered tower.

Abstract: *A critical element in RCA's automated near-field antenna-pattern test facility is the scanner mechanism, or X-Y positioner — a two-axis servo-controlled tower structure operating over a vertical planar area of 18 by 20 feet. This paper presents design features of the scanning mechanism and the methods used in achieving scanner-position accuracies of 0.010-inch RMS in all three directions. The author outlines system and element requirements, discusses error limits and describes the special alignment techniques employed.*

Most of RCA's radar antennas are developed and tested at the Missile and Surface Radar plant in Moorestown, New Jersey. An important part of this development facility is a group of outdoor test ranges, including one pedestal-tower combination suitable for testing large S-band phased-array antennas. This single range, although fully usable for testing developmental antennas, cannot be used to meet the pattern-testing load of antennas produced in quantities.

Accordingly, in 1977 MSR and Navy planners — anticipating a production contract for large numbers of AN/SPY-1A phased-array antennas (awarded in April 1978) — began a study of antenna testing capability. The study showed that although the test load could be partially relieved by multiple-shift operation, it could be resolved satisfactorily only by constructing additional far-field facilities.

Reprint RE-26-4-8

Final manuscript received Oct. 17, 1980.

Of course, this method of testing exacts a price — in the real estate required for far-field antenna operations; in the cost of antenna transport, test setup, and tear-down; in the expensive schedule disruptions due to rain, wind, ice, snow, and temperature variations; in the more subtle effects on antenna performance of solar radiation of varying level and direction; in the measurement errors induced by multipath effects; and in the need for several highly skilled test crews. The situation clearly demanded an alternative solution.

The alternative chosen was the so-called "near-field" testing technique. This approach cuts down the distance required between antenna and test sensor from several hundred feet to a few inches. It moves the sensing probe over the antenna aperture instead of shifting the antenna position relative to a stationary boresight tower which consists of a single RF source and an optical target, mounted on a tower 75 to 100 feet high, with the location of both accurately known with respect to the antenna under test. Perhaps most important, near-field testing can be conducted indoors, in a controlled environment. See box, "How near-field testing works," for a generalized description of near-field testing techniques.

The near-field concept has been under investigation and active experimental development since the early 1960s. The Georgia Institute of Technology and the National Bureau of Standards broke ground first, developing theory and sharing their early findings in the open literature.^{1,2} The results of these pioneering investigations were promising enough to encourage industrial investment, and a few

relatively small test facilities were constructed during the late 1960s and 1970s. RCA's Moorestown facility, the largest production system built at the time, is also described in the literature.^{3,4}

The scanning mechanism in RCA's near-field system is especially interesting because it exemplifies one approach to the problems in meeting extreme accuracies imposed on a heavy, cantilevered structure. This paper describes the concepts and the design practicalities, with a brief summary of near-field testing concepts provided as background. Scanner-accuracy criteria were the driving requirements for the configuration and mechanization of the scanning device. Test results, taken over an 18-month period, verified the device's structural integrity and the rigorous alignment and calibration procedures applied to it.

The problem

The principal objective of the total near-field program was to design and construct an automated near-field test facility that would satisfy the requirements of the AEGIS antenna and be operable by non-engineering, factory-test technicians. Thus, the data output had to be in a form that minimized the amount of technical judgment needed to make a correct decision on whether to accept or reject an antenna.

Another objective was to develop computer routines to aid in aligning the antenna receive beamformer, inasmuch as the near-field technique is well suited to identifying antenna aperture phase variations and predicting necessary adjustments to the waveguide alignment.

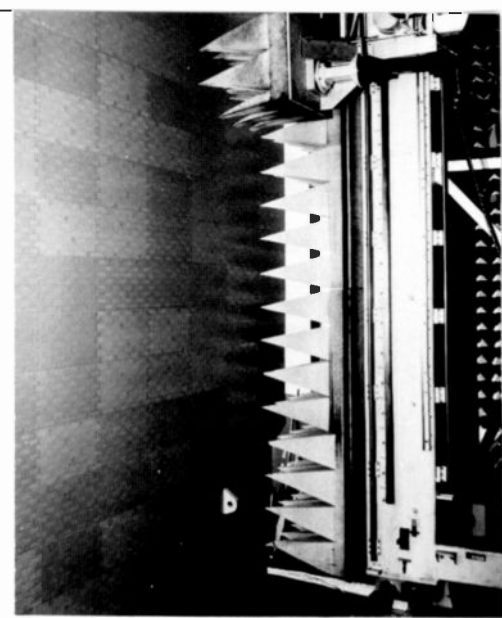


Fig. A. AN/SPY-1A antenna mounted for near-field testing. Waveguide at upper right leads to the scanner probe (hidden by RF-absorbing material).

How near-field testing works

Near-field antenna testing is based on the accurate characterization of the RF field (phase and amplitude) of a radar antenna over a measurement plane parallel to, and displaced a few wavelengths from, the antenna aperture's plane.

For any realizable, planar near-field range, the area of the measurement plane is finite, and the resulting truncation of the measured RF field defines the maximum angles that will yield accurate patterns.⁵ Unlike the standard far-field approach, which uses several hundred feet between the antenna and the boresight tower and which requires rotation of the antenna in both elevation and azimuth, the near-field techniques place a probe just inches from the stationary antenna face and employ linear (X and Y) probe motion. As a result, pattern coverage is limited to less than 180° in near-field testing.

In practice, engineers characterize the RF field by precisely positioning an RF probe at each intersection of an imaginary, uniformly spaced, orthogonal grid system in the measurement plane. As an example, the flat-faced AN/SPY-1A antenna (Fig. A) has nearly 4500 radiating elements arranged and spaced in an octagonal shape that approximates a circular pattern with an inscribed diameter of 12 feet. For the AN/SPY-1A, the scanning probe is driven vertically at constant velocity (about 15 cm/sec) from the bottom to the top of the coverage area (approximately 18 feet) while the tower maintains a fixed horizontal position. The phase and amplitude of the RF signal emanating from the single RF probe are sensed at 3-centimeter intervals over the antenna array's face.

As the slow-speed carriage return (50 cm/sec) brings the probe back to the bottom of the coverage area, the horizontal axis is simultaneously incremented 3 centimeters in preparation for the next cycle of data collection. During this 12-second period, the collected data is sorted and stored on disk. A single data point (a multiplexed collection of frequency setting, antenna channel designated for connection to a single receiver, and selected beam position) is sampled in 2.5 milliseconds, with an additional 2.0 milliseconds allocated for switching and settling. This time, the number of unique data streams and the data-point spacing determine the exact scan velocity.

One cycle of data collection is accomplished in less than one minute and is repeated for 201 scan lines; a complete area scan of the antenna face requires about three hours.

Even slight inaccuracies in probe positioning will produce errors in the measurement of antenna performance. There are three basic error sources in the mechanical scanner.

Two types of probe-positioning error are possible. First, out-of-plane displacement (Z direction) of the RF probe with respect to the measurement plane can occur, and second, in-plane horizontal (X) and/or vertical (Y) direction displacement of the RF probe with respect to the imaginary grid intersections in the measurement plane can happen. Pattern errors introduced by these two types of errors can be a function of antenna frequency, aperture size and illumination factor, and gain. These parameters, in combination with antenna beam-pointing angles, define probe-position-error limits and are critical because the cost of the scanning mechanism is directly affected.

The third source of error is multiple RF reflections from the probe, scanner, or enclosure as observed at the measurement plane. Judiciously placed RF-absorbing material, on and around the probe and scanner, will control these reflections. The ability to prevent RF reflections from the scanner is, to some degree, a function of the scanner configuration.

large size, and the stringent scanner accuracy needed to obtain accurate data (after transformation to the far-field), constituted the major elements of the mechanical engineering task.

System requirements

The overall near-field system specifications ensured a low probability of either acceptance of a defective array or rejection of an acceptable array. The requirements were:

- Reference pattern gain measurement within ± 0.3 dB;
- At least 80-percent probability that errors in measurement of low-level sidelobes will be less than ± 2 dB;
- Beam-pointing errors less than 0.25 mrad RMS;
- Accuracy of beamformer measurement of $< 2^\circ$ RMS for phase characteristics correlated over an array column and $< 3^\circ$ RMS for subarray evaluation;
- Minimum coverage equivalent to far-field coverage of ± 70 degrees from broadside; and
- Data sampling interval of 3 centimeters over the scan area.

These broad system specifications were then used to define critical scanner requirements:

- Scan area of 5.5 by 6 meters (vertical and horizontal, respectively);
- Position accuracy of 0.030 inch RMS in the X, Y, and Z directions; and
- Harmonic variation of 0.020 inch RMS for any single frequency in the X-Y plane or the Z direction

Near-field system performance is critically dependent on scanner accuracy. The scanner geometry of Fig. 1, in turn, influences the scanner error limits listed in Table 1.

The scanner tower and carriage are each viewed as undergoing translation and rotation about each of three orthogonal axes. One axis of translation is desired; all other motions are error sources. Geometric errors derive from crooked or non-parallel linear bearing shafts. These errors define alignment limits for all four shafts. The calibration procedures applied are summarized later in the paper.

Scanner facilitation

The scanner mechanism is a cantilevered tower (Fig. 2) supported by linear bearings

Beamformer adjustments of the array were previously accomplished (with difficulty) on the far-field range.

The size of the facility was determined by the 12-foot-diameter aperture of the

AEGIS array in conjunction with the requirement for far-field sidelobe data at nearly 90 degrees from boresight. These two factors together established the near-field scan plane as 6 by 5.5 meters. This

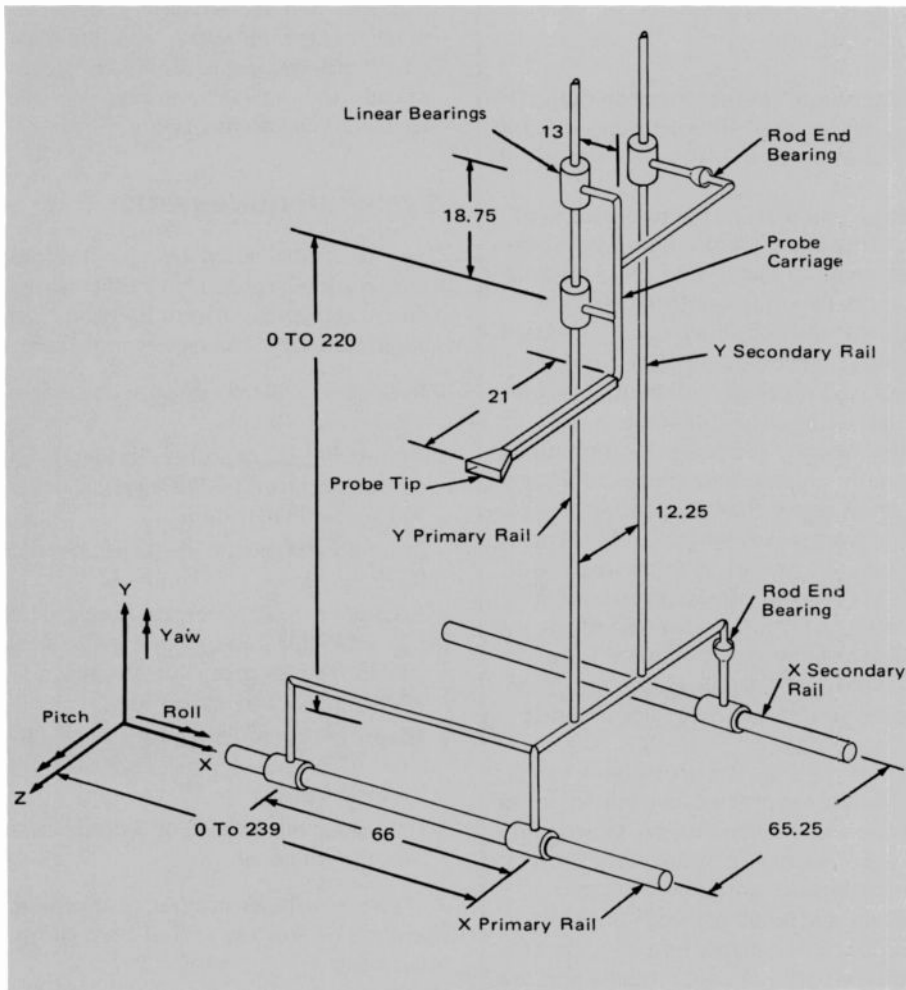


Fig. 1. Scanner geometry and coordinates (all dimensions in inches).

on two horizontal, floor-mounted shafts that allow the tower 6 meters of horizontal (X) travel. A probe carriage is supported by linear bearings on two vertical, tower-mounted shafts that provide for a carriage vertical (Y) travel of 5.5 meters.

A pair of pancake tachometers and a DC torque motor, housed together with a pair of bearings, create the drive-motor package used for both scanner axes (Fig. 3). The motor shaft drives a pinion gear (different tooth count for each axis) which engages a fixed rack gear in each axis.

Dual electro-optical digital encoders (5-bit and 13-bit) are driven from a separate fixed rack gear in each axis to report tower and carriage X and Y position to displays and to the computer. These units are identical for both axes (Fig. 4).

To minimize motor loads, the carriage is mass-balanced by a counterweight and pulley system. Redundant steel cables support the counterweight within the interior of a tower structural column.

Each axis applies two identical limit switches to control over-travel. In addition, six travel-arresting buffers (four in X and two in Y) are used to safely decelerate tower or carriage motion in excess of the travel limits.

An RF probe mounted on the carriage and connected to a remote transmitter is driven by a closed digital-control loop in a prescribed manner to collect RF phase and

Table I. Scanner error summary.

Error source	Errors (in 10^{-3} inches)		
	X	Y	Z
(1) Primary X-rail vertical plane, 0.002-inch straightness	13.9	3.1	0
(2) Primary X-rail horizontal plane, 0.005-inch straightness	3.5	0	7.7
(3) Secondary X-rail vertical plane, 0.003-inch parallel to (1) above	0	2.1	10.5
(4) Primary Y-rail X-Y plane, 0.004-inch straightness	5.3	5.5	0
(5) Primary Y-rail Y-Z plane, 0.004-inch straightness	0	9.0	5.3
(6) Secondary Y-rail X-Y plane, 0.004-inch parallel to (4) above	6.9	0	4.2
(7) Linear bearing clearance (0.005-inch adjusted)	1.5	1.3	0
(8) X-to-Y orthogonality error	8.0	0	0
(9) Encoder least-significant-bit error	0.3	0.3	0
(10) Encoder accuracy	0.3	0.3	0
(11) Encoder-pinion total composite error	0.6	0.6	0
(12) Rack-gear total composite error	13.2	13.2	0
(13) Rack-gear runout error (0.005-inch parallelism)	1.8	1.8	0
(14) Thermal errors ($\pm 5^\circ\text{F}$)	3.5	3.2	0.7
(15) Thermal gradient errors (10°F)	0	6.5	0
(16) Dynamic errors, Y-drive only	1.2	0.5	5.4
(17) Servo-position error	3.0	3.0	0
RMS error	6.3	5.1	6.4
Specification-allowable RMS	30	30	30

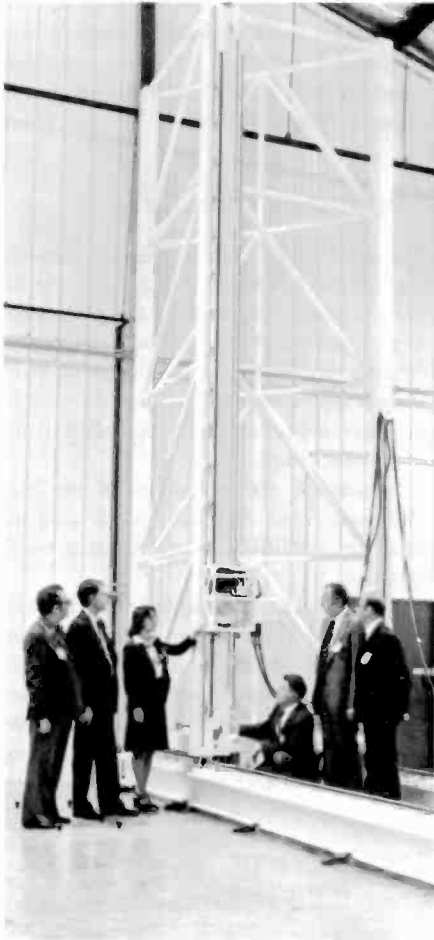


Fig. 2. RCA's near-field scanner mechanism. This photo was taken before the RF probe was installed. Indicated is the RF-probe carriage, which travels up and down the tower. The X rails for horizontal travel are located at knee level on top of the steel "I" beams.

amplitude data on the antenna under test (Fig. 5).

Configuration features

The cantilevered-tower scanner configuration is different from previous smaller units and offers several features that are advantageous in a production test situation. First, the scanner is independent of the building's wall and roof deflections caused by varying external wind, snow/ice or thermal loads. This is important because such deflections can alter the RF-probe position and thereby produce erroneous test results.

Second, the scanner tower and carriage can be completely covered and surrounded with RF-absorbing material to minimize multiple reflections.

Third, the critical horizontal rails are readily accessible for alignment checks — and realignment if necessary. In addition,

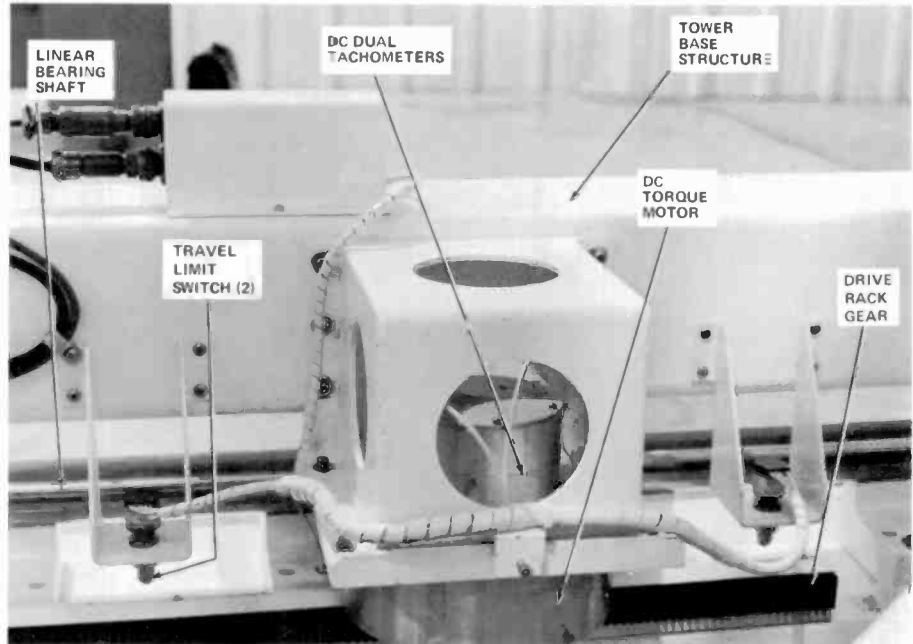


Fig. 3. X-axis drive unit. The motor-tachometer assembly is mounted on an interior face of the structural box beam at the base of the triangular tower. The drive gears are 20-degree pressure angle with a diametrical pitch of 12; the pinion gears use 22 teeth for the X axis and 48 teeth for the Y axis.

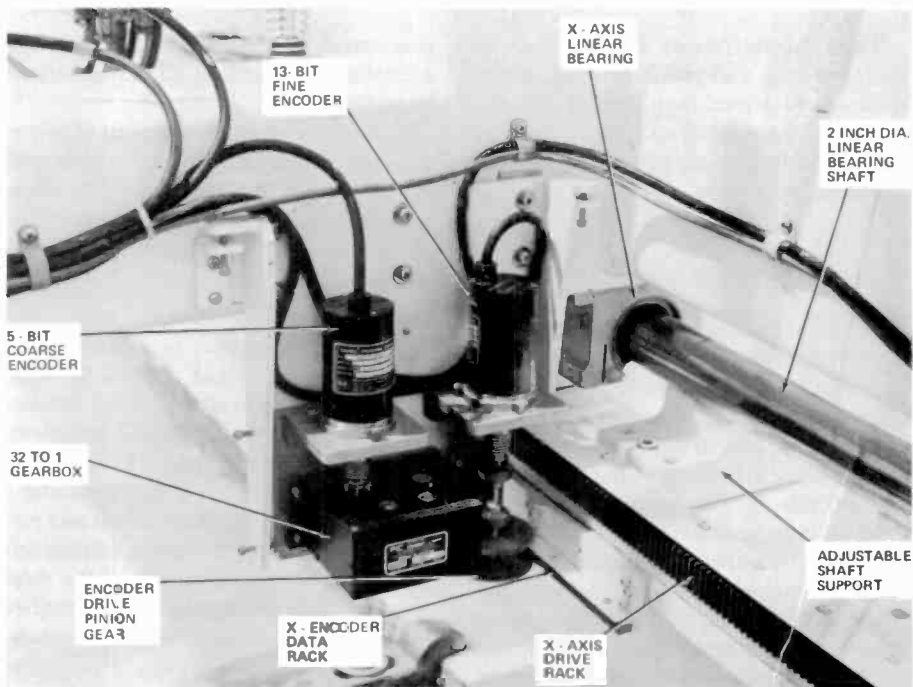


Fig. 4. X-axis dual encoders. The dual-encoder assembly (identical for both axes) is driven by a 20-degree pressure angle, 24-pitch, preloaded pinion gear engaging the data rack gear just below and parallel to the drive rack.

all devices are accessible from floor level for maintenance, repair, and replacement, with or without the test antenna in place.

The RCA system resides in a temperature-controlled environment. This, plus the all-steel construction of the scanner, minimizes thermal deflections of the RF probe and thus improves measure-

ment accuracy.

Since scanner/servo dynamic performance plays a major role in establishing the overall probe positioning accuracy, considerable effort was expended in the detailed system configuration design to overcome recognized sources of dynamic error.

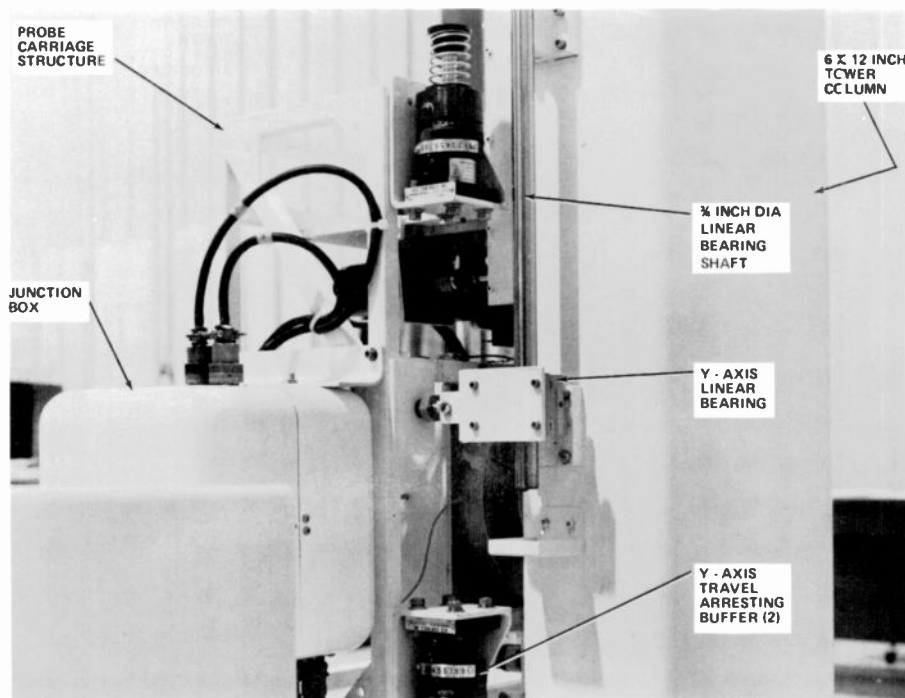


Fig. 5. Y-axis probe carriage. This view shows the single, linear bearing engaging the 3/8-inch diameter rear-bearing shaft. This mechanism and the dual bearings on the front shaft (not visible) constitute the precision carriage "ways."

These considerations included use of standard rack-and-pinion gearing, incorporation of closed-loop analog velocity and damping control, an isolated foundation of 12-inch-thick concrete, and stiff structural load paths.

Scanner calibration

The accuracy of the system depends on the alignment of the individual elements listed in Table I. The most difficult and time-consuming part of the procedure was the alignment for rail straightness, performed on each plane individually (items 1 through 6 in Table I). This alignment was not achievable by ordinary means.

A laser straightness interferometer, with optics arranged to interferometrically measure deviations from the laser-beam centerline in a single plane at a time, was applied to accomplish the rail straightness alignment. In addition, after alignment of all elements, the laser was applied in both distance-measuring (to verify items 9 through 13 in Table I) and straightness modes to provide a direct-accuracy calibration.

Calibration consisted of measuring the X, Y, and Z errors of the RF probe tip as a function of its X and Y position. Five separate error parameters were measured (X, Y, Z, tower-roll, and tower-pitch angle) as a function of X position; three error

parameters (X, Y, and Z) were measured as a function of Y position, all at 3-centimeter intervals.

The nearly 1600 measurements of probe-tip errors were then combined to yield total probe-tip X, Y, and Z errors over the entire scanner coverage area, approximately 37,000 data points for each of the three error components.

The Z-direction errors were then redefined with respect to a least-square error-fitted flat plane which, in turn, defined the plane to which the test antenna was aligned within 0.25×10^{-3} rad about three axes. The RMS and peak values of all three error fields were determined and a two-dimensional Fourier analysis was performed to evaluate harmonic amplitudes.

Table II shows the results of the three separate calibrations, along with specified requirements and the error budget values.

Table II. Summary of calibration results.

Axis	Probe position errors (in 10^{-3} inches)					Maximum harmonic component (in 10^{-1} inches)			
	RMS specified	RMS budget	RMS measured			Specified	Measured		
			11/78	5/79	4/80		11/78	5/79	4/80
X	30	6.3	6.3	9.9	11.0	20	2.8*	5.3*	6.4*
Y	30	5.1	7.5	8.4	7.4				
Z	30	6.4	4.3	7.0	6.7	20	1.3	2.5	2.3

* The X and Y error measurements are combined as complex values and this single array is examined for the maximum harmonic component.

The measured results are significantly better than the specification, indicating a minor impact for S-band antenna measurements and a potential for use at higher RF frequencies.

Alignment stability

The results of Table II indicate that the scanner's RMS error was quite stable for the 18 months spanned by the calibration measurements. Although the X error grew monotonically, this growth resulted from known disturbances. The periodic or harmonic errors are also well controlled within these allocations.

In general, the variations of the May 1979 and April 1980 calibration data are small, as would be expected for a stable system.

The first AEGIS array tested in the near-field range was also tested on the older far-field range. A comparison of the measurements from both ranges showed excellent correlation. These results fully qualified the system for production testing, at a rate of one array per month.

The future of near-field testing

Although the MSR range was designed specifically for AEGIS antenna pattern tests, it is, of course, useful for other antennas. This range is large enough for antennas up to approximately 16 feet in diameter, depending on the angular extent of far-field pattern coverage required.

The facility uses RF equipment selected to match the AEGIS array and is, therefore, limited to a specific frequency band. Near-field pattern measurement accuracy is also influenced by the operating frequency, such that each antenna/frequency combination must be examined in detail.

Only a few working near-field test ranges exist today, but new ranges currently being

implemented will shortly double the total number. The scan area of the near-field systems being built is also increasing significantly, although not so rapidly as the number of ranges.

The present state of scanner accuracy is adequate for lower-frequency antennas, but may become a limiting factor as scan area and frequency increase. This limit may be overcome by computerized position-correction schemes to avoid the high cost of built-in accuracy. Such schemes are already under investigation and may become mandatory as the current trend continues toward antennas with very low sidelobe levels.

The continuing efforts to develop cylindrical and spherical techniques, as opposed to planar methods, should bear fruit in the next several years. These approaches will eliminate the pattern-coverage limit inherent in the planar approach.

Finally, microprocessors will be used increasingly for real-time control, data reduction, and calibration functions. These devices will help to eliminate some of the costly software and provide improved system reliability.

References

1. Kerns, D.M., "Plane Wave Scattering Matrix Theory of Antennas and Antenna-Antenna Interaction: Formulations and Applications," *Journal of Research of NBS*, Vol. 80B, No. 1 (Jan. Mar. 1976).
2. Crawford, M.L. and Newell, A.C., "Planar Near-Field Measurements on High Performance Array Systems," NBSIR 74-380, National Bureau of Standards (July 1974).
3. Harmening, W.A., "Implementing a Near-Field Antenna Test Facility," *Microwave Journal*, pp. 44-55 (Sept. 1979).
4. Staiman, D., "Automating Near-Field Antenna Testing for Phased Array Radars," 1980 IEEE International Radar Conference, *Record*, pp. 248-252.
5. Grimm, K.R., "Antenna Analysis by Near-Field Measurements," *Microwave Journal*, pp. 43-52 (April 1976).

Wayne Harmening is a Principal Member, Engineering Staff, in the Structures and Pedestal Design group of Missile and Surface Radar's Equipment Design and Development section. He joined RCA in 1959 following eight years as a design and dynamics-analysis engineer in the aircraft industry. For the past 20 years he has been involved principally in the conception and design of special structures for precision tracking radars and related systems. As a result of his work on the near-field scanning



device he received MSR's Annual Technical Excellence Award for 1979.

Contact him at:
Missile and Surface Radar
Moorestown, N.J.
TACHET: 224-2397



New Publication from the RCA Engineer

According to the RCA Engineering Information Survey conducted in 1977, the *RCA Engineer* is the second most important source of technical information about RCA, (the most important information source being the engineer's associates). The back issues of the *Engineer* — 150 of them — provide a record of RCA's progress in invention, development, and manufacturing. To make this wealth of technical information accessible to the engineers, a *25-Year Index to the RCA Engineer* has been published.

The *Index* can help you find specific information that is needed in your work. Or the *Index* might provide a vital contact in another RCA business who has related experience and who would be willing to consult with you. The *Index* gives you the opportunity to profit from RCA's technical heritage — to reuse knowledge, to build on past accomplishments.

The *25-Year Index to RCA Engineer* is available in all RCA Libraries. Recipients of the *RCA Engineer* can obtain their personal copies by writing to:

RCA Engineer
 Building 204-2
 Cherry Hill, NJ 08358

The role of mockups in improved equipment design

A mockup of an engineering system is a valuable design tool for the engineer and a visual aid for the customer.

Abstract: *Two- and three-dimensional mockups are increasingly valuable engineering design tools. With appropriate contributions by human-factors engineers and industrial designers, the mockup can increase acceptability and operational efficiency. This article describes a new cost-effective mockup technique and the benefits of involving a human-factors/industrial-design team in mockup formulation. The author also discusses applications other than design tools — marketing displays, system hardware integration, documentation, operator training. The mockup, a full- or reduced-scale three-dimensional representation of hardware, is one of the more effective tools used by human-factors and industrial-design personnel during the development of manned systems. Although mockups are by no means new, this article indicates how their full potential can be realized.*

Human factors engineers help tailor a given system to the abilities and limitations of the eventual equipment user. They bring to this task knowledge of and experience with people's physiological, psychological, and behavioral characteristics. They know how the equipment must be adapted to the operators. The industrial designers share the human-factors specialists' concern for the functional aspects of equipment design. In addition to their general engineering background and their understanding of materials, components, and structural design, the industrial designers can skillfully translate design concepts into sketches, models, and full-scale mockups. Trained in

art, they are sensitive to the equipment's appearance. They know that an aesthetically pleasing, functionally designed device will give the user confidence in, and respect for, the equipment. Industrial designers and human-factors engineers thus have interests and skills that complement each other.

Since the mockup often becomes a focal point for an ongoing design effort, its development provides an excellent opportunity to introduce and implement human-factors engineering and industrial-design consideration. Gaining acceptance for a design recommendation at the mockup stage is far simpler than persuading project office or engineering personnel to modify an existing design to comply with users' recommendations. Construction of the mockup, supervised by an industrial designer, is not generally a goal in itself but is a design tool or a means of communicating industrial-design and human-factors-design principles to other engineers or to the customer.

Mockup applications

An early definition of the objectives to be satisfied by a given mockup will determine the nature and requirements of the mockup development program. Nine possible objectives are:

1. *As design integration aids.* In this era of complex space, military, and commercial hardware systems, no individual has a complete understanding of the detailed design responsibility for the whole system. Consequently, the design of any large system is a piecemeal affair that not only spans the efforts of individual design groups within a company, but often em-

braces the efforts of many companies. With all of the well-known obstacles to effective and timely communications, a mockup can very effectively integrate the efforts of the many and scattered individuals contributing to the program. By using such an integrating device, costly errors that might otherwise require redirection of design efforts can be avoided, depending upon the stage of development when the problem is discovered.

2. *As a means of verifying and validating man/machine interactions.* Conceptualizing the end product from a reduced scale drawing or rendering is often extremely difficult. But determining the ease or difficulty with which the ultimate users will be able to interact with the equipment is even more difficult. In a full-scale mockup, people can dynamically simulate the operational tasks associated with operating or maintaining the equipment. If reading a control, viewing a display or opening an access door is impossible, the mockup will quickly disclose the deficiency. The chances of finding such design errors during dynamic simulations are much better than trying to do so while scanning engineering drawings. The mockup is especially useful in verifying the effectiveness of man-machine interactions when the operator's movements are encumbered by equipment or components, or by items of personal equipment or clothing. The mockup also permits the initial verification of system design and operational/maintainability procedures.

3. *As a means of evaluating alternative approaches.* Depending upon the type of materials and the construction techniques employed, engineers can use the mockup to evaluate alternative design approaches.

Mockups of candidate workstation design made of low-cost foam-core sheeting can be readily assembled using only a knife, some glue and tape. Similarly, low-cost solidified bulk foam (styrofoam) can be used for scale models of equipment shapes. Styrofoam is easily shaped with a hot-wire cutter. The resulting models are particularly useful for facility layout studies. Unworkable arrangements can be rapidly identified and immediately corrected as opposed to situations in which the problems are dealt with in numerous design reviews, where decisions are often difficult to achieve.

4. *As three-dimensional conceptualization aids.* Engineers are usually quite adept at visualizing three-dimensional objects from two-dimensional representations such as scaled-down engineering drawings. But limits exist to the degree of realism or "feel" for the final product they can obtain from such drawings. This is clearly shown by the typical engineer's first reaction to a mockup of a design he worked on for several months. Statements such as "Is that really what it looks like?", "I didn't know it was so big," or "I thought that component would pose a real access problem" indicate that his original visualizations missed their mark.

5. *As documentation aids.* In place of numerous sketches and detailed engineering drawings to record the evolution of a design, a series of photographs can be used to show successive mockup modifications leading to the final configuration. Earlier configurations can easily be recreated if mockup parts are retained. Should pictorial or perspective drawings be desired of the equipment or the workstation layout, an illustrator can more easily work from a photograph taken at the correct angle. This can save many manhours required to develop the appropriate vanishing points and to translate plots from two- to three-dimensional scales prior to creating a desired rendition. The photographic approach is particularly helpful for renderings of complex designs or facility layouts that require many pieces of equipment.

6. *As training aids.* A mockup can be useful long after the hardware design has crystallized. In accelerated programs, the equipment operator and supporting personnel must assume their duties as soon as the equipment is operational. This means that the operators must be trained before the operational equipment is available. In

this situation, mockups often become important training aids. They give the trainee a degree of familiarity with the equipment that cannot be derived from training manuals.

7. *As presentation aids.* A mockup is an excellent "selling" aid. It can be used to persuade management on the merits of investing funds in a new product or to encourage potential customers to sponsor a program. It can also be used to convince a project manager that one layout is superior to another. Furthermore, the mockup is a useful device in apprising management and the customer of progress on a program. A mockup can be shown to a customer at proposal time or during periodic program reviews. Audience reaction and interest is much greater than for the usual vugraph presentations.

8. *As public relations tools.* A coat of paint, a realistic display (perhaps from a slide projector focused on a rear projection screen in the mockup), and an RCA logo can transform a utilitarian mockup into a valuable public relations device. The mockup can be used as the focal point of interest at a proposal presentation, it can be the subject of publicity photographs, or it can be exhibited at various professional meetings. It can be used to acquaint VIPs with a facility layout or to brief visitors on the functions and operational features of a piece of equipment.

9. *As production tooling patterns.* In the case of a military product or a large system, production quantities are often very low. In this situation a suitably constructed

mockup can serve as the production pattern, thus saving the cost of intricate drawings (especially if the equipment contours are complex) or the cost of having a pattern made (if the item is to be a cast or vacuum-formed). Should drawings be required, the mockup represents an ideal means of communicating dimensional and spatial relationships to the draftsman, since it minimizes the need for interpretation and verbal instructions.

Application of a new mockup technique

The idea of a mockup is often overlooked or discarded by a project manager or engineer because of his preconceptions regarding mockup construction and cost. Construction times and costs vary greatly with levels of fidelity and complexity, and with the choice of mockup materials. These investments range from an expenditure of only a few hours construction time and a few dollars worth of cardboard and tape for a console mockup to many hours and dollars for a dynamic, dimensionally accurate mockup; for example, an AEGIS Cruiser Combat Information Center. Quick solutions to man-machine problem areas, not readily solved by resorting to a handbook or making a detailed sketch, can often be obtained using a "design study" mockup.

A case in point was the use of scale models during the facility design for an experimental electronic mail handling center. Realizing the potential uses for a design study mockup and the number of

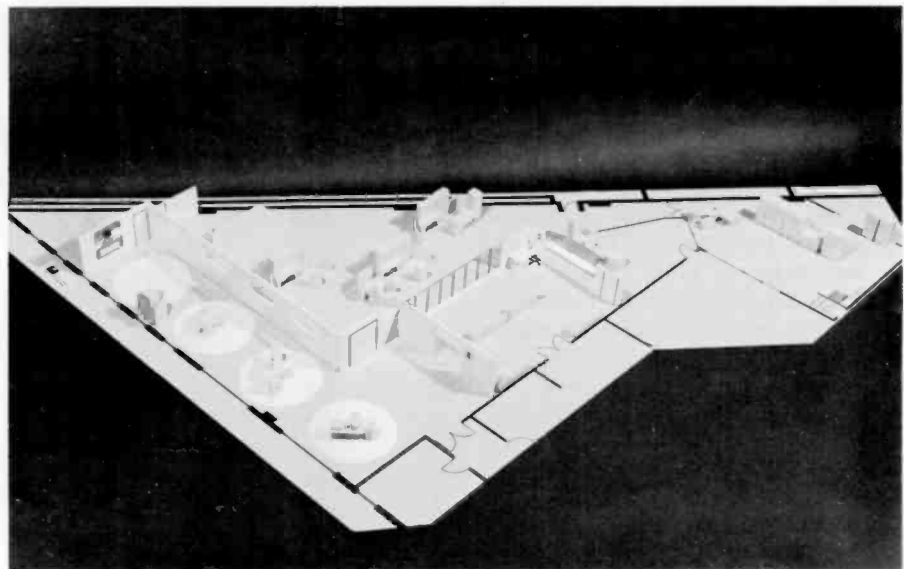


Fig. 1. High-density styrofoam mockup with components formed by hot-wire cutter. Scale is half-inch-to-the-foot. The foldable base is 70 x 30 inches.

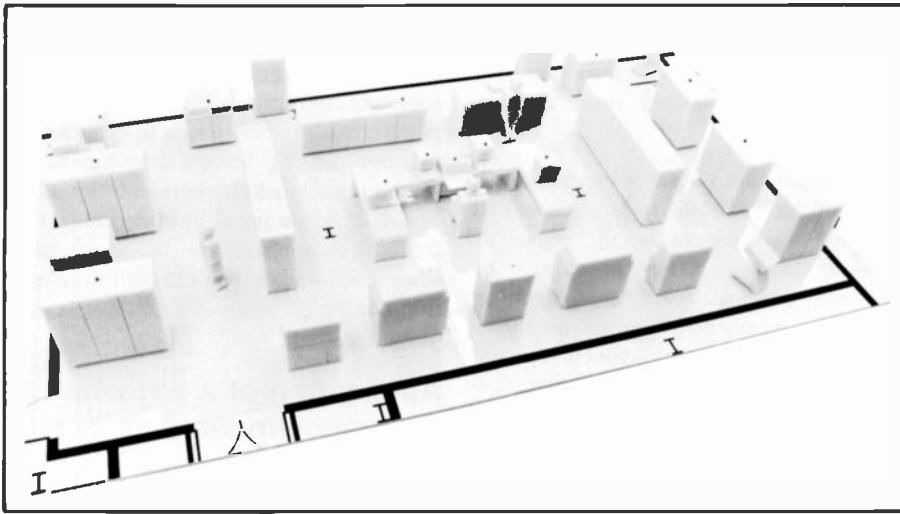


Fig. 2. Computer room layout. Scale is three-quarters-inch-to-the-foot.

questions it can help to answer, the MSR Man-Machine Systems Group, when contacted by the GCS Special Systems Group for layout and interior design recommendations, searched for a fast and inexpensive method to construct scale models. Previously, illustration board or polystyrene sheet materials had been used to create equipment shapes. Both materials require excessive time to cut the material, glue it together, and apply final finishes. After reviewing other materials, we selected a high-density styrofoam, used for insulation by the construction industry, and fabricated a hot-wire cutter to form the shapes.

Figure 1 represents the results of 16 hours of construction time and \$10 worth of styrofoam, illustration board, and tape. The mockup was fabricated at a half-inch-to-the-foot scale and contained 55 separate items of equipment on a foldable 70-by-30-inch base. This mockup — initially built as a design study tool to evaluate equipment-to-equipment and man-to-equipment relationships, material and personnel traffic patterns, and overall facility layout — was used for three design reviews at a remote facility and is now being displayed at the customer's facility where the equipment is being installed. The customer is using this early mockup to orient and brief Government representatives and his potential customers. Moreover, this early mockup formed the basis for plan-view layout drawings, facilitated by the fact that the equipment forms had been placed on one-eighth-inch grid. It was subsequently photographed and the pictures were then easily transformed into detailed three-dimensional illustrations for the facility design report.

The same modeling technique was used to develop a computer room layout for a recent proposal effort. The mockup, pictured in Fig. 2, was designed to a scale of three-quarters-inch to the foot, since it was to be used for presentation, and yet be readily transportable. The entire model could be folded up to suitcase size. Since the equipment was to be located in an existing room, the first design step was to replicate the floor plan and to depict all

known items of interference (columns, door openings, etc.) on the base. After assembling the equipment dimensions and descriptions, engineers formed each item from the rigid styrofoam material and attached a paper base. The paper base cemented to the bottom of each model defined the required maintenance area and access panel or door openings (Fig. 3). To further indicate equipment constraints, equipments that had cable length restrictions to other equipments were coded with colored tacks. Thereafter, the process of laying out the room became a relatively straightforward task of arranging the equipment to satisfy the requirements of the computer room operators.

With the three-dimensional representations, the task of creating an operationally satisfactory layout was aided by the fact that the designer could mentally place himself in the position of each operator. Visual and physical access requirements for seated or standing operators could readily be confirmed, and traffic patterns easily comprehended. Once the layout was approved, final touches were applied to make the model presentable for the customer; the device was then prepared for shipping.

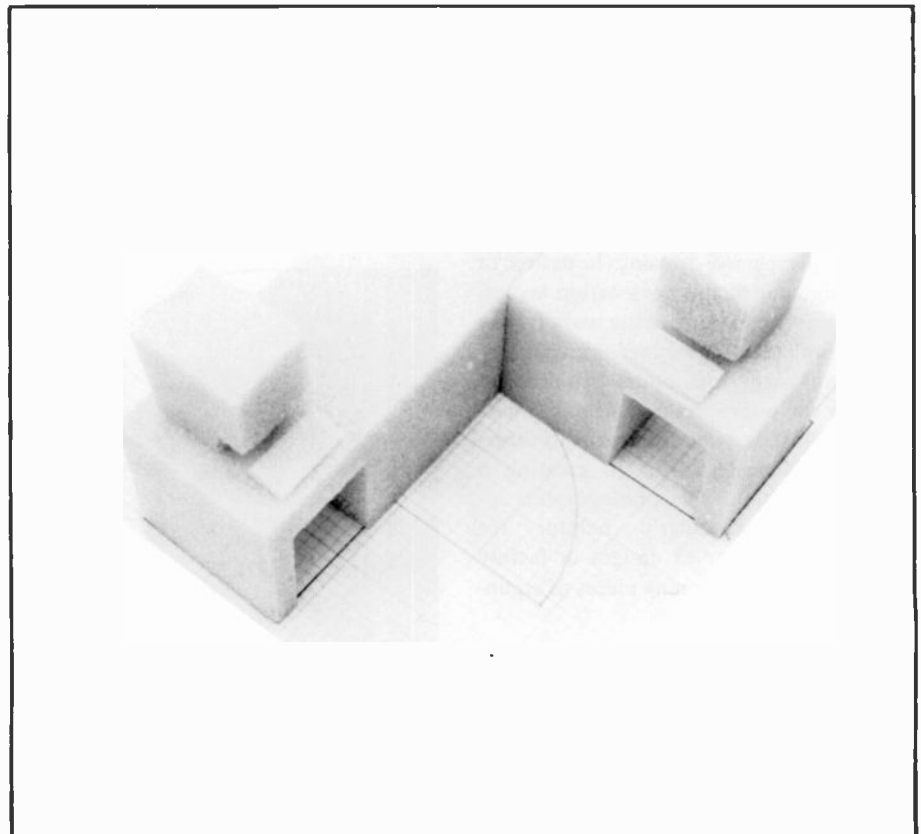


Fig. 3. Close-up of model showing required maintenance area and access panel or door openings.

To reduce the presentation set-up time, the paper bases were removed from each equipment model, and each item was secured to a piece of clear plastic that was keyed to the floor plan base. Equipment labels were prepared for each item in the layout and models of people were introduced to give the reviewers a sense of scale. The final step in the process was to build a "suitcase" for the 27-inch-deep by 45-inch-wide by 5-inch-high mockup that did not exceed the baggage size requirements established by the airlines, and was strong enough to withstand airline baggage handling. The mockup, in its shipping configuration (folded) fit into a special case, made of quarter-inch foam-core board, that measured 28-inches deep, 25-inches wide, and 8-inches high, and weighed only about 15 pounds. The mockup arrived at its destination unharmed and became the focal point of the three-day proposal presentation. The model was subsequently left with the customer.

Conclusion

These inexpensive foam mockups thus served a number of purposes. They were used as design integration aids, allowing a number of disciplines to participate in the design process; as a rapid tryout and evaluation of different design approaches; and as presentation aids/public relations devices. While the foam mockup approach has only been used for scale mockups of facility layouts, this technology is also applicable to full-scale models of small equipments and components.

Charles Tipple is Unit Manager, Industrial Design, within the Man-Machine Systems group at MSR Systems. His group analyzes the functional and operational requirements of equipment and the integration of the requirements into successful product design solutions. Previously, he was Unit Manager of the Human Factors group. He joined RCA in 1969 as a member, Engineer-



ing Staff, Industrial Design group, and he has worked on numerous commercial and military programs.

Contact him at:
Missile and Surface Radar
Moorestown, N.J.
TACNET: 224-3406

Air-lubricated thermal processor for dry silver film

Following a reconnaissance mission, tactical commanders may view dry silver film almost instantaneously, but the quality of the image depends on the processor's ability to give uniform optical density.

Abstract: RCA has developed two thermal processors for dry silver film. Made to give uniform optical density, they are different in implementation but based on the same philosophy. Pressurized air, directed to both sides of the film, supports the film and conducts the heat to the film. Porous graphite is the medium through which heat and air are introduced.

Since dry silver film is processed by heat, it may be viewed on a light table only seconds after exposure. On the other hand, wet films require both bulky chemicals and substantial time before an image can be analyzed. Processing of dry silver film, although simple in concept, is not so simple in practice. The main concern is the effect of film-temperature gradients on the uniformity of optical film density.

RCA has developed two thermal processors, different in implementation but based on the same philosophy. Pressurized air, directed to both sides of the film, supports the film and conducts the heat to the film. Porous graphite is the medium through which heat and air are introduced.

The initial thermal processor was designed to process 9.5-inch-wide film moving at speeds ranging from 0.0034 to 0.008 inch per second. The processor configuration was curved to match the plane generated by the laser recording beam.

The second thermal processor was configured to process 5-inch-wide film moving at a continuously variable rate ranging from 0.15 to 3.5 inches per second. Due to field-flattening optics used in this laser

recorder, the required film processing area was planar. In addition, this processor was sectioned in the direction of film motion, so that the processor could vary both the temperature and the effective processing area.

How do the characteristics of dry silver film affect film-processor design? One important reason for using dry silver film (compared to wet-processed film) is that the processed film may be viewed almost instantaneously. This feature is highly desirable for reconnaissance missions where a tactical decision must be made immediately following surveillance. The quality of the image primarily depends upon the ability of the processor to generate uniform optical density.

Dry silver film is processed by maintaining the film at an elevated temperature (210°F to 330°F) for a fixed time (a few seconds). The film uses an emulsion system in which all elements are built in. A latent image is transformed into a visible image seconds after the heat activation of the process/fix chemistry integral to the dry silver film. Dry silver film, however, does have some unique processing characteristics that a designer must consider in his overall evaluation.

Processing temperature uniformity in the range of $\pm 1^\circ\text{C}$ is a goal, if film-density variations are to be minimized.

General thermal processor background for dry silver film

Many approaches for processing dry silver film have been tried. The two most common approaches employ heat transfer to the film by conduction:

$$q_k = kA \frac{\Delta T}{\Delta X} \quad (1)$$

and convection:

$$q_h = hA\Delta T \quad (2)$$

The conduction approach usually employs a heated roller, which couples the heat into the film as shown in Fig. 1.

The convective processor approach commonly passes film between two surfaces that may be: heated only; or segmented to allow heated, low-pressure air to go through; or porous to allow heated, pressurized air to pass through as shown in Fig. 2. Equations (1) and (2) show that to achieve constant heat transfer, the two parameters of concern are the temperature difference (ΔT) between the heat source and the film, and the heat-transfer coefficient (k or h). The film thickness (ΔX) is basically a constant and the area (A) to be heated can be controlled easily.

Since careful processor design can minimize temperature variations of the

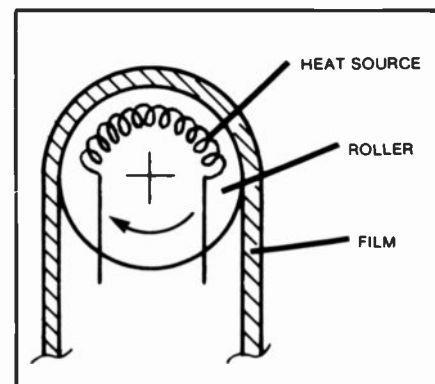


Fig. 1. Dry silver film processing by conduction.

Reprint RE-26-4-10
Final manuscript received Dec. 24, 1980.

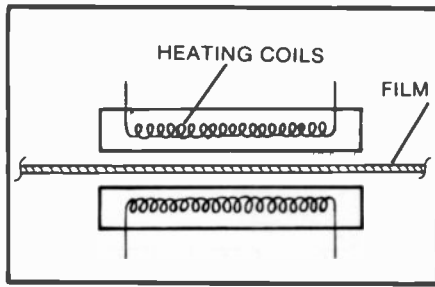


Fig. 2. Dry silver film processing by convection.

heat source, there is some control over that parameter. The parameter that is most difficult to control and that has the most effect on density uniformity is the heat-transfer coefficient. In a conductive processor, the surface contact between the heating surface and the film must be intimate and constant. Air gaps caused by particles of dirt lodged between the film and the heating surface cause "halo"-type density variations. Film-tension irregularities, heating surface (drum) irregularities, and the rms surface finish of the heating surface itself contribute to variations in the heat-transfer mechanism and thus cause density variations on the film.

In a convective processor, the constancy of the heat-transfer coefficient is further compounded by convective air currents and variable air gaps. Film scratching and film softness at elevated temperatures are additional considerations. Relative motion between the emulsion side of the film and its heat source — when in contact — causes scratches that will cause loss of information on the film. Still another film phenomenon, film limpness, has to be considered during processor-design evaluations. The film is so limp at elevated temperatures that it may be thought of as a "wet noodle."

When the concerns stated above are analyzed in detail, it soon becomes apparent that processing by conductive or convective methods involves characteristics that must be carefully considered. To control the parameters described above, and thus minimize density variations, constitutes a formidable design task. In addition, it should be noted that in processor designs where there is only one heating surface, a temperature gradient always exists between the film and the heat-supplying surface. This effect is aggravated if the contact between the film and the heated surface is poor due to dust, tension variation, surface finish, and so on.

Caution has to be exercised when designing a convective processor because the gap

between the film and the heated surface affects the heat-transfer coefficient. An evaluation of the considerations presented above, shows that film-density variations can be minimized if the film is suddenly plunged between two heated, closely spaced plates of equal temperatures. The object is to eliminate ΔT between the film and its surroundings, thus removing the heat-transfer coefficient as a variable. This approach is possible because the mass of the film is relatively small compared to the mass of the surrounding heating elements. The result is very quick heat-up of the film, with the temperature of the surrounding heating elements changing very little.

With the above in mind, we now present a scenario of a convective thermal processor. If heat is supplied at a constant temperature to both sides of the film simultaneously by means of pressurized heated air, the film-density variations will be minimized. Different convective techniques have been tried previously. Using fans in conjunction with coil-heated air, Owsley experimented with a convective processor. But he had difficulty maintaining temperature uniformity, and thus

uniform density, over the width of the film.

Film density normal to the direction of film motion is primarily affected by the uniformity of the processor's heat transfer, whereas the film density parallel to the direction of film motion is primarily affected by the film's speed variations.

RCA's general approach to a convective thermal processor

Previous experience and analysis postulated the following guidelines:

- The film shall pass between two flat surfaces maintained at a constant temperature;
- The film shall not contact the heat-transferring surfaces; and
- The gap between the film and the surfaces shall be minimized (about 0.002 inch) in order to approach heat transfer by conduction as compared to convection.

Film-flotation and air-bearing experience led us to the configuration shown

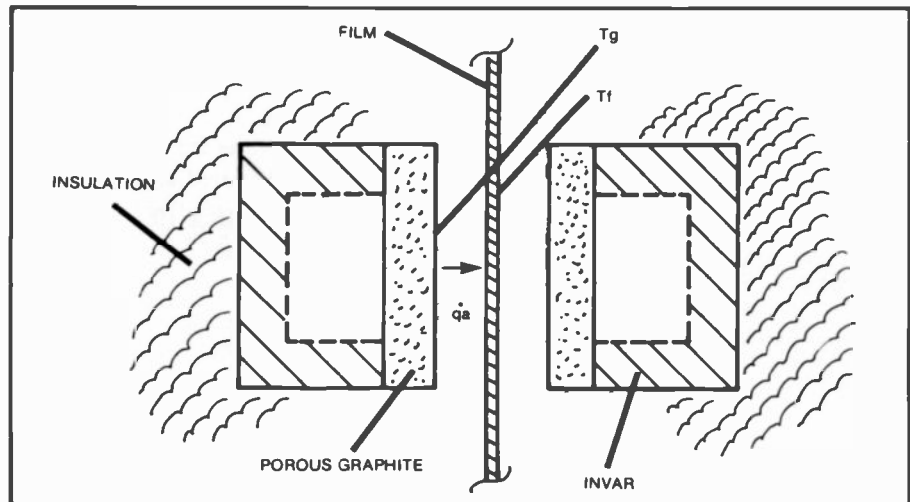


Fig. 3. Dry silver film processing by convection—the RCA approach.

Material	$in/in^{\circ}F \times 10^{-6}$	Thermal Conductivity BTU/hr $ft^{\circ}F$
Graphitar 2	1.9	6.3
Invar 36	0.9	6.05
Aluminum	13.3	117.0
Copper	9.2	224.0
Steel (1%C)	6.5	26.2
303 SS	9.0	12.4
Glass	2.5 - 5.0	0.3 - 0.5

Fig. 4. Linear coefficient of thermal expansion and thermal conductivity data for different materials.

Design Example

Airflow through the porous graphite is:

$$Q_p = \frac{k_p A (P_s^2 - P_a^2)}{2.26 \times 10^{-6} H}$$

where

$$k_p = 0.47 \times 10^{-11} \text{ in}^2$$

$$P_s = 34.7 \text{ psia}$$

$$P_a = 14.7 \text{ psia}$$

$$H = 0.10 \text{ inch}$$

$$A = (0.3)(11) \text{ in}^2.$$

From this

$$Q_p = 6.78 \times 10^{-2} \text{ cfm} \quad \text{and} \quad Q_a = 0.11 \text{ scfm.}$$

If all the energy supplied to the air is used to heat the film, then

$$\dot{q}_a = hA (T_g - T_f)$$

$$\dot{q}_f = mc_p \frac{dT_f}{dt}$$

If $T_g - T_f = \theta$, then $\frac{dT_f}{dt} = -\frac{d\theta}{dt}$ with T_h held constant.

Since $\dot{q}_a = \dot{q}_f$, then $hA\theta = -mc_p \frac{d\theta}{dt}$ and $\int_0^t -\frac{hA}{mc_p} dt = \int_{\theta_i}^{\theta_f} \frac{d\theta}{\theta}$.

This results in $\frac{\theta_f}{\theta_i} = \exp - (hA/mc_p)t$ or $\frac{\theta_f}{\theta_i} = \exp -t/\tau$.

If the required film speed is 0.03 in/s and the film must remain at a specific temperature for 10 s to obtain a specific optical density, then the required processor length is 0.3 inch. Both speed and temperature may be changed while still obtaining the same optical density.

Using the previously presented equations, heat-up time for a film 9.5-inches wide x 0.3-inch long x 0.0034-inch thick is calculated as follows:

Since $\sigma = 0.05 \text{ lb/in}^3$ (density of Mylar), then $m = 0.48 \times 10^{-3} \text{ lb}$.

Since $h \approx \frac{k}{d}$ (for small gaps), then $\tau = \frac{mc_p d}{kA}$

$$\tau = 3.52 \times 10^{-7} \text{ hours, or } 0.0013 \text{ second.}$$

Now, heat-up time to within 0.5°F will be calculated.

$$\text{Since } t = -\tau \ln \frac{\theta_f}{\theta_i}, \quad t = 0.008 \text{ s.}$$

This analysis states that if a section of film 9.5-inches wide, 0.3-inch long, and 0.0034-inch thick is suddenly plunged between two plates at 260°F , it will take the film 8 ms to reach a temperature of 259.5°F . Figures 5a and 5b show how air-gap width (d) and the temperature difference between the temperature reached and steady state temperature (θ_f) affect heat-up time.

in Fig. 3. Graphitar (U.S. Graphite Co.) was known to be a stable porous material with a coefficient of expansion closely matched by Invar 36™ (Carpenter Steel Co.), as shown in Fig. 4.

To obtain better appreciation for the width of the thermal processor, the required air-flow as well as the time required to bring to temperature a section of a film,

a design example (see box) is presented for a configuration shown in Fig. 3.

Design of a narrow curved processor

The curved thermal processor approach is shown in Fig. 6. The intent in this design

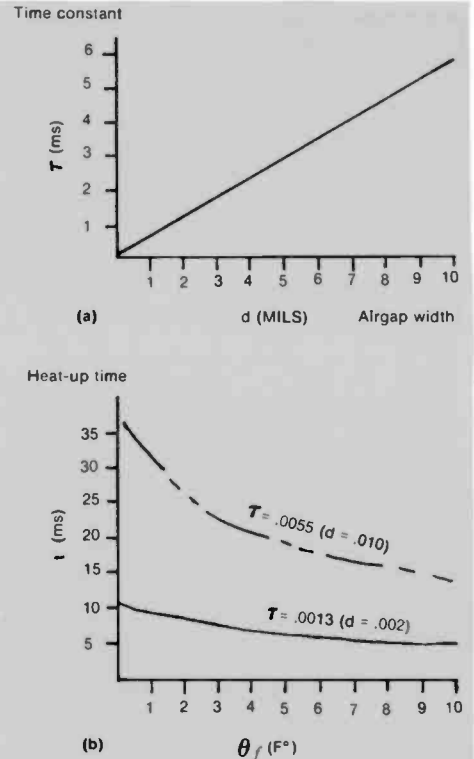


Fig. 5. Film heat-up time—convective approach.

was to process continuous film, 9.5-inches wide, at a speed ranging from 0.008 to 0.0034 in/s. The processor was located immediately following a flying-spot-laser-recording station. The flying spot generated by the laser formed a circle. Since it was desirable to locate the processor very near the recording area, the processor had to be curved (radiused) to conform to the curvature generated by the flying spot. A cross section of the processor is shown in Fig. 7.

Graphitar 2 was used as the porous heat- and air-transfer material, while Invar 36™ was used as the housing for the air chamber that formed the main structure. Thermofiol "guard" heaters acted as "insulators" around the air chamber, to prevent heat loss and to generate a uniform temperature around the air chamber. To further ensure temperature uniformity of the processor, the air chamber was surrounded by a copper housing that, in turn, was insulated from the ambient. Due to physical design restraints, it was anticipated that the two ends of the processor would be cooler as compared to the center and that this condition would form an undesirable temperature profile, resulting in nonuniform density.

To compensate for that condition, heated air was introduced into both ends via small diameter tubes. The tubing

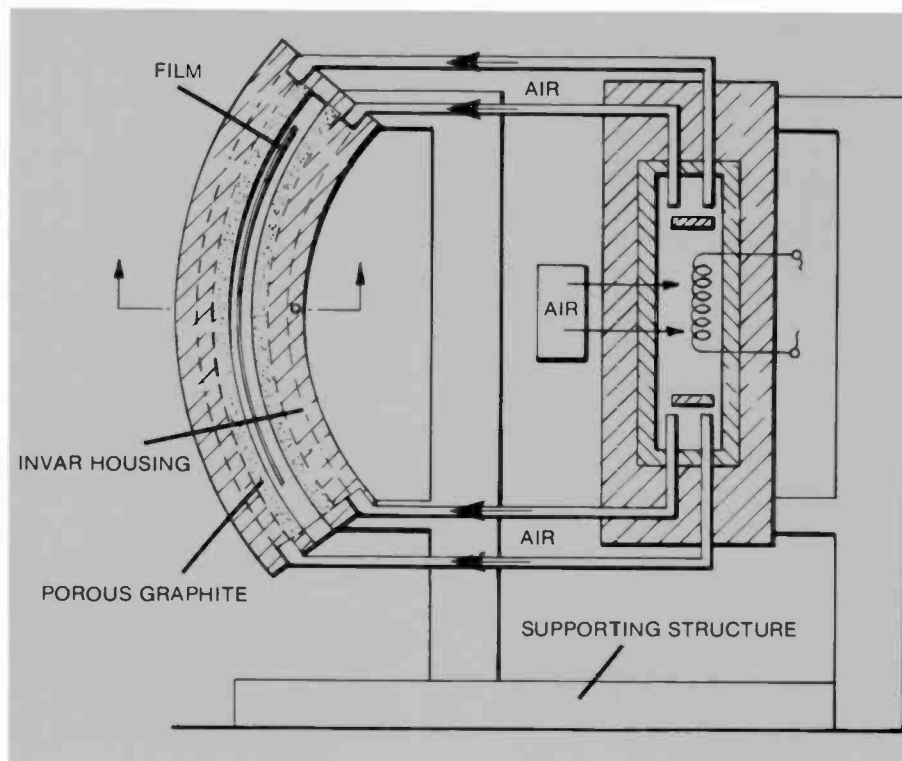


Fig. 6. Curved thermal processor.

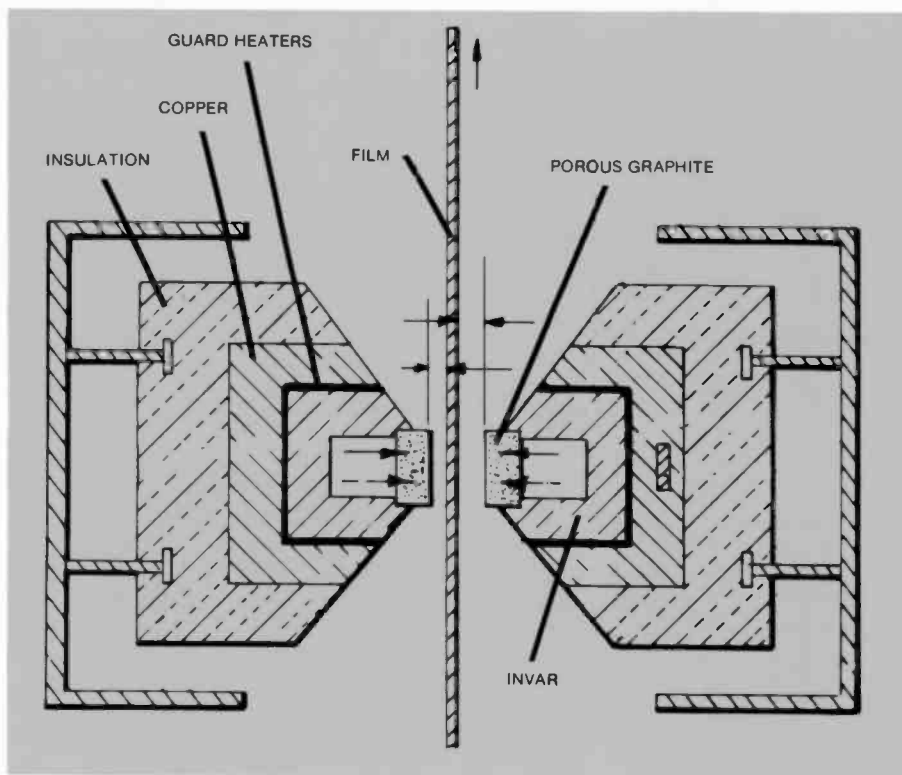


Fig. 7. Curved thermal processor—cross section.

caused air turbulence, thus promoting air mixing that added to temperature uniformity of the supplied air. The two graphite surfaces were separated by shims which allowed for a 0.002-inch thick air film on both sides of the processed film.

Thermistors and proportional controllers sensed and controlled temperatures.

A density profile across the width of 3M's type-7869 dry silver film, gotten through contact printing then pulling the film across rollers in the curved processor,

yielded 0.2 maximum density variation (ΔD_{max}). But another density uniformity test under the same conditions, with 1872-erg/cm² scanning laser beam film exposure, yielded half the ΔD_{max} of contact printing. The nonuniform contact printing exposure source contributed to the initial density variation. The results showed that foil heaters bonded to heat distribution sources satisfactorily distributed the temperature for processor applications.

Design approach for a flat thermal processor

The next application required a processor for dry silver film that can handle a continuous 5-inch-wide film at speeds ranging from 0.09 to 3.5 inches per second. It was also desirable to minimize the expose-process-view distance. These requirements, in addition to processor-design considerations, could best be met if the film could be both exposed and processed in a plane, as compared to the previously described curved configuration. To accommodate the above conditions, field-flattening optics were used in the exposure station. The result was a focused laser spot that could scan the film in a straight line.

On the basis of the previously stated mandates, and especially the 35-to-1 speed range, it was determined that a sectioned, flat, thermal processor was the optimum solution since both temperature and time-at-temperature would have to be varied. The concept used two porous graphite platens spaced 0.008-inch apart for both air-bearing and heat-transfer purposes. Because of available material limitations and the ease of design implementation, the processor was subdivided into three sub-assemblies with four sections each. Each section was 0.7-inch wide with a separately controlled foil heater. In addition to the foil heaters, which heated the material surfaces directly, an air preheater was used in each section. It preheated the air before it entered the main chamber, and thus reduced another source of possible temperature gradients. A typical sub-assembly is shown in Figs. 8 and 9. Figure 9 shows a typical cross section, B-B, through one of the 12 thermally controllable sections. The cross section depicts a thermofoil heater with orifices bonded to a copper heat-transfer plate that, in turn, is spring loaded into intimate contact with the porous graphite. A thermistor, directly attached to the foil heater, was used as a

sensing element while a proportional controller maintained the temperature at a set point. The reason for spring loading the heating elements (compared to bonding directly) was to ease assembly, as well as to ease maintainability by treating each foil assembly as a separate module.

The width of the processing surface (distance normal to film motion) was designed to be 8 inches, though the film was only 5-inches wide. The purpose of this approach was to exceed the processor by 1.5 inches on each side of the film, thus allowing for temperature roll-off at the ends.

Flat thermal-processor test results

Typical uniformity of gap temperatures as measured is shown in Fig. 10. Initial testing indicated longitudinal density streaks when the film was pulled through the processor by hand. Further investigation showed that the air that supports the film took the path of least resistance and was exited by the shortest distance to atmosphere. Because the film was soft at testing temperature, the air formed convolutions in the film (sine waves) with crests parallel to the film length, which acted as air channels. This phenomenon was most prevalent about the film's centerline. To alleviate this streaking, channels 0.032-inch wide and 0.015-inch deep were cut in the graphite between sections, thus providing each section with an exiting port.

Laser exposed films were unavailable at the time of the testing, so most of the test data were generated with a contact printing table as an exposure source. The results are presented in Figs. 11 and 12. At film speeds of 1.5 and 1.0 in/s, the maximum density variation (ΔD_{max}) was measured to be 0.04 (Fig. 12a) and 0.14 (Fig. 11), respectively. The ends contribute to almost all of the density variation. A similar density profile characterizes the 2.6 in/s speed also. It is believed that heat loss through both processor ends is the prevalent contributing factor that caused the previously presented density variations. The gap-temperature profile in Fig. 10 shows a similar characteristic.

Figure 12b depicts density variations along the length of the film with a maximum density variation equal to 0.04. As anticipated, the longitudinal density variation is primarily a function of speed control and, under servoed capstan conditions,

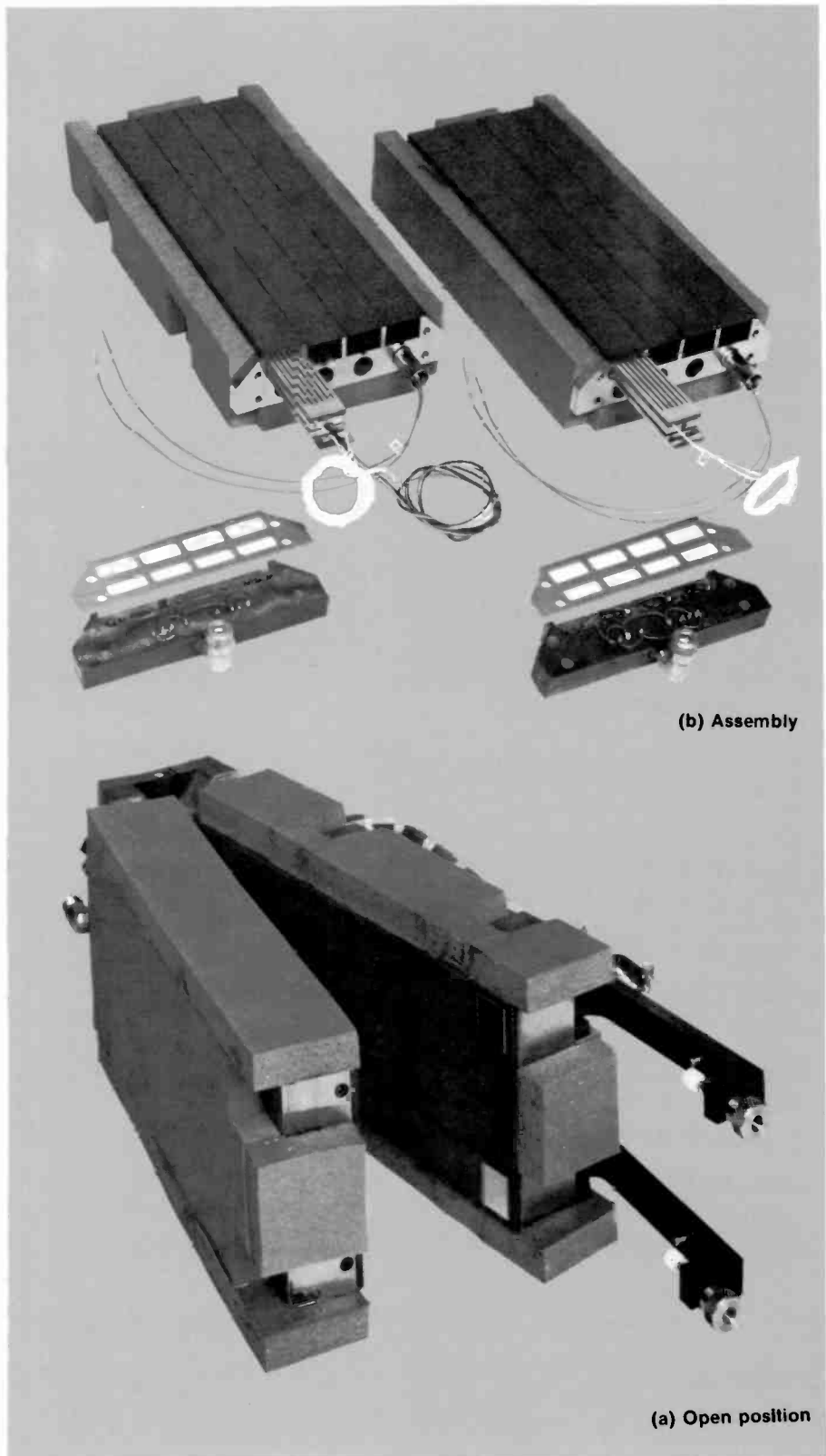


Fig. 8. Flat thermal processor.

should be minimal. Acceptance tests conducted at a film speed of 1.2 in/s resulted in 0.10 and 0.08 density variations when 3.0-mm and 0.1-mm apertures used, respectively.

Conclusions and recommendations

If pressurized air is available, the convective processor approach should

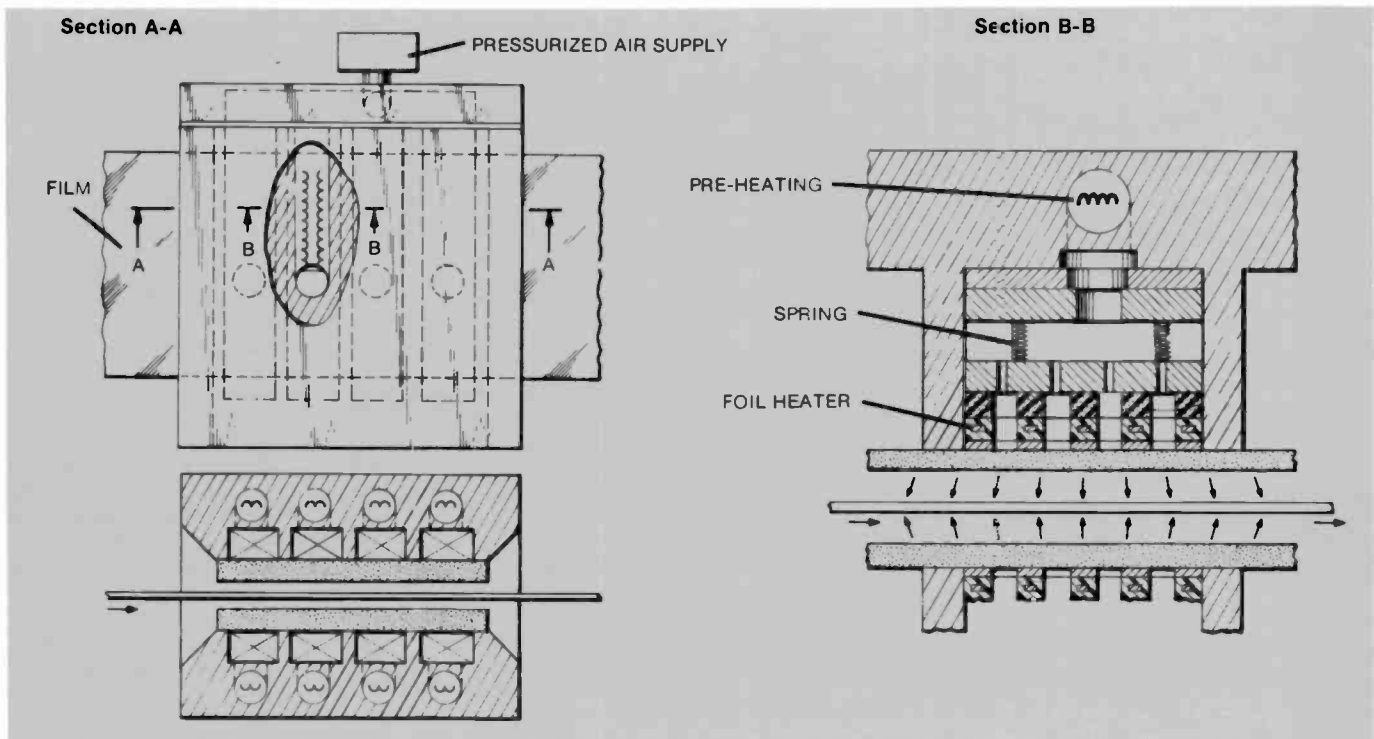


Fig. 9. Flat thermal processor.

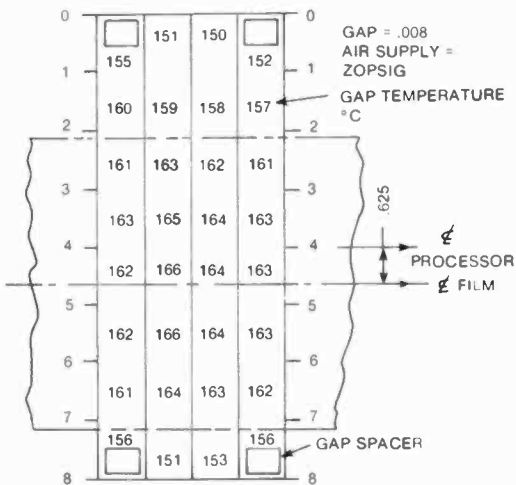


Fig. 10. Flat thermal processor gap temperatures.

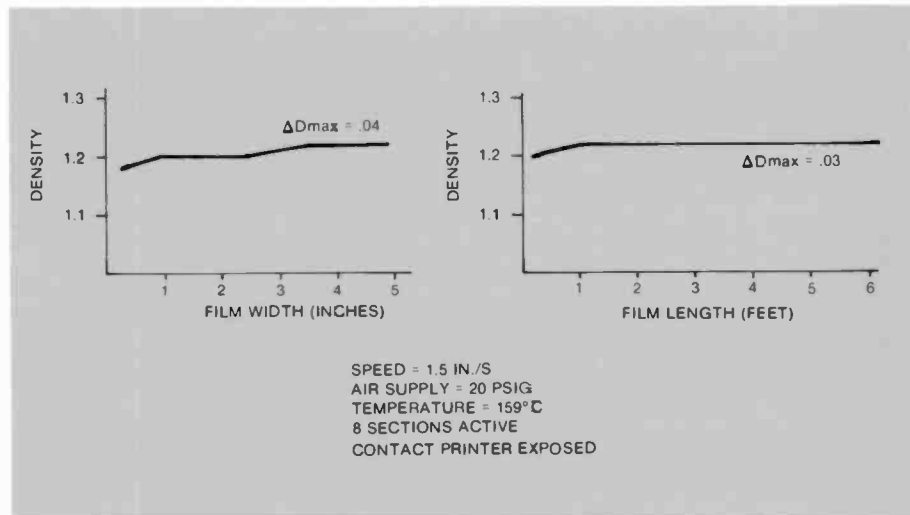


Fig. 12. Flat processor—width- and length-density variations.

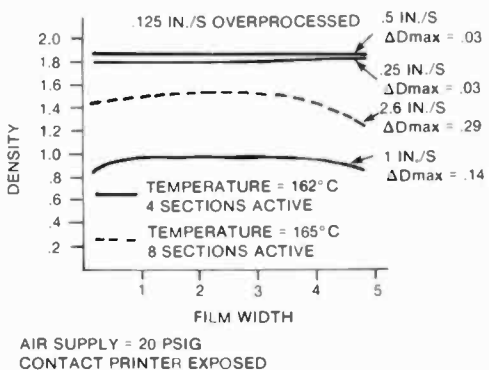


Fig. 11. Flat processor—density variations across film width for different film speeds.

definitely be considered since it presents a conceptually simple, reliable way to process dry silver film. In addition, film tension is of no consequence since the film is supported by an air bearing with no contact between it and its heat/air transfer plates. At least to some extent, the film is self-cleaning; we have never encountered a dust problem, although the initial testing was conducted under normal laboratory conditions, which are far from being dust free.

Some processor-design improvements should be developed to eliminate the temperature falloff effects at the processor

ends. Quick heat-up and quick cool-down still need investigation in designs where film speeds should be changed quickly and over a wide range.

Acknowledgment

The author wishes to thank Mr. M. Crouthamel, at ATL, for his help in formulating the thermal model for the film processor, as well as Mr. J. Covert, at ATL, for his unequivocal devotion to the program during the design, construction and testing phases.

Appendix: nomenclature

A	—	area
c_p	—	specific heat
d	—	air gap
H	—	thickness of porous material
h	—	film coefficient of heat transfer
k_p	—	permeability of porous material
k	—	thermal conductivity
m	—	mass of film
P_a	—	ambient pressure
P_s	—	supply pressure
Q_p	—	volumetric airflow at mean pressure
Q_a	—	volumetric airflow at ambient pressure
q_h	—	heat flow by convection
q_k	—	heat flow by conduction
\dot{q}_a	—	heat flow in air gap
\dot{q}_f	—	heat flow in film
T_g	—	temperature of graphite
T_f	—	temperature of film
ΔT	—	temperature difference
ΔX	—	thickness of film
t	—	heat-up time
τ	—	time constant



Bohdan Siryj, Principal Member of the Engineering Staff, Advanced Technology Laboratories, joined RCA June 1959. He helped to design tape mechanisms as well as packaging of electronic equipment for military applications. After an absence of two years, Mr. Siryj rejoined RCA in 1965 as a Member of the Engineering Staff with Applied Research. Here his engineering involvement consisted of laser and holographic film transport design, video and

optical disc related design, enhancement of IR detection systems for perimeter defense, development of scanning cursors for digitizing of cartographic material, the state-of-the-art advancement and implementation of thermal processors for dry silver film, high speed air and ball bearing supported scanner construction for laser recorder applications, helical and digital magnetic tape transport design and parcel conveyor development for the U.S. Postal Service.

At present, he is the Program Manager for the Erasable Optical Recorder Materials Evaluation Program. He is a registered professional engineer, has four patents and is the author of several technical articles. In 1979, he received the David Sarnoff Award for Outstanding Technical Achievement for research, development and implementation of laser-beam image-recording systems.

Contact him at:
Advanced Technology Laboratories
Camden, N.J.
TACNET: 222-3051

Electronic packaging for an artillery-delivered sensor

Now, a unique electronic modular design enables an artillery-delivered sensor to survive a 16,000-g gun-launch and ground-impact shock.

In July 1976, RCA was selected as prime contractor for the engineering development phase of the REMBASS system, the U.S. Army's new generation of battlefield sensors for the 1980s. REMBASS, an acronym for Remotely Monitored Battlefield Sensor System, is an integral family of seven sensors, three datalink

Abstract: *As prime contractor for the Army's REMBASS system, RCA was required to develop an electronic packaging technique suitable for an artillery-delivered sensor. The program objective was to devise a modular system—low in acquisition cost and easily maintainable—enabling the electronics to operate reliably after surviving an extremely severe 16,000-g gun-launch and impact-shock environment. The gun-hardened module's design consists of a circular, printed-circuit board supported by and encapsulated within an aluminum-alloy ring. A number of these "puck-like" modules were plugged together in a stack.*

A conservative stress and dynamics analysis was performed to size the hardware components. A materials-evaluation study was conducted to select the optimum encapsulants. Test modules were shocked in air and rail guns at the Picatinny arsenal's test facilities. Temperature-cycling and temperature-shock tests were conducted. Analytical results, substantiated by actual gun tests at Yuma Proving Grounds, demonstrated that the electronics packaging technique achieved the desired design integrity.

relays, and two monitoring sets. The sensor system is intended for use by battlefield commanders for covert detection of enemy activity around the defense perimeter, forward battle area, or other selected sites. The sensors and relays are emplaced at strategic monitoring locations by a specially trained company. When access by troops or airdrop is denied, the DT-570 GSQ artillery-delivered sensor will be used.

The sensor can actually discriminate and identify the type of activity near the site, using real-time seismic and acoustic stimulus sampling that is analyzed by a resident microprocessor with a sophisticated algorithm. Detections are transmitted to sensor monitoring sets via one of 600 datalink frequency channels which are preprogrammed in the unit. The DT-570 can be remotely deployed by a 155-mm howitzer up to ranges of approximately 20 km.

The sensor electronics are housed within the XM-694 Terminal Delivery Vehicle (TDV) developed by ARRADCOM on an earlier program. The TDV is installed in a 155-mm carrier projectile as shown in Figs. 1 and 2. The artillery deployment scenario is: launch by 155-mm gun, ballistic flight to target area, TDV expulsion from the carrier projectile, TDV free-flight, then impact and implantation—as shown in Fig. 3.

The shock environment encountered in these events is unusually severe. The gun launch imparts a 16,000-g, 12-ms shock pulse on the projectile in the gun tube; also, the rifling in the barrel spins the projectile with an angular acceleration of 332,000 rad/s^2 to 16,260 r/min when it exits the muzzle (zone-8 charge conditions). In a timed sequence, the TDV is expelled from

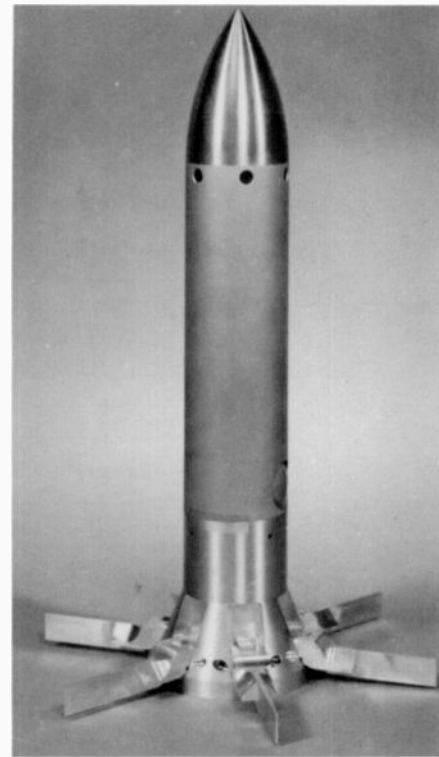


Fig. 1. The Terminal Delivery Vehicle (TDV), housing the sensor electronics, is installed in a 155-mm carrier projectile.

the carrier projectile by an explosive charge that imparts approximately a 5000-g, 2.5-ms shock pulse on the TDV in the reverse direction from gun launch. With a terminal velocity of 300 ft/s at impact, the sensor TDV experiences another 5000-g, 2.5-ms shock (implant shock level varies depending on soil conditions), again in the reverse direction from gun launch.

The program objective was to develop an electronic packaging technique that was suitable for the 2.75-inch-diameter and 6.3-inch-long cylindrical payload volume of the artillery-delivered sensor. Previous packaging design for similar applications consisted of a stack of circular boards, hardwired and encapsulated within an aluminum cannister using a structural foam. Any failure, during manufacture or storage, necessitated costly replacement of the entire package. A detailed trade-off analysis indicated it was necessary to devise a modular system, low in acquisition cost, to satisfy the REMBASS constraints. The expendable sensor was to be produced in a substantial quantity of 3600 units, but commonality was an important driver because the basic module stack could be used in another air-dropped REMBASS sensor with the addition of a unique timer module. Also, the transmitter, synthesizer and voltage regulator modules could be used in the two REMBASS air-dropped

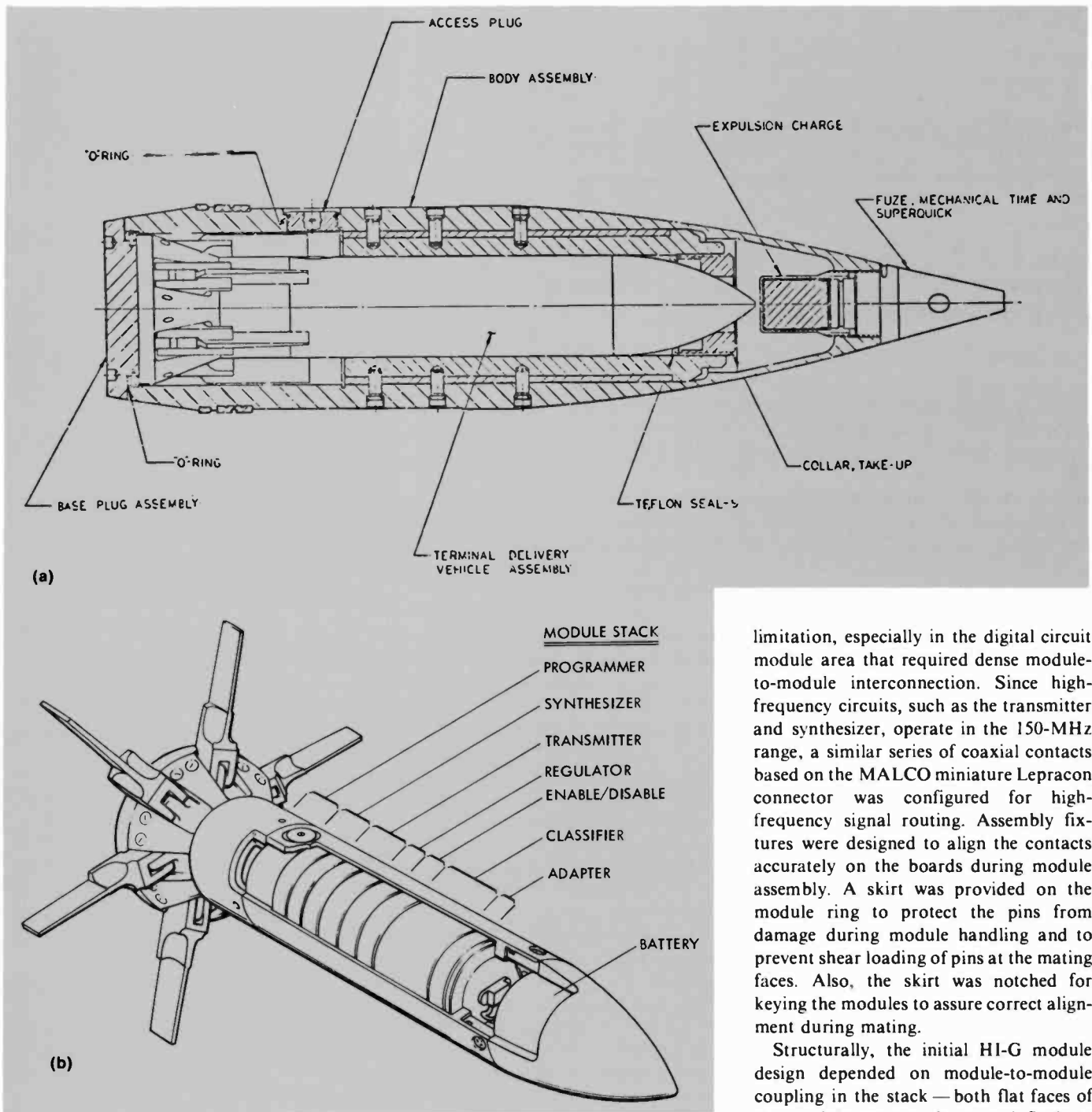


Fig. 2. Artillery deployment scenario shows stresses the unit must withstand.

repeaters. Modularization would also provide ease of manufacture and test, and enhance maintainability.

The basic design concept for the gun-hardened module derived from the effort consists of a circular, printed-circuit board supported within an aluminum-alloy ring with the electronic parts volume totally encapsulated. The puck-like modules are then plugged together in a stack to form a cylindrical unit. For electrical interconnection provision between modules, a basic

48-pin connector is built into the printed-circuit (PC) boards using individual pin/jack contacts placed on a standardized pin circle, near the periphery of the module. The pin/jack contacts had been used by RCA in previous, lesser HI-G environment applications and provided a viable candidate as an interconnect system. A series of pin-only, jack-only and pin/jack contacts was designed to provide interconnection versatility up and down the module stack and to preclude pin-count

limitation, especially in the digital circuit module area that required dense module-to-module interconnection. Since high-frequency circuits, such as the transmitter and synthesizer, operate in the 150-MHz range, a similar series of coaxial contacts based on the MALCO miniature Lepracon connector was configured for high-frequency signal routing. Assembly fixtures were designed to align the contacts accurately on the boards during module assembly. A skirt was provided on the module ring to protect the pins from damage during module handling and to prevent shear loading of pins at the mating faces. Also, the skirt was notched for keying the modules to assure correct alignment during mating.

Structurally, the initial HI-G module design depended on module-to-module coupling in the stack — both flat faces of the module were to be potted flush to permit the encapsulant to transfer the load between modules up and down the stack during setback, expulsion and impact shock loads.

It was relatively difficult, however, to economically encapsulate the modules to the flatness of mating surfaces desired for effective load transferral, and to mask the pins/sockets reliably to prevent adhesive contamination of contact surfaces. Additionally, the dynamic load buildup on the bottom module supporting the stack overstressed the candidate encapsulants in compression. Artillery design experience

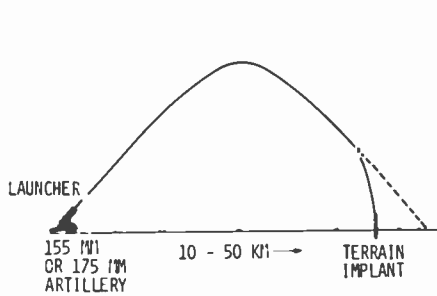
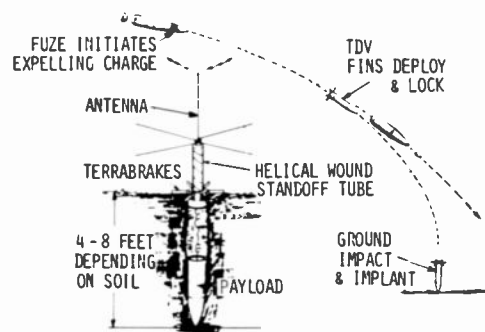


Fig. 3. Typical high frequency module.

indicates encapsulants are virtually liquefied under these huge dynamic loads.

An alternate approach was taken in the basic design philosophy, which was an "uncoupled" approach. Each module became structurally independent. A PC board with a relatively high electronics-part population mounted on it will be overstressed in flexural bending in the 16,000-g acceleration environment. The board could be stiffened by a ribbed support structure (or central column as used in the copperhead gun-launched missile), but expulsion and implant load reversals left the electronic parts virtually unsupported. Thus, encapsulation was the reasonable solution, and the problem became one of selecting the encapsulant with the appropriate Young's Modulus and yield strength properties to form a composite beam of adequate stiffness that would not overstress either the encapsulant or the PC board material. In the module design, the PC board is supported by a peripheral ledge during the initial setback shock, thus transferring the load into the aluminum-alloy ring, then down this metallic shell to the TDV-stack-support surface. The encapsulation of the parts is simply a "meniscus pour" with virtually no pin masking or potting fixtures necessary. For shock direction reversals, the PC boards are bonded to the metal ledge, and the encapsulant adheres to and is locked into grooves in the inner sidewall of the module support ring.

Although the dynamic stresses within the vehicle are quite complicated, the stress analysis of the module used a simple static model that was assumed to be a solid, circular, uniformly-loaded, composite-material flat plate to approximate expected stresses and deflections. The edge restraint of the flat plate was considered to be somewhere between fixed and simply supported, probably closer to fixed conditions. The module's natural frequency was calculated to be in a range above 3000



Hz. The shock transmissibility would probably be very low due to the f_n/f_d ratio exceeding 15 to 1. Because of the unpredictability of the structural responses and materials behavior in this dynamic environment, any attenuation advantage was ignored, and this conservative analysis was performed using material yield strengths and $F = MA$ loads multiplied by 1.25 to provide a margin of safety. Artillery projectile designers use this same analytical

philosophy for developmental design, especially where dynamic testing will be performed for early verification. Subsequent hardware design refinement would use finite-element analysis techniques for optimization or problem-area analysis.

The selection process of the encapsulant for the HI-G module design resulted in a rather extensive materials evaluation program. The primary candidates were selected for their previous HI-G applications usage. Others exhibiting a high Young's Modulus and low cure shrinkage or good damping characteristics were also considered, including rigid, lightweight foams. Initially, all encapsulant materials were cast into test pucks of the approximate module geometry with an aluminum ring. These were subjected to thermal shock and thermal cycling testing (-70°F to $+165^\circ\text{F}$) to evaluate their ability to withstand the REMBASS environmental requirements. Stress deflection and load analyses were also performed with the candidate encapsulants in combination with the PC board as a composite-material

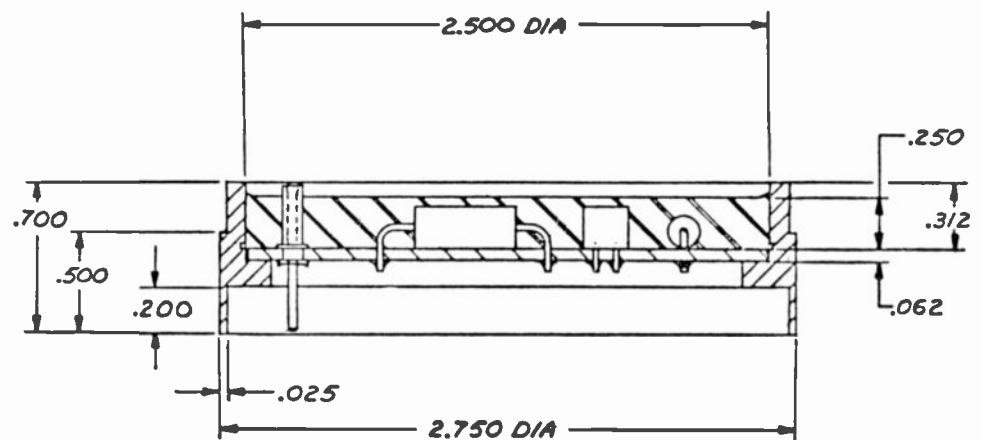


Fig. 4. (a) Basic module configuration with circular PC board mounted in ring.

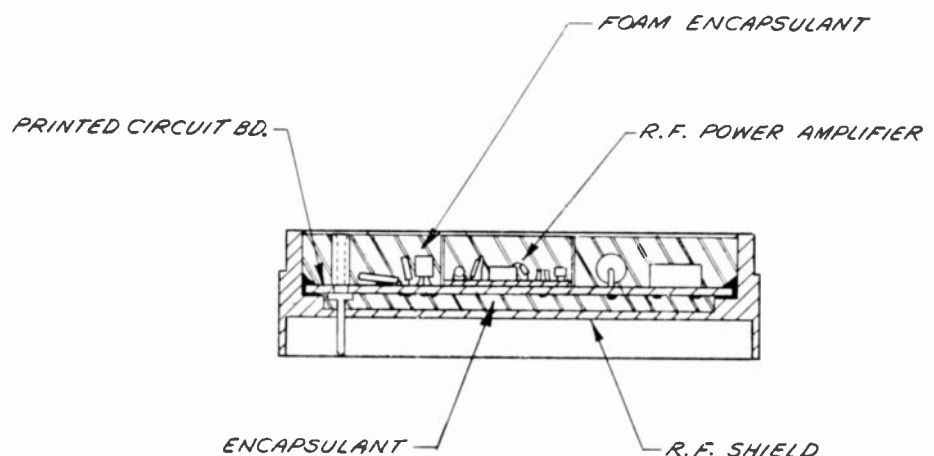


Fig. 4. (b) Typical high-frequency module with a thin-walled plate (composite structure) and foam encapsulant with low dielectric constant.

plate. The module designs exhibiting the lowest deflections were thought to have the best chance of surviving the HI-G environment without fracturing the PC boards or electronic parts.

Two groups of modules using the promising candidate encapsulants were fabricated in functional circuit form, either as a voltage regulator or digital programmer module. All test pucks had PC boards and connector pins. Thermal shock and cycling tests were performed on all test items. HI-G shock tests were then performed on these pucks in the air gun facility, Picatinny Arsenal in Dover, New Jersey. The pucks were first subjected to the 16,000-g shock, then electrically tested. Direction was reversed, and the 5000-g separation and implant shocks were simulated. Although the air gun cannot simulate the actual pulse width of setback shock (1 ms is typical in the air gun) or spin, it does provide full g-level testing capability for step-by-step developmental projects. The results indicated that Emerson and Cuming STYCAST 1090 SI, HYSOL C9-R246 with H-A248, and Hexcel URALITE 3125 encapsulants provided the necessary rigidity. STYCAST 1090 SI was chosen as the prime candidate since it was the preferable encapsulant for low-cost production.

However, the STYCAST 1090 SI was not optimum for use in the high-frequency (150 MHz) transmitter and synthesizer modules because its dielectric constant of 2.9 severely affected the circuit performance of these modules. A variation of the basic module added a thin-walled bottom plate to the arrangement as shown in Fig. 4. The plate formed a stiff composite-beam structure with the PC board, using STYCAST 1090 SI between them as a filler. The sensitive volume around the electronic parts was encapsulated with Emerson and Cuming ECCOFOAM EEF-14, a low-dielectric-constant foam material. The addition of the metallic bottom plate to the module also provided a substantial improvement in EMI shielding between the sensitive modules in the stack. Analytical results for this high-frequency module design were substantiated in air-gun tests using prototype pucks.

Two full payload stacks of functional modules with simulated classifier sections were installed in the forward section of the XM694 TDV for rail-gun testing. The scoop-nosed projectiles were fired in the 155-mm howitzer rail-gun. These tests introduced spin and 14,000-g actual setback shock, and the projectiles were recovered intact after traversing a 100-yd



Fig. 5. Electronic stack.

water trough that gradually slows the projectile before it impacts 20 ft. of crushable, corrugated cardboard. After the rail-gun, the two module stacks were shock tested in the airgun to simulate separation and implant. The test sequence was successful with only minor adjustments necessary to several transmitter module tunable elements which should have been adhesive staked.

As a final step in the HI-G test sequence, six full-up DT-570 sensors (without classifiers) were prepared and loaded into their 155-mm carrier projectiles. The electronic stack is shown in Fig. 5. These rounds were fired at Yuma Proving Ground where five of the six TDVs implanted successfully, approximately 15-km downrange. The test firings were con-

ducted with an M-190 gun at zones 7 and 8. Setback shock levels at zone 7 were 12,500 g's and 13,500 g's at zone 8. The actual gun tests performed on the prototype hardware proved that this electronic packaging technique is viable. Electronic parts and circuits can be gun-hardened for the most severe shock environment possible and can survive and function successfully. An implanted TDV is shown in Fig. 6.

Acknowledgment

The author would like to acknowledge the valuable contribution of O.A. DeMarco, J. Thornhill, R. Turransky, and D.R. McCarthy. Their dedicated efforts assured the success of this development program.

Miles Kurina has over 24 years experience in aerospace mechanical engineering design and management. Areas of experience include wind-tunnel design/test, air-to-air missiles, shipboard radar, B-52 pulse doppler radar avionics, and several EW expendables/sensors programs including REMBASS.

Since joining RCA in 1962, he has been involved in mechanical design of automatic satellite detection equipment, a four-frequency radar transmitter, the LM-Apollo rendezvous radar, Phase III air-dropped sensors, and a B-52 airborne pulse doppler radar developmental system. As Manager, he has been responsible for the mechanical design of the QRC-418 and AN/ALQ-127 pulse doppler radar systems, F-15 radar antenna development, NAVY EW systems, PROUD ARROW development and, most recently, the REMBASS sensors and repeaters, which include the artillery-



delivered DT-570. He was a member of the Lunar Module Team that won the David Sarnoff Team Award in 1970.

Contact him at:
RCA Automated Systems
Burlington, Mass.
TACNET: 326-3627

Pen and Podium

Recent RCA technical papers and presentations

Patent listings, omitted from this issue, will appear in the next issue.

To obtain copies of papers, check your library or contact the author or his divisional Technical Publications Administrator (listed on back cover) for a reprint.

Advanced Technology Laboratories

A. Feller|I. Abeyta
High-Speed Standard Cell CMOS/SOS Custom LSI Devices for Advanced Signal Processing Applications—IEEE 1980 International Conf. on Circuits and Computers (ICCC) for Large Scale Systems, Port Chester, N.Y., *Proceedings* (10/80)

A. Feller|R. Noto
Automatic Layout and Design Verification of Random Logic LSI Devices—1980 CANDE Workshop at Lake Tahoe, Calif. (9/80)

A. Feller|R. Noto|A. Smith
Standard Cell Approach for Generating Custom CMOS/SOS Devices Using a Fully Automated Layout Program—IEEE 1980 International Conf. on Circuits and Computers (ICCC) for Large Scale Systems, Port Chester, N.Y., *Proceedings* (10/80)

R.F. Kenville
Fifteen Years of Laser Recording—Where We've Been and Where We're Going—12th annual Electro-Optics/Laser 80 Conference, Boston, Mass. (11/80)

T. Lombardi|R. Pryor
Megarad Radiation Hardened Array Design for a Fault-Tolerant Spaceborne Computer—IEEE 1980 International Conf. on Circuits and Computers (ICCC) for Large Scale Systems, Port Chester, N.Y., *Proceedings* (10/80)

R. Noto|F. Borgini|B. Suskind
The Automated Universal Array (AUA)—1980 IEEE SOS Workshop, Snowmass, Col. (9-10/80)

R. Noto|F. Borgini|B. Suskind
Automated Universal Array—IEEE 1980 International Conf. on Circuits and Computers (ICCC) for Large Scale Systems, Port Chester, N.Y., *Proceedings* (10/80)

S. Ozga|J. Saultz|A. Cornish
CMOS/SOS High-Performance Microprocessors—IEEE 1980 International Conf. on Circuits and Computers (ICCC) for Large Scale Systems at Port Chester, N.Y., *Proceedings* (10/80)

M. Stebnisky|A. Feller
State-of-the-art CMOS/SOS Technology for Next-generation Computers—IEEE 1980

International Conf. on Circuits and Computers (ICCC) for Large Scale Systems, Port Chester, N.Y., *Proceedings* (10/80)

J. Tower
A Microprocessor-controlled CCD Analog-Binary Correlator—IEEE SSCTC Fall Workshop, New Paltz, N.Y. (9/80)

Americom

M. Shumila|R. Langhans
Digital Audio for Satellite Distribution—1981 Southcon Professional Program, Atlanta, Ga. (1/81)

Astro-Electronics

F. Chu, *et al.*
S/C Modal Testing Using Systematic Multi-Shaker Sine-Dwell Testing Technique—51st Shock and Vibration Symposium, San Diego, Calif. (10/21/80)

F. Chu
Experimental Determination of Damping in Materials and Structures—ASME Winter Meeting, Symposium on Damping, Chicago, Ill. (11/17/80)

S. Hawkins|P. Holtzman
Microprocessor Controlled Telemetry System—NASA/AIAA Workshop on Aerospace Applications of Microprocessors, Greenbelt, Md. (11/3/80)

J. Horan
Highlights of 1980: Sensor Systems—Aeronautics & Astronautics Journal (12/80)

C. Hubert
Dynamics of the Generalized Dual-Spin Turn—*RCA Review*, Vol. 41 (9/80)

C. Voorhees
Predicting the Random Acoustic Response of a Complex Structure Using FEM Techniques—100th Mt. of the Acoustical Society of America, Los Angeles, Calif. (11/17/80)

Automated Systems

L. Arlan
High Resolution Computer-Controlled Television System for Hybrid Circuit

Inspection—Eta Kappa Nu Electrical Engineering Honorary Society Meeting, Univ. of Mass., Amherst, Mass. (12/80)

L. Arlan
Automatic Electro-Optical Inspection of Hybrids Demonstrated—*Electronic Packaging and Production Magazine* (9-10/80)

M.J. Cantella
Application of Schottky Barrier IR Focal Plane Arrays—EASCON '80, Arlington, Va. (9/80)

M.J. Cantella|F.F. Martin
W.F. Kosonocky (Princeton)
Schottky Barrier Focal Plane Array Review—Navy Focal Plane Array Review, Naval Research Labs, Washington, D.C. (11/80)

O.T. Garver
Trends in Automatic Test Equipment—AIAA Support Systems Group, Washington, D.C. (1/80)

R.T. Cowley
New Generation of Test and Monitoring Systems—ASME Student Chapter, Northeastern Univ., Boston, Mass. (10/80)

M.J. Gilbert
Microprocessor Applications—IEEE Student Chapter, Univ. of Vt., Burlington, Vt. (10/80)

R.J. Gildea
AN/GVS-5 Laser Rangefinder and Improved Modules—Low Energy Laser Applications Symposium, Ft. Belvoir, Va. (10/80)

J.M. Goode
Hardware-Software Tradeoffs—IEEE Student Chapter, Tufts Univ., Medford, Mass. (11/79)

T.E. Kupfrian
Reliability in the LSA Process—Boston IEEE Reliability Group, Lowell, Mass. (12/80)

J.M. Laskey
An Automated System for Hybrid Circuit Visual Inspection—12th Annual Manufacturing Technology Advisory Group Conf., Bal Harbour, Fla. (10/80)

J.F. McCarthy
Broad-based Technology at RCA Automated Systems—IEEE Student Chapter, Univ. of Lowell, Lowell, Mass. (10/80)

R.J. Monis
DEPOT Automatic Test Equipment—AUTOTESTCON '80, Washington, D.C. (11/80)

C.F. Morrissey
Technical Publications Facilities—Aerospace Industries Assoc. Automated Publications Symposium, Danvers, Mass. (9/81)

A.R. Pelletier
Shock and Vibration Applied to Design—ASME Student Chapter, Univ. of Lowell, Lowell, Mass. (10/80)

Government Communications Systems

H. Barton, Jr.
User's Guide: RCA Unit Production Cost Tracking Model (UPCT4)—EIA-G-47 Committee Meeting, Washington, D.C. (11/18/80)

D. Hampel
Application of VLSI to Smart Sensors—GOMAC Conf., Houston, Texas, *Proceedings (GOMAC Digest)* (11/19-21/80)

D. Hampel
Advanced Remote Expendable Sensor/Processing Techniques—AIAA Conf. on Sensor Systems for the 80s, Colorado Springs, Col., *Conference Record* (12/2-4/80)

D.G. Herzog
Using Optical Disc to Solve High Data Rate Recording (20-75 Mb/s) and Mass Storage of 10¹⁴ Bits—AIAA Conf. on Sensor Systems for the 80s, Colorado Springs, Col., *Conference Record* (12/2-4/80)

R.B. Hines
Technical Writing in the Corporation—Fall Conf. of the Delaware Valley Writing Council, Drexel Univ., Phila., Pa., *Proceedings* (10/80)

J.B. Howe
Communications for Rapid Deployment Forces—RCA Panel - Armed Forces Communications & Electronics Assoc., *SIGNAL* (6/80)

J. Springer
Error Management in a Distributed System—ICCC 80 (IEEE Conf.) New York, N.Y., *Proceedings* (10/80)

Laboratories

I. Balberg
Determination of States Distribution in Hydrogenated Amorphous Silicon Using MIS Tunnel Junctions—Physical Review B, Vol. 22, No. 1 (10/15/80)

D. Botez
Single-mode AlGaAs Laser Diodes—SPIE, Fiber Optics for Communications and Control, Vol. 224 (1980)

D.J. Channin
High Data-Rate Modulation of Laser Diodes—SPIE, Fiber Optics for Communications and Control, Vol. 224 (1980)

J. Dresner
Hall Mobility for Electrons in Undoped a-Si: H—Appl. Phys. Lett., Vol. 37, No. 8, 1980 American Institute of Physics (10/80)

B. Goldstein|D.J. Szostak
Surface Photovoltage, Band-Bending and Surface States on a-Si: H—Surface Science 99, pp. 235-258, North Holland Publishing Co. (1980)

W.F. Kosonocky|M.J. Cantella
F.F. Martin (Burlington)
Schottky Barrier Focal Plane Array Review—Navy Focal Plane Array Review, Naval Research Labs, Washington, D.C. (11/80)

H.W. Lehmann|R. Widmer
Dry Etching for Pattern Transfer—J. Vac. Sci. Technol., Vol. 17, No. 5 (9-10/80)

R.U. Martinelli|A. Rosen
The Effects of Storage Time Variations on the Forward Resistance of Silicon p⁺-n-n⁺ Diodes at Microwave Frequencies—IEEE Transactions on Electron Devices, Vol. ED-27, No. 9 (9/80)

Y. Okada
Glow-Discharge-Polymerized Difluoroethylene Film—Thin Solid Films, Elsevier Sequoia S.A., Lausanne, Printed in the Netherlands, Vol. 74, pp. 69-76 (1980)

G.H. Olsen
InGaAsP Laser Diodes—SPIE Fiber Optics for Communications and Control, Vol. 224 (1980)

J.I. Pankove|J.E. Berkeyheiser
Light-Induced Radiative Recombination Centers in Hydrogenated Amorphous Silicon—Appl. Phys. Lett., 1980 American Institute of Physics, Vol. 37, No. 8 (10/80)

A. Rosen|R.U. Martinelli|M. Caulton
Temperature Dependence of Storage Time in Silicon p⁺-n-n⁺ Switching Diodes and Reduction of Harmonic Distortion—Electronics Letters, Vol. 16, No. 2, pp. 66-68 (1/17/80)

D.L. Staebler|J.I. Pankove
Conductivity Changes in Dehydrogenated and Rehydrogenated Discharge-Produced a-Si: H—Appl. Phys. Lett., Vol. 37, No. 1, American Institute of Physics (10/1/80)

C.W. Struck (two others not RCA)
Two-Photon Excited Luminescence of Thulium-Activated Lanthanum Oxysulfide (La₂O₂S-Tm³⁺)—J. Chem. Phys., Vol. 73, No. 8, 1980 American Institute of Physics (10/15/80)

G.A. Swartz|D.W. Wern|P.H. Robinson
Large-Area Varactor Diode for Electrically Tunable, High-Power UHF Bandpass Filter—IEEE Transactions on Electron Devices, Vol. ED-27, No. 11 (11/80)

M. Toda
Elastic Properties of Piezoelectric PVF₂—J. Appl. Phys., Vol. 51, No. 9, 1980 American Institute of Physics (9/80)

Missile and Surface Radar

J.A. Bauer
The Impact of New Technology—Burlington County College (12/80)

W.C. Grubb, Jr.
Mini Computers and Microprocessors for Non-Electrical Engineers and Solid State Electronics for Non-Electrical Engineers—ASME Winter Meeting, Chicago, Ill. (11/80)

W.C. Grubb, Jr.
Mini Computers and Microprocessors for Non-Electrical Engineers—George Washington Univ., Washington, D.C. (12/80)

J.T. Nessmith
A View of Systems Engineering—Univ. of Pennsylvania Moore School, Phila., Pa. (11/80)

W.A. Mulle
R-76 Fire Control Radar... Performance and Versatility for Small Ships—International Naval Technology Expo '80, Proceedings, p. 299 (11/80)

E.J. Stevens|J. Halat
RTE Driver for the 8542A Automatic Network Analyzer—Automatic RF Techniques Group, Dallas, Texas (11/80)

NBC

C. Spicer, Sr. Staff Engineer
NTSC Color Field Identification—122nd SMPTE Technical Conference, N.Y. (11/80)

Attention: TRS-80 Users

The results of a survey in TREND showed a large number of TRS-80 owners among RCA's personal computer users. These owners voiced a strong interest in exchanging programs. As a result, a Corporate TRS-80 Users Group has been formed with the purpose of, initially, providing a means for program exchange and, later, offering other services.

If you are interested in this activity, contact the organizer: **George E. Haas**, TRS-80 Users Group, RCA Labs, W-238B, Princeton. TACNET: 226-2491.

Engineering News and Highlights

James B. Feller Named Division Vice-President



James B. Feller is Division Vice-President, Engineering for RCA Government Systems Division, reporting to **John D. Rittenhouse**, Division Vice-President and General Manager, RCA Government Systems Division.

Mr. Feller is responsible for coordinating and reviewing the engineering and technology activities of the division's business units in Moorestown, Camden and Princeton, New Jersey, and in Burlington, Massachusetts.

He is also responsible for the division's Advanced Technology Laboratories in Camden, and administers the independent research and development programs. The division has a staff of more than 2,000 engineers.

Mr. Feller joined RCA in 1959 as an electronics engineer in what is now the Government Communications Systems operation in Camden. He was named a Unit Manager in Advanced Communication Systems Design in 1968. In 1974 he was promoted to Engineering Manager in Advanced Communication Systems and Computing Systems.

Mr. Feller served as manager for a group of programs, including a major effort in information processing for the Department of Defense in 1976. He had served as Manager of Information Processing Systems since 1978.

Sherman is new EdRep at Automated Systems



Dale Sherman has been appointed Editorial Representative for Automated Systems, Government Systems Division, Burlington,

Massachusetts. He joined RCA in August of 1980 as Senior Publications Engineer.

Mr. Sherman began his career as a technical writer in the Technical Publications department of Pratt & Whitney Aircraft where he authored numerous technical reports, articles, speeches, presentations and industrial movie scripts. He has produced, directed and written copy for television commercials and designed multi-media ad campaigns for assigned clients. Working with the U.S. Department of Labor, he helped to design and implement recommendations for the nationally recognized Disabled Veterans Outreach Program in the Commonwealth of Massachusetts. He returned to private industry to teach proposal writing before joining RCA.

Contact him at:
Automated Systems
Burlington, Mass.
TACNET: 326-2985

Staff Announcements

Consumer Electronics

J. Peter Bingham, Division Vice President, Engineering, announces the organization of Engineering as follows: **Larry A. Cochran**, Manager, Signal Systems and Components;

Arthur Kaiman, Manager, Systems Applications; **Eugene Lemke**, Chief Engineer, Advanced Projects; **Perry C. Olsen**, Manager, Product Design Engineering; and **J. Peter Bingham**, Acting Manager, Engineering Development.

Laboratories

William M. Webster, Vice-President, RCA Laboratories, announces that **Henry Kressel**, Staff Vice-President, Solid State Research, will have responsibility for the research program of Laboratories RCA, Ltd. (Zurich). Dr. Kressel will also continue his present responsibilities.

Henry Kressel, Staff Vice-President, Solid State Research, announces the organization of Solid State Research as follows: **Phillip K. Baltzer**, Head, LSI Systems and Applications; **Bernard Hershenov**, Director, Solid State Devices Laboratory; **Walter J. Merz**, Director, Laboratories RCA, Ltd., Zurich; **Louis S. Napoli**, Staff Scientist; and **David E. O'Connor**, Director, Integrated Circuit Technology Research Laboratory.

William M. Webster, Vice-President, RCA Laboratories, announces the appointment of **Alfred H. Teger**, Staff Vice-President, Systems Research.

David D. Holmes, Director, Consumer Electronics Research Laboratory, announces the organization of the Consumer Electronics Research Laboratory as follows: **Robert H. Dawson**, Manager, New Technology Applications Research (Somerville); **Leopold A. Harwood**, Fellow, Technical Staff; **David D. Holmes**, Acting, Signal Processing Research; **Dalton H. Pritchard**, Fellow, Technical Staff; **Stanley P. Knight**, Head, Signal Conversion Systems Research; **Lubomyr S. Onyshkevych**, Head, Electronic Packaging Research; **Martin Rayl**, Head, Product Assurance Research; **Werner F. Wedam**, Head, Television Receiver Systems Research; and **Kern K.N. Chang**, Fellow, Technical Staff.

Solid State Division

Carm J. Santoro, Division Vice-President, Integrated Circuits, announces the organization of Integrated Circuits as follows: **Marvin B. Alexander**, Manager, IC Operations Analysis; **Ronald J. Costlow**, Director, SS Offshore Manufacturing; **James K. George**, Director, LSI Operations; **Heshmat Khajezadeh**, Director, Bipolar & MOS Logic Operations; **Donald W. Laird**, Director, Offshore Support and Assembly Development; and **John P. McCarthy**, Director, Government & HiRel Operations.

James K. George, Director, LSI Operations, announces the organization of LSI Operations as follows: **Michael S. Fisher**, Manager, LSI Marketing and Applications;

L.H. Yorinks—for his pioneering analysis work on the influence of "edge effects" on sidelobe performance of very low sidelobe array antennas. His investigation of this little-known area has resulted in a simple, direct means of quantifying the sidelobe contribution of edge effects, and establishment of a direct relationship between antenna aperture dimension and edge effect impact on sidelobes.

Manufacturing Engineering Symposium

Art Barrett, Division Vice-President, Manufacturing, Camden, welcomed about 130 manufacturing engineers and managers, as well as members of RCA Laboratories who are involved in manufacturing support, to a manufacturing engineering symposium in Moorestown.

The symposium, held on December 10 and 11, reviewed many programs directed at

productivity increases in the RCA manufacturing activities. Also, the business units reported on specific productivity accomplishments.

The invited dinner speaker, **Larry Matthews**, a management consultant from Philadelphia, Pa., addressed opportunities to increase productivity.

Fred Pfifferling, Manager, Test Engineering, Camden, was the symposium organizer and chairman.

Copies of the viewgraphs used in the talks will be available in RCA technical libraries.

Pridgen is Award Winner

The Technical Excellence Award has been made to **Junius Pridgen** of ATL for his significant contribution to LSI array development for COMSEC equipment.

Specifically, as Project Engineer on the BANVILLE Program, his objective was to replace four arrays—213 x 231 mils—containing 2348 active devices, with a single array—235 mils square—containing approximately 9,000 active devices. Junius designed a unique set of logic cells for the chip with interface connections on all four sides and with geometrics which permitted an efficient mosaic of these connections. His resulting design contains 8178 active devices and is 202 x 215 mils—smaller than any of the four chips it replaced. A measured operating speed of the array was more than an order of magnitude higher than that of the previous design.

This successful and innovative design, called COMPEP, considerably enhances CMOS/SOS technology in general, as well as RCA's reputation as a high-technology, state-of-the-art developer of DoD equipment. The performance and yield of the COMPIP was well beyond expectations, and is expected to considerably accelerate the acceptance of the CMOS/SOS technology in DoD applications.

Consumer Electronics presents Technical Excellence Awards

The Consumer Electronics Technical Excellence Committee received a large number of nominations for the Third Quarter 1980 Award. **Dr. D.J. Donahue**, Division Vice-President, Operations, has informed the following winners of their selection:

Don Willis—for significant creative contributions to the advanced development of a new TV regulator/deflection system with wide application in the TV product line.

Wayne Harlan—for expedient design of a cost-effective automatic circuit for use in F line receivers, years before original expectations.

Jim Hettiger—for enhancement of IC yields with low-cost novel solutions which were implemented when the early performance of those ICs fell short of the necessary design goals.

Charles Coyle, Bob Schoentrup, and Ken Meyer—for the introduction of microcomputers to component production assembly and test techniques.

Jim Grayson, Dave Ward, Bob Atkins, Tom Stiller, Stu Golin, and Duane Piper—for design of the M.A.C.S. factory information system which provides real-time quality factory information and discrete product history.

Ed Christensen, Don Over, Harry Martin, Charles Key, and Joe Case—for implementation of the low-cost custom magnetized tape beam bender used in all RCA in-line picture tubes and design of unique production line magnetizer.



Willis



Harlan



Hettiger



Coyle



Schoentrup



Meyer



Grayson



Ward



Atkins



Stiller



Golin



Piper



Christensen



Over



Martin



Key



Case

Editorial Representatives

Contact your Editorial Representative at the TACNET numbers listed here to schedule technical papers and announce your professional activities.

*Technical Publications Administrators, responsible for review and approval of papers and presentations, are indicated here with asterisks before their names.

Americom

TACNET

* Murray Rosenthal Princeton, New Jersey 258-4192

Commercial Communications Systems Division (CCSD)

Broadcast Systems

* Bill Sepich Camden, New Jersey 222-2156
* Krishna Praba Gibbsboro, New Jersey 222-3605
* Andrew Billie Meadowlands, Pennsylvania 228-6231

Cablevision Systems

* John Ovnick Van Nuys, California 534-3011

Consumer Electronics (CE)

* Clyde Hoyt Indianapolis, Indiana 422-5208
* Francis Holt Indianapolis, Indiana 422-5217
* Chuck Limberg Indianapolis, Indiana 422-5117
* Don Willis Indianapolis, Indiana 422-5883

Distributor and Special Products Division (DSPD)

* Charles Rearick Deptford, New Jersey 225-2299

Globcom

* William Hartweg New York, New York 323-7300

Government Systems Division (GSD)

Astro-Electronics

* Ed Goldberg Princeton, New Jersey 229-2544

Automated Systems

* Ken Palm Burlington, Massachusetts 326-3797
* Dale Sherman Burlington, Massachusetts 326-2985

Government Communications Systems

* Dan Tannenbaum Camden, New Jersey 222-3081
* Harry Ketcham Camden, New Jersey 222-3913

Government Engineering

* Merle Pietz Camden, New Jersey 222-2161

GSD Staff

* Ed Moore Cherry Hill, New Jersey 222-5833

Missile and Surface Radar

* Don Higgs Moorestown, New Jersey 224-2836
* Jack Friedman Moorestown, New Jersey 224-2112

National Broadcasting Company (NBC)

* Bob Mausler New York, New York 324-4385

Patent Operations

TACNET

Joseph Tripoli Princeton, New Jersey 226-2992

Picture Tube Division (PTD)

* Ed Madenford Lancaster, Pennsylvania 227-3657
* Nick Meena Circleville, Ohio 432-1228
* Jack Nubani Scranton, Pennsylvania 329-1499
* J.R. Reece Marion, Indiana 427-5566

RCA Limited (Canada)

Bob McIntyre Ste Anne de Bellevue 514-457-9000

RCA Records

* Dave Devarajan Indianapolis, Indiana 424-6109

RCA Service Company

* Joe Steoger Cherry Hill, New Jersey 222-5547
* Ray MacWilliams Cherry Hill, New Jersey 222-5986
* Dick Dombrosky Cherry Hill, New Jersey 222-4414

Research and Engineering

Corporate Engineering

* Hans Jenny Cherry Hill, New Jersey 222-4251

Laboratories

Maucie Miller Princeton, New Jersey 226-2322

"SelectaVision" VideoDisc Operations

* Woody Workman Indianapolis, Indiana 426-3235

Solid State Division (SSD)

* John Schoen Somerville, New Jersey 325-6467

Power Devices

Harold Ronan Mountaintop, Pennsylvania 327-1633
or 327-1827
John Cadra Somerville, New Jersey 325-6909

Integrated Circuits

Dick Morey Palm Beach Gardens, Florida 722-1262
Sy Silverstein Somerville, New Jersey 325-6168
John Young Findlay, Ohio 425-1307

Electro-Optics and Devices

John Grosh Lancaster, Pennsylvania 227-2077

Solid State Technology Center

Judy Yeast Somerville, New Jersey 325-7357

RCA Engineer

A technical journal published by
Corporate Research and Engineering
"by and for the RCA engineer"

Bldg 204-2, Cherry Hill, NJ 08358
Return postage guaranteed

BULK RATE
US Postage

PAID

Phila., Pa.
Permit No. 2906

EM MUSSELMANN LCTT
PO BOX 9
STRASBURG
PA 17579